LOSS OF COOLANT ACCIDENT SIMULATION FOR THE CANADIAN SUPERCRITICAL WATER-COOLED REACTOR USING RELAP5/MOD4

LOSS OF COOLANT ACCIDENT SIMULATION FOR THE CANADIAN SUPERCRITICAL WATER-COOLED REACTOR USING RELAP5/MOD4

By MENGMENG LOU, B.ENG.

A Thesis

Submitted to the School of Graduate Studies

In Partial Fulfillment of the Requirements

For the Degree

Master of Applied Science

McMaster University

Master of Applied Science (Engineering Physics)

McMaster University
Hamilton, Ontario

TITLE: Loss Of Coolant Accident Simulation For The Canadian Supercritical Water-Cooled Reactor Using RELAP5/MOD4

AUTHOR: Mengmeng Lou, B.ENG. (Shanghai Jiao Tong University)

SUPERVISOR: Professor D. R. Novog

NUMBER OF PAGES: XII, 143

Abstract

Canada has participated in the Generation IV International Forum (GIF) collaboration in the area of Super Critical Water-cooled Reactors (SCWR). Similar to the current CANDU technologies, in the Canadian SCWR design the low pressure heavy water moderator system is separated from the supercritical coolant system (25MPa). The High Efficiency Re-entrant Channel (HERC) design in the Canadian SCWR has multiple coolant regions (i.e. coolant in the downward center flow tube and coolant in the upward outer fuel region) and provides thermal isolation between the moderator and heat transport system fluid. Although the overall reactivity feedback in the channel is negative for equilibrium density decrease transients, a temporary positive reactivity may be induced during non-equilibrium conditions such as cold-leg Loss of Coolant Accidents (LOCA). The primary objective of this study is to investigate the fuel and coolant behaviors under postulated LOCA transients, in particular those caused by cold-leg breaks, and to demonstrate the effectiveness of several proposed safety systems in the Canadian SCWR.

The one-dimensional thermalhydraulic system code RELAP5 has been used for the safety analysis in many LWRs. The latest version RELAP5/MOD4 has been improved to accommodate supercritical water and is used in this study. A RELAP5 model is constructed based on the most recent Canadian SCWR design. The 336 fuel channels are split into two representative groups each with a series of hydraulic and heat structure models. A benchmark study is conducted by comparing RELAP5 to CATHENA simulations and shows good agreement for both steady-state and transient predictions.

The RELAP5 model is then used to predict the system response to several postulated LOCA transients. For a 100% (single-ended) cold-leg break located in between the feedwater pump and the inlet plenum, the system pressure immediately drops followed closely by a flow reversal with rapid discharge from the break. A brief power pulse (178%FP) is observed under this non-equilibrium depressurization scenario. The transient simulations show the potential for two sheath temperature maxima, one early in the transient as a result of the power pulse and the subsequent flow-power mismatch, and another later peak resulting from the fuel heat-up under near stagnant channel flow conditions (such as in the failure of the Emergency Core Cooling Systems) as the heat transfer regime changes to radiation dominated. The Automatic Depressurization System (ADS) located on the hot-leg side mitigates the later fuel heat-up by introducing forward channel flows. This effect is enhanced by additional coolant supplied from Low Pressure Coolant Injection (LPCI) which is part of the Emergency Core Cooling System (ECCS). Under the 100% break LOCA/LOECC transient, the core inventory is depleted rapidly after the break and thermal radiation becomes the dominant heat removal mechanism. The highest MCST, 1331 K, is achieved approximately 136s after the break and

meets the safety criterion (1533 K). Beyond this time the sheath temperatures gradually decrease either by the continuous LPCI from the reactor sumps, gravity driven core cooling, or in the event of a failure of those systems by the Passive Moderator Cooling System (PMCS).

LOCAs initiated by break sizes varying from 5% to 100% of the cold-leg cross-section area are simulated under loss of ECCS. In this specific design, break sizes less than 15% are defined as SBLOCAs and show an early pressure increase up to the Safety Relief Valve (SRV) setpoint. During SBLOCAs, the first MCST peak is more limiting than the large LOCA case because of insufficient fuel cooling caused by relatively low reverse flow. However, these lower reverse flows prolong the period of blowdown cooling and hence help to mitigate the secondary MCST peak. The worst LOCA case occurs in the 15% break case with a maximum cladding temperature of 1450 K. The results showed the most sensitive parameters are delays associated with SDS action, emissivity and ADS actuation parameters.

Acknowledgements

I would like to express my sincere gratitude to my supervisor Dr. David Novog for his inspiring and patient guidance through this two-year program. I would never finish this thesis without his invaluable suggestions and generous assistance in thesis editing. The research approaches, analysis methodology, creative way of thinking that I've learnt from him will absolutely benefit me for my future career.

It is also my duty to record my thankfulness to Dr. Luxat and Dr. Rashkovan for their critical comments on my oral presentation and my thesis. They inspired me to think deeply and further beyond my study.

I would also like to thank Dr. Chris Allison, Dr. Richard Wagner, Mr. Zheng Fu and Mr. Brian Allison From the Innovative System Software LLC for their generous help of RELAP5/MOD4 during my one month summer internship in the US and continuous technical support since I came back.

Also I want to thank my friends and colleagues at McMaster: Hummel, James, Fred, Feng, Yang, Travis, Chris, Matt, Dion, Changrui, Izaak, Remon, Xiaopan, Jason, et al. for their help from all aspects.

Finally, special thanks to my beloved parents, my young brother and my dearest boyfriend for their fully support. Love you all.

Table of Contents

Contents

List of Figures

List of Tables

Nomenclature

Letters

A	area
α	void fraction
ρ	fluid density
v	fluid velocity
x	distance in the flow direction
t	time
Γ	vapor/liquid generation
B	body forces
FWG	wall friction against vapor
FWF	wall friction against liquid
FIG	Interface frictional drag on vapor
FIF	Interface frictional drag on liquid
C	Virtual mass coefficient
U	internal energy
P	Pressure
Q_w	wall heat transfer rate
Q_i	interface heat transfer rate
h^*	enthalpy associated with bulk interface mass transfer
h'	enthalpy associated with wall interface mass transfer
$DISS$	energy dissipation by wall friction and pump effect
φ	neutron flux
β	delayed neutron fraction
λ	decay constant
Λ	prompt neutron generation time
C_i	delayed neutron precursor number
Σ_f	macroscopic fission cross-section

E_f	energy released per fission
P_f	immediate fission power
ρ	reactivity
a	reactivity coefficient
W	weighting factor
F	power fraction
c_p	specific heat
K	thermal conductivity
T	temperature
d	density
q'''	volumetric power generation rate
q''	heat flux per unit area
h	heat transfer coefficient
N_u	Nusselt Number
Re	Reynolds number
Pr	Prandtl number
D	hydraulic diameter
N	kinematic viscosity
E	radiation emission rate
ε	emissivity
σ	Stephen-Boltzmann constant
F_{ij}	view factor from surface i to surface j

Subscript

g	vapor phase
f	liquid phase
m	mixture of liquid and vapor
i	interface
B	biased

Abbreviation

ACR	Advanced CANDU Reactor
AFS	Auxiliary Feedwater System
BOC	Begin Of Cycle
CANDU	CANada Deuterium Uranium reactor
CATHENA	CAnada THErmal-hydraulic Network Analysis
CDF	Core Damage Frequency
CFD	Computational Fluid Dynamics
CHF	Critical Heat Flux
CNL	Canadian Nuclear Laboratories
CVR	Coolant Void Reactivity
DNBR	Depart from Nucleate Boiling Ratio
ECCS	Emergency Core Cooling System
EOC	End Of Cycle
GDCS	Gravity Driven Coolant Injection system
GFCIS	Gravity-Fed Coolant Injection System
GEOFAC	GEOmetry FACtors
GFR	Gas-cooled Fast Reactor
GIF	Generation IV International Forum
HEM	Homogenous Equilibrium Model
HERC	High Efficiency Re-entrant Channel
LWR	Light Water Reactor
HPLWR	High Performance Light Water Reactor
HWPR	Heavy Water Pressurized Reactor
IAPWS	International Association for the Properties of Water and Steam
ICS	Isolation Condenser System
INEEL	Idaho National Engineering and Environmental Laboratory
LBLOCA	Large Break LOCA
LERF	Large Early Release Frequency
LFR	Lead-cooled Fast Reactor

LOCA	Loss of Coolant Accident
LPCI	Low Pressure Coolant Injection
MCST	Maximum Cladding Surface Temperature
MOC	Middle of Cycle
MSIV	Main Steam Isolation Valve
NIST	National Institute of Standards and Technology
NRC	Nuclear Regulatory Commission
PCCS	Passive Containment Cooling System
PDO	Post DryOut
PMCS	Passive Moderator Cooling System
PRHR	Passive Residual Heat Removal systems
PT-SCWR	Pressure Tube SCWR
R&D	Research and Development
RIA	Reactivity Initiated Accident
SBLOCA	Small Break LOCA
SBO	Station BlackOut
SCW-FFP	Supercritical Fossil-Fired Power Plants
SCWR	Supercritical Water-Cooled Reactor
SCWR-M	Mixed-spectrum SuperSritical Water Reactor
SDS	ShutDown System
SDTP	SCDAP Development Training Program
SFR	Sodium-cooled Fast Reactor
SJTU	Shanghai Jiao Tong University
SRV	Safety Relief Valve
TDJ	Time Dependent Junction
TDV	Time Dependent Volume
TMI	Three Mile Island
VHTR	Very-High Temperature Reactor
XJTU	Xi'an Jiao Tong University
YSZ	Yttria-Stabilized Zirconia

1. Introduction

1.1 Background

With the growing environmental concern from greenhouse gas emissions and the finite nature of fossil fuel reserves, clean abundant energy is in urgent demand. Nuclear power has become increasingly important in today's energy market for its high power density, economic competitiveness, sustainability and it's near zero carbon dioxide emission. Nuclear power technology has evolved from the first prototype generation, to the second generation to which most of the currently operating nuclear power plants belong, and then to the third generation presently under construction [1]. The most significant lesson people have learnt from the three nuclear power catastrophes in history, i.e. the Chernobyl accident, the Three Mile Island (TMI) accident and the Fukushima Daiichi accident, is that safety and accident management are of paramount importance in the deployment of this advanced technology.

The Generation IV International Forum (GIF) was established in 2001 to formalize international collaboration on research and development (R&D) for the next generation nuclear power technology. Six types advanced reactor concepts were selected based on the criteria involving sustainability, safety and reliability, economics and proliferation resistance with a goal of deployment beyond year 2030 [1]. These concepts include the Gas-cooled Fast

Reactor (GFR), the Lead-cooled Fast Reactor (LFR), the Molten Salt Reactor (MSR), the Sodium-cooled Fast Reactor (SFR), the Super Critical Water-cooled Reactor (SCWR) and the Very-High Temperature Reactor (VHTR).

As the only water-cooled Gen IV reactor, the SCWR is considered the logical extension from contemporary Light Water Reactors (LWRs) or Heavy Water Pressurized Reactors (HPWRs) technologies [3]. Extensive knowledge of the design and operation from previous reactor generations reduces the technical gaps and enhances confidence that such design can be realized in the next 20 to 30 years. In addition, successful operation of supercritical fossil-fired power plants (SCW-FFPs) provides expertise with materials and chemistry, equipment reliability and balance of plant design.

1.2 SCWR advantages and challenges

The SCWR is designed to operate above the thermodynamic critical point of water (22.064 MPa and 649.76 K), usually at 25 MPa with a high temperature (up to 898 K) outlet coolant. The SCWR has several important advantages that make it attractive as a candidate of GEN-IV nuclear reactors [3]:

- Remarkably improved economics because of the increased steam temperature and the resultant increased thermal efficiency (45-50%), which is much higher than that of the existing reactors (33-35%);

- Economic enhancements from a simplified heat transport system achieved by incorporating a once-through thermodynamic cycle. The steam separator and dryer as well as the internal/external recirculation loop in BWRs are avoided. As compared to PWRs the steam generator is removed. Such changes may allow for reduced capital cost and containment size;
- Since two-phase flow is avoided while at power, boiling crises are no longer a safety concern while the core remains above the critical pressure;
- Some components such as the high pressure turbine have been manufactured for application in SCW-FFPs and can be directly adopted in SCWRs.

However, some challenges arise because of the supercritical water thermodynamic properties. These challenges are significant, and to some extent expected, given the early stages of conceptual design. Of prime importance is the issue of in-core materials selection. The high pressure, high temperature and corrosive nature of supercritical water limit the type of material available for in-core components, in particular those for the pressure boundary and the fuel sheath. Corrosion of materials, its activation, and transportation/deposition in the turbine issues are similar to modern BWRs, with the added caveat that corrosion is expected to be more significant in the SCWR designs. Additional materials and/or operability issues such as those related to the thermal insulators and channel reliability also remain open. A large amount of R&D is focused on overcoming these issues.

Furthermore, at a given pressure above the critical point, the coolant properties vary as the temperature changes. A sharp peak of specific heat appears at what is called the pseudo-critical temperature (T_{pc}) [4]. The pseudo-critical temperatures at different pressures constitute the pseudo-critical line. In addition to specific heat, other thermodynamic properties such as density, viscosity and thermal conductivity undergo substantial variation as well (Figure 1-1). Thus, the forced convective heat transfer under supercritical pressure is more complicated than that of the single-phase fluid flow under subcritical pressure [5], even though there is no boiling crisis. Because of the strong variation of coolant properties, heat transfer can either be unchanged, enhanced or impaired depending on the wall surface heat flux and geometry [6]. Many empirical heat transfer correlations have been proposed to predict the onset of heat transfer deterioration and the resultant limiting fuel cladding temperature in [5].

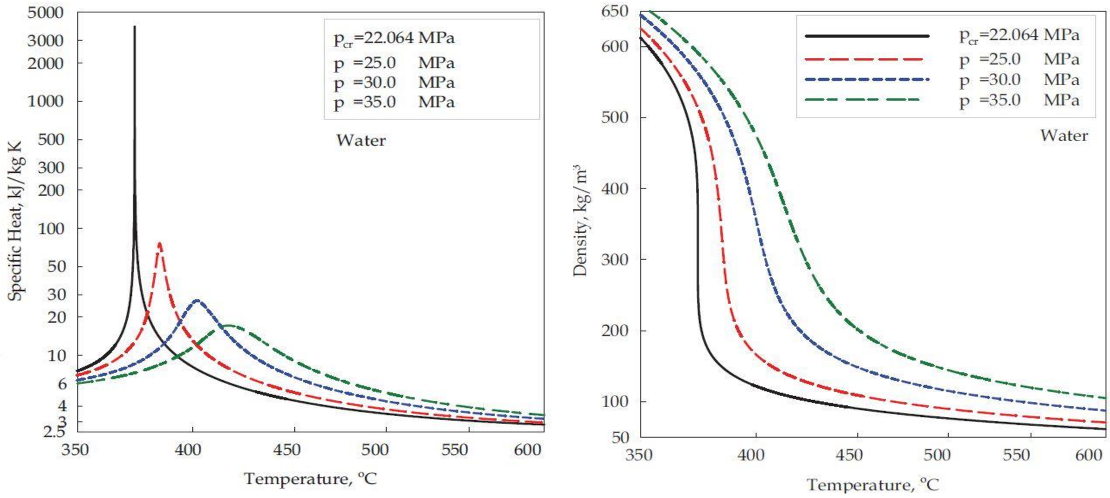

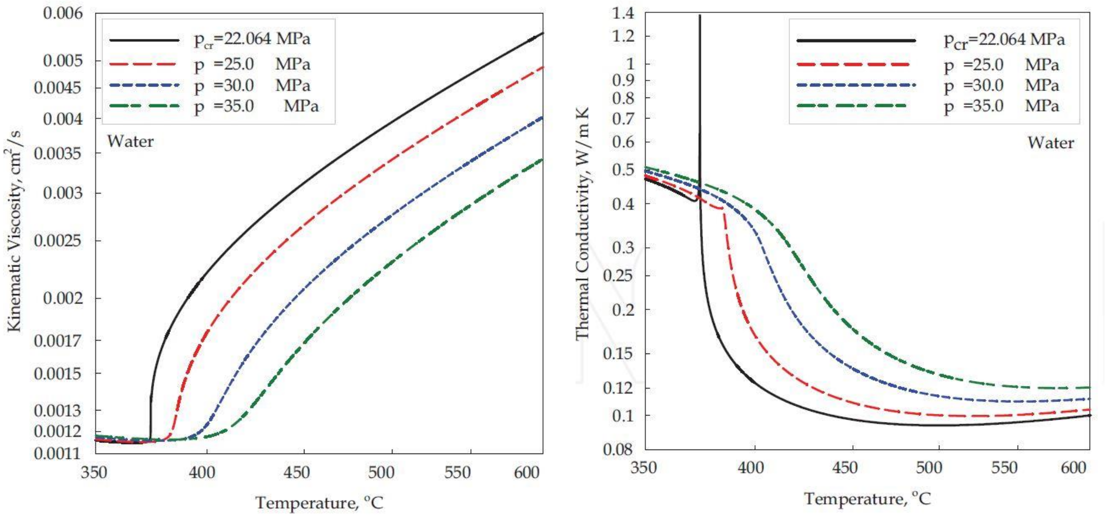

Figure 1-1 Coolant thermodynamic properties under supercritical pressure [4]

The drastic variation of coolant density through the pseudo-critical point not only affects the thermalhydraulic behavior but also has a significant impact on SCWR neutron kinetics since the coolant nuclei density affects the reactor fission rate. This effect has been confirmed by some neutronic/thermalhydraulic coupling simulations for SCWRs [7] and is expected to be significant during Loss of Coolant Accidents (LOCAs).

Several SCWR concepts have been proposed by the GIF members [8] including thermal, fast or mixed-neutron spectrum reactor concepts. In terms of the pressure boundary, two types of SCWR designs are being considered, one using a large pressure vessel similar to PWR geometry and the other using distributed pressure tubes like CANDU reactors. The University of Tokyo in Japan have come up with two pressure vessel type SCWRs, one with a thermal spectrum known as the Super Light Water Reactors (Super-LWR), and the other with a fast spectrum called the Super Fast Reactor (Super FR). The European Consortium developed a pressure vessel type SCWR referred to as the High Performance Light Water Reactor (HPLWR). Shanghai Jiao Tong University (SJTU) from China proposed a mix-spectrum pressure vessel type SCWR called SCWR-M. Canada has participated in the GEN IV program with a unique pressure tube type SCWR (PT-SCWR). Extensive R&D has been performed through worldwide collaboration to demonstrate the feasibility and safety of these SCWR concepts, although the challenges above remain.

1.3 Canadian PT-SCWR

The Canadian SCWR is a pressure tube type reactor cooled by supercritical light water and moderated by low pressure heavy water. It has evolved from the well-established CANDU reactors in several aspects. Some of the key features of this design include:

- A Thorium-Plutonium ceramic fuel mixture with a batch refueling scheme is utilized instead of the online refueling using natural uranium. With the removal of online refueling, the reactor core orientation is vertical rather than the traditional CANDU horizontal configuration;
- Feeder pipes are eliminated as the fuel channels are directly coupled to the inlet and outlet plena, which simplifies the heat transport system and reduces material issues related to feeders at such high pressures.

- The fuel assembly design has evolved from the initial 43-element CANFLEX arrangement (design of ACR), to the 54-element, the 78-element, the 62-element and eventually to the most recent 64-element design [35]. A single fuel assembly is used in each channel with a collapsible stainless steel fuel sheath that maintains direct contact with the fuel pellets;
- The fuel channel geometry is significantly different from the previous CANDU designs. In the SCWR, a separate calandria tube is not required, but rather the pressure tube is in direct contact with the moderator. To insulate the pressure tube from the high temperature coolant, a ceramic insulator is used on the coolant-facing side of the pressure tube. The flow arrangement in the SCWR channels is from the inlet plenum and down through the interior flow tube which contains no fuel. When the flow reaches the bottom of the tube it is redirected upwards through the concentric fuel rings, and finally to the outlet plenum. The new channel design concept is named the High Efficiency Re-entrant Channel (HERC) [35].
- The separated heavy water moderator system at low pressure and low temperature is retained [9].

A schematic figure of the PT-SCWR reactor core is in Figure 1-2 and some design parameters of significant importance are listed in Table 1.1.

The Canadian SCWR concept satisfies the GEN IV requirements as follows [3]:

1) Improved economics. The coolant outlet temperature of 898 K increases the cycle thermal efficiency to 47% [3]. Heat transport system simplification reduces the capital cost, maintenance cost as well as the containment size;
2) Enhanced safety and reliability. Negative Coolant Void Reactivity (CVR) is an inherent safety feature that ensures the reactor shutdown during LOCAs. Under emergency conditions decay heat can be removed in a number of ways: a) the passive isolation condenser system, b) the active low-pressure core injection system, c) the passive gravity-fed coolant injection system, or d) the passive moderator cooling system. The redundancy and diversity of these emergency cooling systems makes the design more accident tolerant than previous designs while also significantly reducing safety metrics such as Core Damage Frequency and Large Early Release Frequency;
3) Improved sustainability. The SCWR uses the thorium-plutonium fuel cycle which is an intermediate step in developing a fully sustainable Thorium based fuel cycle [8];
4) Improved proliferation resistance and security. The Thorium fuel does not irradiate U-238 and therefore does not produce transuranic atoms like Plutonium, Americium, Curium, etc. In addition, the presence of a highly radioactive isotope U-232 poses a difficulty during the reprocessing course due to the need of thick lead shielding. Although U-233 has been determined to be at least as efficient as U-235 as a weapon material, it can be easily diluted by a relatively small amount of natural uranium, which creates an effective barrier to diversion of U-233 [10].

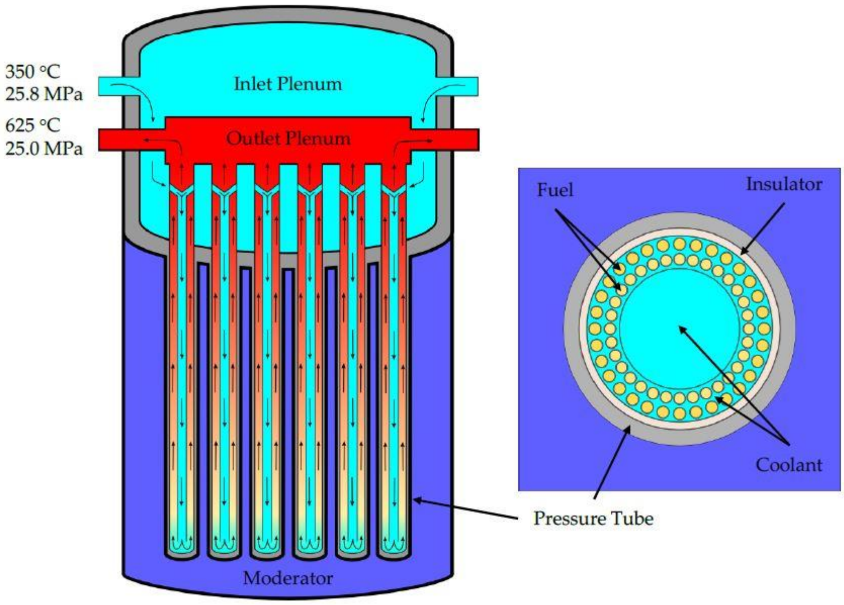

Figure 1-2 Schematic figure of the Canadian PT-SCWR reactor core [2]

Table 1-1 Important design parameters of the Canadian PT-SCWR

Parameter	Value
Thermal/Electrical Power [MW]	2540/1200
Thermal efficiency [%]	47
Inlet/outlet coolant temperature [K]	623/898
Inlet/outlet coolant pressure [MPa]	25.8/25.0
Core mass flow rate [kg/s]	1272
Fuel channel numbers	336
Active core length [m]	5
Moderator pressure [MPa]	0.336
Moderator temperature [K]	328

1.4 Thesis objectives and outline

The modeling tool used in this study is RELAP5/MOD4, which is the latest version of RELAP5 for application in SCWRs. The primary objective of this study is to investigate the behavior of the PT-SCWR under postulated LOCA in the inlet (i.e. cold-leg) piping break. This includes building the RELAP5 model for the PT-SCWR and benchmarking the code and the reactor model against alternative toolsets. The LOCA analysis including all the relevant feedbacks is performed and the effectiveness of each safety system is investigated.

To be specific, the objectives of this study are to:

1) Establish a model of Canadian PT-SCWR using RELAP5/MOD4;
2) Assess the RELAP5 modeling capacity for SCWR by a code-by-code benchmark against CATHENA;
3) Use the RELAP5 to simulate both steady-state and postulated LOCA transients;
4) Evaluate the effectiveness of safety systems such as Emergency Core Cooling System (ECCS) and PMCS in mitigating the accident consequences;
5) Assess system behavior for a wide range of inlet break sizes;
6) Provide suggestions to the SCWR designers for future improvement.

Chapter 2 gives a summary of several system codes improved for application in SCWRs and a literature review of the safety analyses conducted for different SCWR concepts. Further details about the PT-SCWR safety systems are provided in this section.

Chapter 3 covers the important theoretical framework within RELAP5, including the conservation equations, the point kinetics model and heat transfer models. Also discussed are the important code modifications implemented by the developers to enable modeling of SCWR transients as well as property routine enhancements done by the author.

Chapter 4 describes the procedure of constructing the RELAP5 model for the Canadian SCWR, from hydraulic components, heat structures, kinetics model, and radiation heat transfer model to system control mechanisms. A code-to-code comparison performed with CATHENA indicates good agreement in steady-state and postulated transients, providing additional confidence in the RELAP5 models.

Chapter 5 introduces the transient scenario for the 100% cold-leg break LOCA. The effectiveness of safety systems is discussed by comparing the results from cases with partial or total failure of certain safety system. Sensitivity analyses are performed on break sizes, solid surface emissivities, ADS size, critical flow models, etc.

Chapter 6 summarizes the work in this study and draws the main conclusions. Suggestions for design improvement for the PT-SCWR and future code modifications are also included.

2. Literature Review

This chapter reviews the modeling tools that have been improved for application in thermal-hydraulic simulations of SCWRs. Following that is a summary of the available literature related to the applicable safety criterion for SCWRs as well as safety systems and safety analyses relevant to PT-SCWR design. The last section of this chapter describes some alternative SCWR concepts under investigation.

2.1 Thermalhydraulic codes for SCWR simulation

There are a large number of thermalhydraulic codes available for investigation of coolant flow in nuclear reactor system involving different levels of complexity. Starting from the large scale and system wide behavior, system codes typically analyze one-dimensional average flow, the main heat transport system components, system boundary conditions, control system interactions and safety systems in order to predict the bulk response of a reactor to a given initiating event. Subchannel level codes model one-dimensional flow in each sub-channel of a fuel assembly as well as subchannel mixing to provide pseudo two-dimensional flow information inside the fuel assemblies. Computational Fluid Dynamics (CFD) codes attempt to model micro-scale phenomena such as turbulence and heat transfer with the minimal use of correlations. This thesis focuses on the system wide phenomena and as such the literature below covers mostly this area.

One-dimensional system codes (e.g. RELAP5, CATHENA, TRACE, etc.) are commonly used for thermalhydraulic simulations in safety analyses. Those codes have been validated by a large number of experiments under subcritical pressure and thus are widely used for simulations of LWRs and HPWRs. However, the unique thermo-physical properties and heat transfer mechanisms of supercritical water present challenges to those codes. While implementation of fluid properties and SCWR specific correlations is fairly straight forward, the large magnitude gradients in fluid properties in the vicinity of the critical point, and also near the pseudo critical temperature, pose unique numerical challenges.

2.1.1 RELAP5/MOD4

The Reactor Excursion and Leak Analysis Program (RELAP5) is a one-dimensional thermalhydraulic code designed to predict the reactor coolant systematic responses under normal and postulated accident conditions. It is characterized by a two-fluid, non-equilibrium, non-homogenous hydraulic model for two phase flow [30]. Its modeling capability for thermalhydraulic response, control system behavior, reactor kinetics and various special reactor system components (i.e. pressurizer, turbine) has been confirmed by extensive experimental data for LWR type conditions and accidents. In order to extend RELAP5's application in advanced reactors and to improve its simulation performance, Innovative System Software (ISS) has participated in the international SCDAP Development & Training Program (SDTP) [12]. On the basis of the publicly accessible RELAP5/MOD3.3 models developed by the US Nuclear Regulatory Commission (NRC), ISS released RELAP5/ MOD4 as the first version of RELAP5 which is completely rewritten in FORTRAN 90/95 [13], resulting in increased flexibility in adding alternative working fluids and correlations.

RELAP5/MOD4 has incorporated the NIST (National Institute of Standards and Technology) property database Version 10 based on the International Association for the Properties of Water and Steam (IAPWS) 1995 formulation for water thermodynamic properties [14]. Compared to the original database in RELAP5, NIST 10 provides improved accuracy of water properties in the supercritical region, especially in the vicinity of the pseudo-critical line. Above the critical pressure, the fluid properties change continuously without the presence of phase change phenomenon. However, at constant pressure and over a very narrow range of temperatures near the pseudo-critical temperature threshold, fluid properties vary significantly. Below this threshold the fluid property magnitudes and sensitivities closely resemble those of liquid water at high pressure. Above this threshold, the magnitudes and sensitivities resemble those of gaseous water at high pressure. In RELAP5/MOD4 the fluid properties in the supercritical region are determined from the NIST database and the void fraction is set to zero in the two-fluid equations (i.e. the equations are solved as if there were only a liquid within a pipe component, and using the fluid properties of the supercritical fluid). Special techniques have been implemented in MOD4 to cope with the water property transitions through the pseudo-critical temperature range as well as when pressure transitions through the critical pressure. These modifications together with some important models and basic conservation equations will be covered in Section 3.1.

2.1.2 Other system codes applicable for SCWR

The most difficult challenges for numerical simulation of SCWRs is to cope with the discontinuities resulting from fluid transitions from supercritical to subcritical pressures. In particular for codes that model the supercritical region as a single fluid with zero void fraction, there may be volumes which transition to the vapor region (void fraction being 1), the liquid region (void fraction being 0) or the mixture region (void fraction between 0 and 1). Numerical errors and discontinuities are likely to occur when the void fraction suddenly changes from 0 to 1 within one time step (or a few time steps). To overcome these potential discontinuities, the "pseudo-two-phase" method has been proposed and it assumes that pseudo-critical line divides the supercritical region into two sub-regions of pseudo-liquid and pseudo-gas [15] phases. Over a small range of enthalpies, the approximation assumes the properties change in a similar fashion as in the two-phase region in subcritical flows, and is termed the pseudo-two-phase region. The void fraction for pseudo-liquid is set to 1 and for pseudo-vapor is 0. The pseudo-two-phase fluid properties change according to the pseudo-void fraction over the range of transition enthalpies. Therefore unlike RELAP5 which attempts to model the supercritical region as a single-fluid, these codes treat the supercritical pressure identically as the subcritical two-phase transition. This has the advantage of avoiding potential discontinuities when a volume transitions from pseudo-vapor to subcritical vapour since both situations have a consistent void fraction in the pseudo-two-phase method. This concept was adopted by many one-dimensional systems codes, including APROS, SCTRAN and ATHLET-SC. While these codes have systematic error in the pseudo two-phase transition region (e.g., the pressure and temperature become dependent whereas in reality they are not), such approximations have improved stability characteristics as discussed below.

APROS

The 6-equation two-fluid APROS model adopted the concept of pseudo-two-phase method with an extension of the saturation line in subcritical region along the pseudo-critical temperature line when the pressure exceeds the critical pressure [15]. The code has been improved in the following ways:

- Water properties based on IAPWS-IF 97 were used to provide sufficient accuracy;
- The latent heat of pseudo-vaporization was set to a constant value to formalize the interfacial heat and mass transfer in the two-fluid model;
- The wall heat transfer above critical pressure was determined by the Jackson's correlation, while at near critical pressure the subcritical nucleate boiling correlation with a multiplier was used during the pseudo-boiling process;

- The interfacial friction between pseudo-liquid and pseudo-vapor is interpolated between the subcritical interfacial friction and a constant (and large value) for the supercritical state. This has the effect of making the flows homogeneous for all practical values in the pseudo-two-phase region and also near the critical pressure;
- Two separate wall friction multipliers were created to estimate the pseudo-phasic distributions on the wall of the flow channel.

The aforementioned modifications were incorporated in APROS and tested against two simple pipe blowdown tests [15]. Various initial states and boundary conditions proved that transients from supercritical to subcritical pressure were simulated by APROS without numerical discontinuities and with acceptable accuracy.

SCTRAN

SCTRAN is a Homogeneous Equilibrium Model (HEM) two-phase thermalhydraulic code based on RETRAN. It has previously been modified by researchers from Xi'an Jiao Tong University (XJTU) for transient simulations where both supercritical and subcritical regimes were encountered [16]. The modifications include:

- The saturation specific enthalpies and their derivatives with respect to pressure near the critical point were updated;

- Consistent with the pseudo-two-phase methodology above, the fluid was treated as pseudo liquid and the void fraction was 1 if its specific enthalpy was greater than the pseudo-critical specific enthalpy, otherwise the fluid was pseudo steam and the void fraction was zero;
- New correlations for temperature and specific volume as functions of pressure and specific enthalpy are incorporated for fluid in supercritical regions;
- Updated critical heat flux (CHF) and Post Dryout (PDO) heat transfer look-up table for pressure up to 21 MPa. Jackson's correlation was used as the convective heat transfer correlation for supercritical region;
- The surface to surface radiation heat transfer model was included.

Since experimental data are sparse, the verification of SCTRAN was performed by code-to-code comparisons with APROS and RELAP5-3D for blowdown phenomena from supercritical pressures [16]. LOCA/LOECC transient simulations of the Canadian SCWR performed using SCTRAN are reviewed in Section 2.3.2.

<u>ATHELET-SC</u>

The thermalhydraulic code ATHELET has two models: i) a 5-equation model with separate phasic conservation equations of mass and energy and a mixture momentum equation; ii) a 6-equation two-fluid model. The 5-model ATHELET was improved based on the pseudo-two-phase concept in Reference [17] to include:

- The fictional narrow region of latent heat at supercritical pressure was assumed so as to ensure the continuous transition of void fraction and to avoid numerical errors;
- It was stated that the pseudo-enthalpy would be highly sensitive to pseudo-critical temperature. A fitting equation for fast calculation of pseudo-critical temperature with high precision was proposed;
- The water properties were calculated directly based on the IAPWS-IF97 formulations instead of the original look-up table approach. Several computational optimization techniques were included with the new water property calculation module.

The new version of ATHELET-SC is used for LOCA transient of SCWR-M and is reviewed in Section 2.4.2.

<u>RELAP5-3D</u>

RELAP5-3D has been developed at the Idaho National Engineering and Environmental Laboratory (INEEL). It was improved in several aspects to resolve the numerical issues encountered with 27 slow transient calculations and 85 blowdown transient calculations [18].

- A more dense steam table especially near the critical point was used and the specific volume and isothermal compressibility were obtained using linear rather than cubic spline interpolations;

- Modifications were made to the transport properties of thermal conductivity and viscosity based on the 4th edition of the 1967 ASME steam tables.

The combination of above modifications corrected all the execution failures encountered in the test cases. The application of RELAP5-3D in the US SCWR simulation will be discussed in Section 2.4.3.

CATHENA

The two-fluid code CATHENA MOD-3.5/Rev3 and later releases were enhanced to perform thermalhydraulic simulations at supercritical pressure [19]. The light water properties were extended from subcritical to supercritical region and the Dittus-Boelter correlation was chosen as the heat transfer coefficient for supercritical pressures. Even though the trans-critical issue has not yet been fixed in CATHENA for depressurization events, its simulation capability above the critical pressure was of considerable importance in the preliminary thermal-hydraulic studies of SCWR.

For all the above codes, experimental data of blowdown transients from supercritical pressure are necessary for further code validation.

2.2 Safety criteria for SCWR

In most LWRs it is crucial to maintain the primary coolant in contact with the fuel (e.g., a safety goal in a BWR is to prevent the CHF from occurring during an accident and to maintain post-accident liquid level above the top of the active core). As such, safety criteria on the prevention of CHF (e.g., minimum critical channel power ration or minimum departure from boiling ratio) and/or liquid level requirements are common in the LWR safety analyses. However, the phase change phenomenon and resultant boiling crisis do not exist in the supercritical region. Thus the CHF related criteria are not suitable for the SCWRs safety analysis.

Kitoh et al. developed the transient criterion for the Japanese SCWR with consideration of the unique characteristics of supercritical water cooling [20]. The maximum cladding surface temperature (MCST) was regarded as the most important safety criterion rather than the minimum DNBR in a PWR reactor. Kitoh stated that the heat transfer deterioration at pseudo-critical temperature is much milder than that of the departure from nucleate boiling under subcritical pressure. This means if the supercritical heat transfer deterioration does occur, the associated cladding temperature increase will not challenge fuel integrity. Similar to LWRs, the safety criteria require that: 1) the cladding sheath remains intact; 2) no fuel pellet damage; 3) no pressure boundary damage. Kitoh proposed the following criteria in view of the above safety philosophy [20]:

a) MCST is <1260℃ or 1533K (to ensure fuel rod integrity);

b) Reactor pressure is <110% of the design pressure of 27.5MPa (to ensure pressure integrity);

c) Maximum fuel enthalpy is <230 cal/g (963J/kg) (to ensure fuel pellet integrity).

To a large extent the same criteria are used for the Canadian SCWR as its sheath material and operating conditions are similar to Super LWR.

Ishiwatari claimed that the fuel enthalpy criterion should be considered for reactivity initiated accidents (RIA) as the potential reactivity insertion was over one dollar [21], which is also true for the Canadian SCWR given that the delayed neutron fraction is small compared to traditional thermal reactor designs. In a pressure vessel type SCWR it is necessary to consider reactivity insertion accidents resulting from potential control rod ejection, which is basically precluded in the pressure-tube type SCWR since the control rods are located in the low pressure moderator system. Therefore, rod-ejection events are of rather low probability in pressure tube based designs and the fuel enthalpy criterion is not considered in this study. However, if LOCA reactivates were to be significant such criterion may need to be considered in future studies.

The Canadian SCWR retains the Safety Relief Valve (SRV) to maintain the system pressure below 26.0MPa [22] with redundant means of depressurization available through the ADS valves. Thus overpressure events beyond the SRV setpoints are also not considered. Generally speaking, the cladding integrity criterion of MCST is of paramount importance for the safety analysis in this study.

2.3 Safety-related research for Canadian SCWR

2.3.1 Safety systems in Canadian SCWR

As a GEN IV reactor concept, the Canadian SCWR is expected to achieve enhanced safety through improvements in its accident tolerance characteristics as well as reductions in the risks of core damage and release of fission products to the environment. The overall negative coolant void reactivity ensures reactor shutdown in a LOCA [7]. In addition the design includes a mixture of active and passive safety systems aiming for significant improvements in the Large Early Release Frequency (LERF) and Core Damage Frequency (CDF) [23]. These include:

a) Active fast acting shutdown systems (SDS),
b) Emergency Core Cooling System comprising of a low pressure core injection system, long term pumped injection from the reactor sumps or external water source, and a passive gravity-fed injection system,
c) Active Automatic Depressurization System,
d) Passive Containment Cooling Systems,
e) Passive buoyancy driven Isolation Condenser System and
f) Passive Moderator Cooling System [24].

The details of each are provided below.

The MCST is used as the primary safety criterion in this study. In most accident scenarios the safety requirements can be satisfied by assuring continuous post-accident core coolant flow. This is maintained by keeping the coolant supply from the inlet and keeping the steam outflow through the hot-leg pipe. The proposed safety systems in the primary heat transport system are very similar in nature to BWR, ABWR and ESBWR designs and include:

- isolation valves at inlet and outlet of the reactor core,
- overpressure protection (i.e. Safety Relief Valve, SRV) located in the hot-leg piping,
- ADS, Low Pressure Coolant Injection (LPCI), and a Gravity-Fed Coolant Injection System to maintain flow in LOCA scenarios,
- ICS to provide a primary heat sink during station blackout events.

In addition to the typical BWR safety systems, the Canadian SCWR contains a PMCS as a backup decay heat removal path during transients where insufficient core cooling can be maintained via heat sinks connected to the primary heat transport system.

Furthermore, the Canadian SCWR design retains the shutdown systems similar to a traditional CANDU reactor (two redundant fast acting shutdown systems). Figure 2-1 and Figure 2-2 show the layout of the safety systems in the PT-SCWR.

The SRV is intended to provide overpressure protection in case of pressure control system failures or power to flow ratio increase in the core. The SRVs are spring-loaded and actuate on high pressure signal and close as the pressure drops below the closing setpoint.

The ADS is designed to maintain forward flow in the fuel channels in case of a cold-leg break and hence acts to prevent flow stagnation in the core during the early-phases of LOCA events. The ADS is activated by detection of low pressure signal and quickly depressurizes the system with a capacity designed to ensure forward flow in a 100% cold-leg LOCA event. It should also be noted that as a result of the work presented in Section 5.3, alternate action based on sustained low flow (indicating either a failure of ICS during core isolation events or a SBLOCA) should also be considered in the design. After depressurization ECCS can inject water into the core and compensate for the coolant loss through the break. In addition, ADS may be used as a redundant backup to the SRVs in the event of an unmitigated overpressure transient.

The ECCS is intended to provide intermediate and long-term core cooling under postulated accident conditions. It consists of long term Gravity-Fed Coolant Injection System (GCIS) and an active Low Pressure Coolant Injection system (LPCI). The LPCI system uses pumped flow either from the suppression pool, the containment sumps, or external water make-up, and hence can provide both intermediate and long term active post-accident core cooling, similar to the ECC systems in many GEN II and III designs. In the event of a loss of power the GCIS can deliver low pressure coolant to the reactor core from the Gravity Driven Water Pool, while the gravity pool inventory is resupplied from the condensation in the PCCS, similar to the ESBWR design.

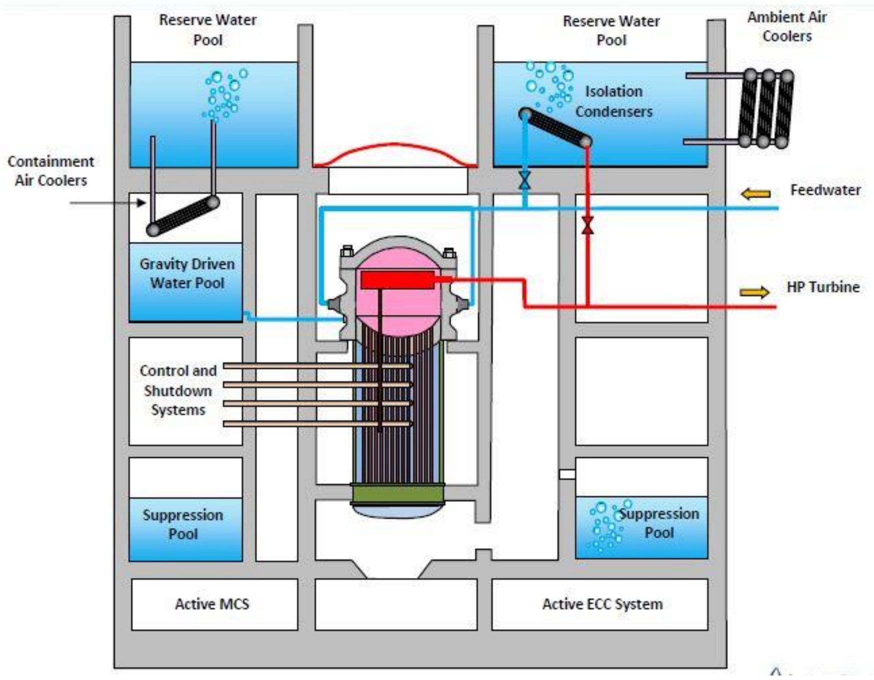

Figure 2-1Coolant-based safety systems in the Canadian SCWR [2]

The ICS is a passive heat removal system with its primary function to remove decay heat in the event of a Station Blackout (SBO). The ICS heat exchangers are located in the Reserve Water Pool above the reactor core and cool the primary side by natural circulation. The ICS is pressurized and on hot standby under normal operation. During a LOCA, sustained natural circulation in the heat transport system cannot be established due to the break, therefore the ICS and its inventory are not considered in this work.

The PMCS is an important part of the PT-SCWR design and is driven by both active (i.e. pumped) and passive (i.e. natural circulation) components under normal operating conditions and passively for post-accident emergency cooling. It serves as a diverse, redundant and separated safety system compared to the conventional safety systems discussed above. Under normal high-power conditions the active portion of the MCS removes approximately 95% of the moderator heat load while the passive components handle the remaining 5%. In the event of an accident, the passive components remain capable of removing 5%FP. It is a unique feature of the Canadian design that the PMCS is in operation continuously from full-power conditions through all accident phases without the need of actuation. During an emergency, decay heat flows through the channel insulation layer, through the pressure tube and is eventually deposited to the moderator. The hot moderator fluid surrounding the pressure tubes rises and eventually flashes into steam in the moderator riser pipes. This heat is subsequently exchanged with cold water in the Reserve Water Pool. In case of a SBO with coincidental loss of ICS, or a LOCA with loss of ECCS, while the active components of moderator cooling are lost, the flashing-driven natural circulation continues passively operation and is capable of removing decay heat [19]. The passive moderator heat removal system is designed to remove approximately 5% of the full power (FP) under normal operating and accident conditions, which guarantees that the decay heat can be removed effectively. In this study the PMCS is credited in all transients as the ultimate heat sink to the primary heat transport system.

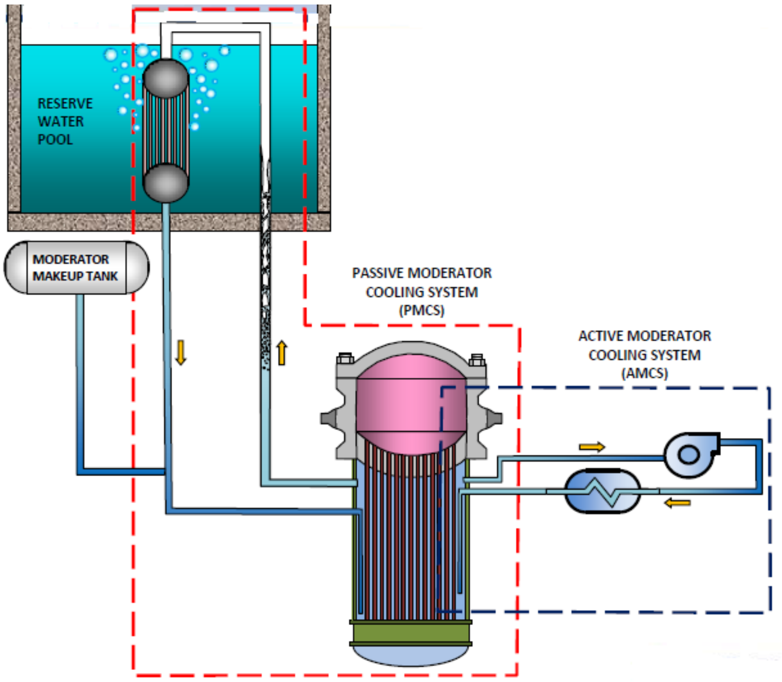

Figure 2-2 Passive and Active Moderator Cooling Systems

2.3.2 LOFA and LOCA/LOECC transients

Several LOFA and LOCA transient analyses have been performed using the most recent version of SCTRAN and CATHENA by researchers from XJTU and McMaster University. The transient responses of the Canadian SCWR to the postulated accidents were studied along with some sensitivity analyses.

Wu et al (2015) assessed the effectiveness of the heat transfer to the moderator via thermal radiation under a postulated LOCA with loss of ECCS transient using SCTRAN for the 64-element fuel design [26]. The 336 fuel channels were divided into 5 groups according to the channel power. A double-ended cold-leg break occurred at 0.5s and the reactor scram signal was initiated on low pressure (24MPa). A limitation of this work is that it did not include the effect of non-equilibrium voiding feedback on reactor power. The reactor shutdown and turbine stop valve closure occurred at the same time with a delay of 0.5s. The inlet coolant flow was assumed to continue for the first 10s and then linearly decrease to zero within 5s to simulate pump inertia. The MCST occurred on the inner ring fuel pins in the highest power channel group with a value of 1278℃, which is lower than the melting temperature of SS310 (1400℃). Sensitivity analysis on emissivity, outlet plenum size and convective heat transfer rate to moderator were performed and emissivity showed a significant impact on the MCST predictions.

Wu performed a LOFA transient for the Canadian SCWR based on a 2-channel-group model and a 4-channel-group model [19]. The CATHENA idealization including primary cooling system and moderator system were constructed and system responses to SBO scenarios were investigated with the simultaneous failures of the ICS and emergency power supplies. Radiation and convective heat transfer modes were present during the initial phase of the transient with a peak MCST of 1059℃. Natural circulation induced convective heat transfer became dominant in the intermediate phases of the transient. The development of natural circulation driven by the density difference between inlet and outlet plena was sensitive to the grouping scheme and the orifice sizes. In the later phases of the transients, a secondary MCST peak was predicted which resulted from the loss of inventory from the SRVs and the subsequent breakdown of natural circulation. Beyond this time radiation to the PMCS was capable of removing decay heat.

A CATHENA model of the Canadian SCWR including ICS and PMCS was studied for postulated SBO scenarios [25] in support of the design. It was concluded that the decay heat can be adequately removed by crediting both ICS and PMCS. In absence of ICS, the fuel elements can be cooled effectively by the PMCS only if backup power for the auxiliary Heat Transfer Pump and moderator pump failed 1 hour after the SBO. It is unclear from Reference [25] why radiation heat transfer to the moderator was insufficient to provide cooling within the first hour, when the literature above demonstrated adequate cooling.

The effect of neutron feedbacks was investigated using coupled thermalhydraulic and 3-D neutron kinetics responses by Hummel [7] showing that the multiple coolant regions in the HERCs give rise to different neutronic feedbacks as compared to traditional CANDU designs. The coolant density reactivity (denoted as void for consistency with previous CANDU literature) around the fuel was found to be positive, while the inner channel region voiding reactivity was negative, which resulted in a temporary positive power excursions in several postulated transients. The study also demonstrated that the reactor can shut itself down shortly after the break due to the strong negative reactivity feedback as the coolant densities further decrease. Hummel suggested that a fast acting shutdown system would mitigate the power-pulse phenomenon during the early phases of the transient. For the work in this thesis, a shutdown system with comparable speed and reactivity as a traditional CANDU is employed.

2.4 LOCA analysis conducted for other SCWR designs

As a design basic accident (DBA), LOCA is of particular importance as historically it has been one of the most limiting accidents. The LOCA consequences in an SCWR may be more significant than LWRs since the initial pressures are higher, coolant inventories in SCWR tend to be lower, and blowdown heat transfer coefficient may be lower for supercritical fluids compared to the subcritical counterparts. A large number of studies of the responses to postulated LOCA transients have been conducted by researchers for various GEN-IV SCWR concepts.

2.4.1 Japanese Super LWR

University of Tokyo has actively designed two pressure-vessel concepts of supercritical water reactors with either thermal or fast neutron spectrums, referred to as Super LWR and Super FR [27]. They both adopt the once-through steam cycle which eliminates the recirculation system, the steam separator and steam dryer from BWRs. Figure 2-3 shows the plant systems (including heat transport system and safety systems) of the high-temperature Super LWR. The active Auxiliary Feedwater System (AFS) and LPCI are designed to provide coolant supply to the core, while SRV/ADS relieve pressure and maintain forward coolant flow under postulated accidents. Coolant inventory in the upper dome and downward flowing water rods act as in-vessel core accumulators and supply coolant to the fuel containing region of the core during the early stages of the LOCA transients.

Ishiwatari performed hot- and cold-leg LOCAs with various break sizes (1-100%) [28]. For cold-leg breaks they claimed that the fuel heat-up in LBLOCAs (15-100%) was mitigated by the ADS actuation and the highest MCST prediction was 830℃. For smaller breaks (1-14%) in the cold-leg predictions showed higher MCST than large breaks because the ADS was not activated (i.e. the pressure remained higher than 24.0MPa, which was the ADS setpoint). The highest MCST occurred at the critical break (14%) with a value of 1000℃. The hot-leg break LOCAs were demonstrated to be less severe than cold-leg because they can induce forward flow through the core. The fuel temperature was not expected to increase as long as the LPCI provided continuous coolant in the latter stages of the accidents. It should be noted that these sheath temperature predictions were approximately 150 to 200 C less severe than the analysis available for the HPLWR (which has many similar characteristics), the Chinese SCWR, the US SCWR and the CATHENA/SCTRAN simulations for the Canadian design. The causes for this discrepancy are not apparent at this time.

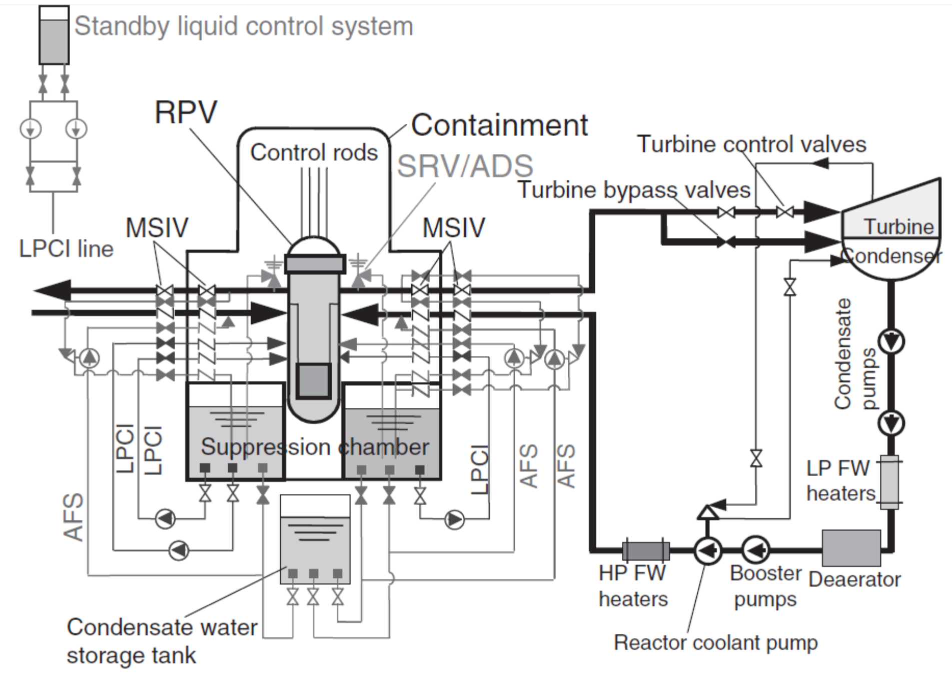

Figure 2-3 Plant systems of the Super LWR [28]

2.4.2 Chinese SCWR-M

Shanghai Jiao Tong University (SJTU) has proposed a mixed spectrum supercritical water reactor (SCWR-M) whose safety systems are derived from AP1000. The safety systems include two ICS, two accumulators (ACC), two Gravity Driven Coolant injection System (GDCS) and four-stage ADS (Figure 2-4). A check valve is incorporated immediately upstream of the inlet plenum to minimize the potential for reverse flow during some cold-leg break scenarios. The code ATHLET-SC was used for simulating three different break sizes in both the cold-leg and hot-leg of the SCWR-M [29].

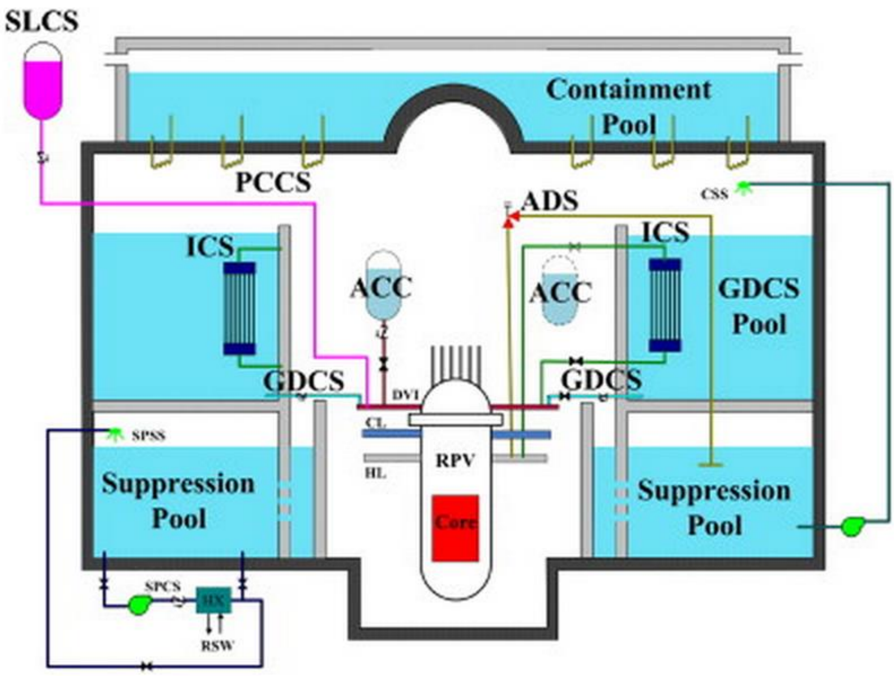

Figure 2-4 Outline of the SCWR-M safety system [29]

The peak cladding temperatures under all six cases were estimated to be lower than the safety criterion. It was found that the larger breaks were less challenging since they caused earlier initiation of ADS and the passive safety systems. The peak cladding temperature of 1200℃ occurred for smaller inlet break sizes and the author recommended future optimization of the safety systems and trip parameters.

2.4.3 US SCWR

The US SCWR design was modeled using RELAP5-3D for LOCAs located at cold-leg, hot-leg and steam line [22]. The feedwater tanks were designed to provide sufficient inertia to reduce the need for early plant intervention and mitigate several design basic accidents. The safety relief valves, main steam isolation valves, turbine stop valves and isolation condensers are also included in this model, shown in Figure 2-5. A best estimate point kinetics model was used for reactor power calculations. In the cold-leg break transient, the power decreased rapidly after the break due to the negative coolant void reactivity. The initial power/flow mismatch caused the fuel temperature to reach 1160℃. After this early peak, the flow reversal from the hot-leg pipes then provided significant cooling and the cladding temperature decreased temporarily. The MCST limit of 1205℃ was approached at 130s when the hot-leg piping inventory was depleted. This provides enough time for the emergency core cooling system intervention to mitigate the fuel temperature to an acceptable low value.

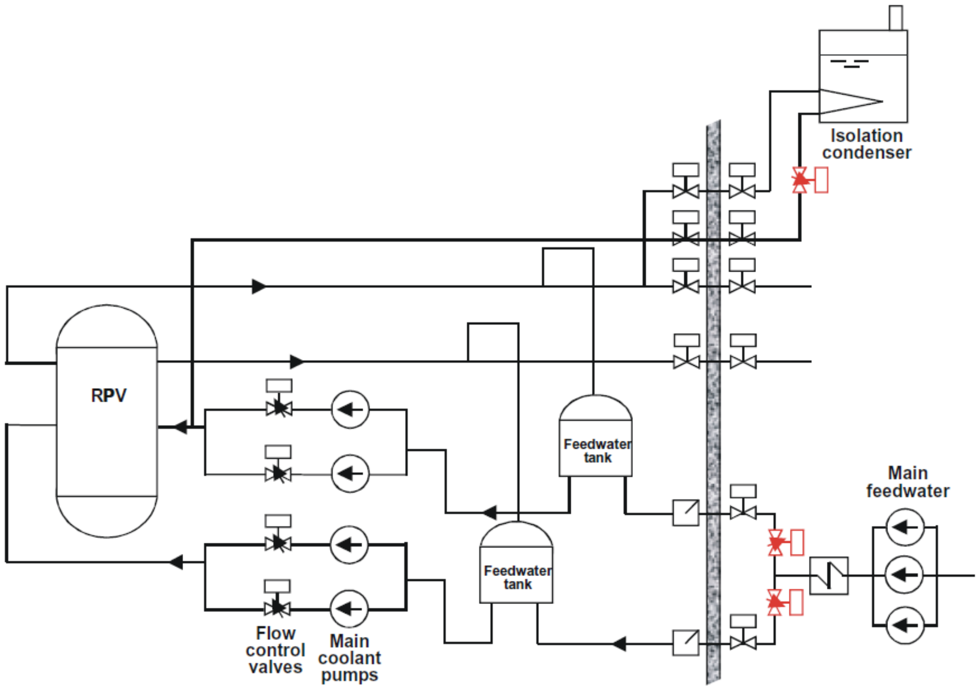

Figure 2-5 US SCWR reactor core cooling system [22]

2.5 Summary

This chapter reviewed the thermalhydraulic codes that have been modified for application in SCWRs. The safety criterion of limiting cladding temperature was selected for SCWR safety analysis due to the unique single-phase heat transfer characteristics. The safety systems designed for the Canadian SCWR were then introduced followed by a critical review of some LOFA and LOCA safety analyses. Results from previous studies have generally shown that cold-leg break LOCAs tend to be the most limiting transients with respect to MCST, and that the unique design of the Canadian SCWR (with temporary positive density feedbacks) would also be challenging. Most analyses of the various designs show two MCST peaks, and initial peak resulting from the power deposition and a later peak as inventory was depleted and cooling switched to alternate phenomena/systems (E.g., ECC in the US SCWR). The previous results have also shown that SBLOCAs tend to be limiting due to the reduction in blowdown cooling during these transients. This thesis focuses on the same break size range (5% to 100% break) as theses previous analyses and adopts similar acceptance criteria.

3. Theory

Similar to the other one-dimensional system codes such as TRACE, CATHENA and SCTRAN, the RELAP5 thermalhydraulic code is derived from the conservation of mass, momentum and energy. The equations are defined for each of the control volumes and solved in conjunction with the equations of state and various constitutive relationships. In this chapter, the basic conservation equations and some important constitutive equations in RELAP5 are presented. In addition to thermalhydraulics, RELAP5 performs point kinetics and decay heat calculations to assess neutron feedback effects and core power changes throughout a transient. The point kinetics and decay heat parameters for the SCWR are also briefly discussed in this chapter.

3.1 Conservation equations

RELAP5 uses a one-dimensional, non-equilibrium, non-homogenous two-fluid model for two phase flow below the critical pressure. Six primary dependent variables for each control volume, including pressure (P), phasic specific internal energies (U_f, U_g), vapor void fraction (α_g) and phasic velocities (v_g, v_f), are obtained by solving six conservation equations with respect to time (t) and distance (x) in the flow direction. The fundamental field equations for the two-fluid model contain two sets of phasic continuity equations, phasic momentum equations and phasic energy equations and are listed in Equation (3-1) to Equation (3-6)[30].

The phasic mass continuity equations are

$$\frac{\partial}{\partial t}\left(\alpha_g\rho_g\right)+\frac{1}{A}\frac{\partial}{\partial x}\left(\alpha_g\rho_g v_g A\right)=\Gamma_g \tag{3-1}$$

$$\frac{\partial}{\partial t}(\alpha_f\rho_f)+\frac{1}{A}\frac{\partial}{\partial x}(\alpha_f\rho_f v_f A)=\Gamma_f \tag{3-2}$$

where Γ_g and Γ_f are the vapor and liquid generation rates and satisfy $\Gamma_g=-\Gamma_f$ with no mass sources or sinks.

The momentum conservation equations:

$$\alpha_g\rho_g A\frac{\partial v_g}{\partial t}+\frac{1}{2}\alpha_g\rho_g A\frac{\partial {v_g}^2}{\partial x}=-\alpha_g A\frac{\partial P}{\partial x}+\alpha_g\rho_g B_x A-\left(\alpha_g\rho_g A\right)FWG\left(v_g\right)+\Gamma_g A\left(v_{gI}-v_g\right)-\left(\alpha_g\rho_g A\right)FIG\left(v_g-v_f\right)-C\alpha_g\alpha_f\rho_m A\left[\frac{\partial\left(v_g-v_f\right)}{\partial t}+v_f\frac{\partial v_g}{\partial x}-v_g\frac{\partial v_f}{\partial x}\right] \tag{3-3}$$

$$\alpha_f\rho_f A\frac{\partial v_f}{\partial t}+\frac{1}{2}\alpha_f\rho_f A\frac{\partial {v_f}^2}{\partial x}=-\alpha_f A\frac{\partial P}{\partial x}+\alpha_f\rho_f B_x A-(\alpha_f\rho_f A)FWF(v_f)+\Gamma_g A(v_{fI}-v_f)-(\alpha_f\rho_f A)FIF\left(v_f-v_g\right)-C\alpha_f\alpha_g\rho_m A\left[\frac{\partial\left(v_f-v_g\right)}{\partial t}+v_g\frac{\partial v_f}{\partial x}-v_f\frac{\partial v_g}{\partial x}\right] \tag{3-4}$$

The force terms in the right side of the above equations are, pressure gradient, the body forces (i.e. gravity or pump head), wall friction, momentum transfer due to interface mass transfer, interface frictional drag, and force due to virtual mass, respectively [30].

The phasic energy conservation equations are:

$$\frac{\partial}{\partial t}\left(\alpha_g\rho_g U_g\right)+\frac{1}{A}\frac{\partial}{\partial x}\left(\alpha_g\rho_g U_g v_g A\right)=-P\frac{\partial\alpha_g}{\partial t}-\frac{P}{A}\frac{\partial}{\partial x}\left(\alpha_g v_g A\right)+Q_{wg}+Q_{ig}+\Gamma_{ig}h_g^*+\Gamma_w h_g'+DISS_g \tag{3-5}$$

$$\frac{\partial}{\partial t}\left(\alpha_f \rho_f U_f\right) + \frac{1}{A}\frac{\partial}{\partial x}\left(\alpha_f \rho_f U_f v_f A\right) = -P\frac{\partial \alpha_f}{\partial t} - \frac{P}{A}\frac{\partial}{\partial x}\left(\alpha_f v_f A\right) + Q_{wf} + Q_{if} - \Gamma_{ig} h_f^* - \Gamma_w h_f' + DISS_f \tag{3-6}$$

where Q_{wg} and Q_{wf} are the phasic wall heat transfer rates per unit volume, Q_{ig} and Q_{if} are interface heat transfer terms, h_g^* and h_f^* are phasic enthalpies associated with bulk interface mass transfer, h_g' and h_f' are phasic enthalpies associated with wall interface mass transfer, $DISS_g$ and $DISS_f$ are phasic energy dissipation terms as a combined effects of wall friction and pump [30].

Water in the supercritical region is treated as single-phase liquid in MOD4, despite the large variation of thermo-physical properties near the pseudo-critical line. These properties are retrieved via linear or cubic interpolations from the property table derived from the NIST database for a temperature range of 273.16-5000 K and a pressure range of 611.57-100e6 Pa. Above the critical pressure the vapor void fraction is set to zero. Under normal operational conditions, the primary system of SCWR stays above the critical pressure thus the single-phase model (liquid) is utilized by solving one set of conservation equations as follow:

$$\frac{\partial \rho_f}{\partial t} + \frac{1}{A}\frac{\partial}{\partial x}(v_f A) = \Gamma_f \tag{3-7}$$

$$\rho_f A\frac{\partial v_f}{\partial t} + \frac{1}{2}\rho_f A\frac{\partial {v_f}^2}{\partial x} = -A\frac{\partial P}{\partial x} + \rho_f B_x A - (\rho_f A)FWF(v_f) \tag{3-8}$$

$$\frac{\partial}{\partial t}\left(\rho_f U_f\right) + \frac{1}{A}\frac{\partial}{\partial x}\left(\rho_f U_f v_f A\right) = -\frac{P}{A}\frac{\partial}{\partial x}\left(v_f A\right) + Q_{wf} + DISS_f \tag{3-9}$$

However, two specific challenges arise in using RELAP5 for trans-critical pressure simulations:

a) When a volume (node) transitions from super to subcritical pressure, over the course of a single time step, a volume may transition through the critical pressure and resultant fluid may either be i) subcooled liquid with void fraction 0; ii) superheated steam with void fraction 1.0, or iii) a saturation mixture with $0 < \alpha < 1$ (Figure 3-1). While a transition from supercritical to subcooled liquid is straight forward (since the void fraction remains at zero and all properties change continuously), transition into ii) or iii) is more challenging. For volume transitions from supercritical to superheated steam, the void fraction is set to 1.0, the subcritical vapour properties are set to the supercritical density, velocity and internal energy from the previous time step, while the liquid properties are set to the saturated liquid density, supercritical velocity and saturated liquid internal energy at the new pressure. In this way, the fluid properties transition continuously, albeit with a small lag since it essentially freezes the property change for the time step corresponding to supercritical pressure transitions[1] .

For volume transition from supercritical conditions to a two-phase mixture, the liquid and vapor densities are set to their respective saturated conditions, the vapor and liquid velocities are both set equal to the supercritical velocity from previous time step, and the

[1] In many ways this is analogous to the treatment of recursive heat transfer relationships which inherit the fluid properties from the previous time step

void fraction is determined based on a homogenous equilibrium formulation. The homogeneous mixture assumption during the time step immediately following transition seems qualitatively justified since the flow is likely well mixed during this brief period, however experimental evidence to this effect is not available at this time.

Following the logic above, RELAP5 then has the state properties and flow variables for the volume in transition. It is worth mentioning that RELAP5 allows the time step size to automatically reduce to such extent that the water property change at critical transition is numerically acceptable. After the transition time step the node's calculation will proceed normally using the RELAP5 two-fluid equations.

b) When a volume is already subcritical and its neighbors remain in the supercritical state. Under subcritical flow conditions, RELAP5 normally uses a volume junction arrangement where the properties at the junction of two volumes are inherited from the upstream volume according to an upwind-style difference scheme. At the junction between a supercritical volume and a subcritical volume, the standard RELAP5 logic is replaced such that the junction inherits the density and internal energy of the upstream node (at supercritical pressure), but the void fraction is inherited from the downstream node (which is subcritical and hence has an appropriate void fraction). This logic change is required to prevent the transport of zero void fraction values from the supercritical node to the downstream node which may already either be two-phase mixture or superheated steam.

While the above alterations to RELAP5 logic overcome a majority of the trans-critical issues, some numerical issues remain due to possible sudden changes in some state variables as a result of the transitions. In general the fluid properties are stored in a tabular binary form at discrete values of pressure and temperature (i.e. internal energy). Two dimensional interpolation (either cubic or linear) is used to determine the other state variables based on the nearest tabulated values. In addition to the absolute value of the fluid properties, RELAP5 stores the derivative of many properties with respect to pressure and internal energy. Given the large changes in properties over small changes in pressure and internal energy (near the critical pressure), their associated derivatives are very large and cause instability in the numerical routines. To overcome this, when assessing the derivative properties MOD4 ignores the tabulated values immediately adjacent to the critical point and uses linear interpolation of table entries on either side of the problematic (i.e. large) values. In this way the steep property gradients are smoothed and numerical issues are avoided. This smoothing of the very steep gradients only occurs in very few nodes in the simulations within a given time step and hence its impact on system transient is likely minimal. However no validation by experimental data is available at this time.

Given these changes a significant amount of code validation under these transitions is warranted. However, experimental data is not yet available for full code validation. In lieu of validation, these modifications have been tested in code-to-code comparisons with other system codes which utilize differing solutions to the above issues. These results are discussed in subsequent chapters.

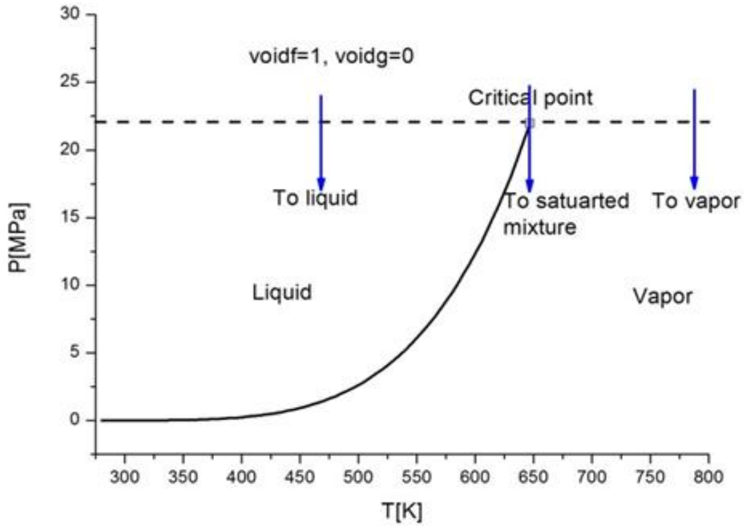

Figure 3-1 Trans-critical transition mechanisms in RELAP5/MOD4

Apart from the thermodynamic properties in the look-up table, the accuracy of fluid transport properties such as viscosity and thermal conductivity are of great importance in determining the Reynolds Number and Prandtl Number, which in turn have significant impact on the wall surface heat transfer coefficient. The author updated the viscosity and thermal conductivity formulations in the REALP5 source code based on the latest publication from IAPWS. The thermal conductivity modification is discussed below. Before modification, a constant thermal conductivity of 0.274148 W/m.K defined by the 1967 ASTM formulation was used for liquid above the critical temperature (647 K) at any given pressure, which is inaccurate. The most recently published IAPWS formulation 2011 (IF-2011) for ordinary water substance is incorporated in the source code to improve the thermal conductivity computation [31]. The pseudo-critical enhancement in conductivity is represented by an additive term in the IF-2011 formulation. Details about the correlating equation, necessary constants, range of validity and estimation of uncertainty can be found in Reference [31]. Figure 3-2 shows RELAP5 predictions of thermal conductivities at different temperatures before and after the author's modification. The NIST 23 database is the most recent water property database developed by the National Institute of Standards and Technology and therefore thermal conductivity predicted by NIST 23 is used as the reference value. The improvement in thermal conductivity accuracy results in a higher MCST prediction at the same coolant temperature (in range of 700K to 900K) profiles along the fuel channels compared to the RELAP5 version used previously. In this Canadian SCWR model, the steady-state MCST increases from 990.5K to 1060.4K after the modification.

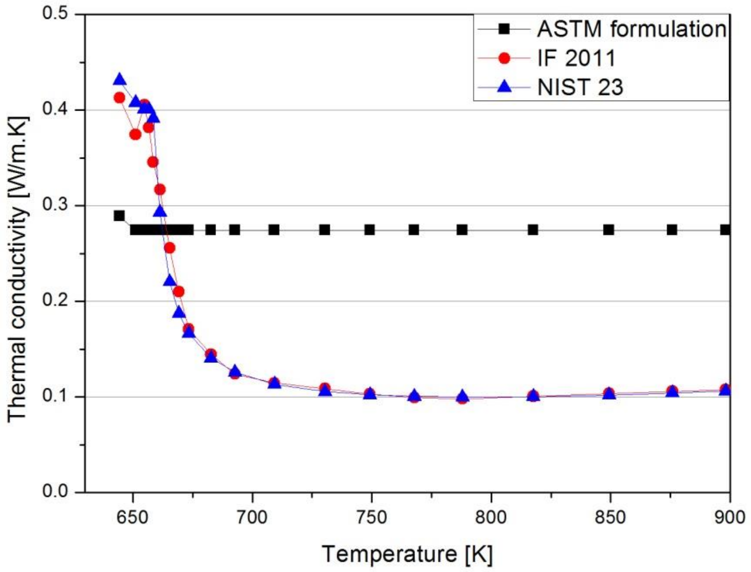

Figure 3-2 Thermal conductivities before and after the author's modification

3.2 Point kinetics model

RELAP5 provides users with two options to define the power generation in the reactor core, either specified in a power table or calculated from the point kinetics model depending on various reactivity feedbacks. A power table defines the total power in the reactor as a function of time. For instance, a constant power for steady-state or a decay heat curve after reactor shutdown can be defined using power tables. The point kinetics model on the other hand computes the reactor power using a space-independent reactivity feedback approximation, which assumes the fission power can be separated into space and time functions and where the spatial function is invariant in time. This model provides sufficient accuracy for cases in which the spatial power distribution remains nearly constant, and avoids complex spatial kinetics calculations (for example in [7]). The point kinetics model has been selected for this research to realistically simulate the power behavior during the LOCA transients, allowing for the strong coolant density effects on PT-SCWR neutronics. In order to examine the accuracy of the point kinetics model as compared to 3D-kinetics, a code-to-code benchmark is performed in Chapter 4.

The fundamental point kinetics equations are [30]

$$\frac{d}{dx}\varphi(t) = \frac{[\rho(t)-\beta]\varphi(t)}{\Lambda} + \sum_{i=1}^{N_d}\lambda_i C_i(t) + S \tag{3-10}$$

$$\frac{d}{dx}C_i(t) = \frac{\beta_i\varphi(t)}{\Lambda} - \lambda_i C_i(t) \quad i = 1,2,\dots,N_d \tag{3-11}$$

$$P_f(t) = E_f \Sigma_f \varphi(t) \tag{3-12}$$

where φ is the neutron flux, ρ is the reactivity, β_i is the delayed neutron fraction for group i which satisfies $\beta = \sum_{i=1}^{N_d} \beta_i$, Λ is the prompt neutron generation time, C_i is the number of delayed neutron precursor in group i, λ_i is the decay constant of delayed neutron precursor in group i, S is neutron source term, Σ_f is the macroscopic fission cross-section, E_f is the energy released per fission and P_f is the immediate fission power rate. The various kinetics parameters for the SCWR fuel are listed in Table 4-7 in Chapter 4.

There are two reactivity feedback mechanisms in RELAP5 [30]: a separable model and a tabular model. The separable model assumes that each feedback effect is independent of the other effects, while the tabular model generates the reactivity feedback based on a multi-dimensional look-up table which computes reactivity as a combination of several variables. The former is adopted in this study to provide direct consistency with the feedback tables generated in a separable lattice physics code.

The reactivity from the separable model is computed as:

$$\rho(t) = \rho_0 - \rho_B + \sum_{i=1}^{n_s} \rho_{si}(t) + \sum_{i=1}^{n_c} V_{ci} + \sum_{i=1}^{n_\rho} \left[W_{\rho i} \cdot P_d\big(d_i(t)\big) + a_{Wi} \cdot T_{Wi}(t)\right] +$$

$$\sum_{i=1}^{n_F} [W_{Fi} \cdot P_F\big(T_{Fi}(t)\big) + a_{Fi} \cdot T_{Fi}(t)] \tag{3-13}$$

ρ_0 is the user-defined steady-state reactivity at time zero (usually set as zero), ρ_B is the bias reactivity calculated during the input processing to ensure that the initial reactivity is equal to the input reactivity after including the feedback terms. ρ_{si} are reactivity contributions from n_s scram curves as a function of time. V_{ci} are reactivity contributions from n_c user-defined control variables. P_d is the reactivity feedback table as a function of water density d_i weighted by factor $W_{\rho i}$ for volume i. P_F is the reactivity feedback table as a function of fuel temperature T_{Fi} and W_{Fi} is the fuel temperature weighting factor for the i-th heat structure. a_{Wi} and a_{Fi} are the coolant density and fuel temperature reactivity coefficient, respectively [30]. The reactivity feedback tables were generated by the reactor physics code SCALE using the similar methodologies defined by Ahmad and Novog [32] and are provided in Table 4-8~4-10 in Chapter 4.

The coolant density from each region of the fuel channel in the Canadian SCWR has different reactivity feedback characteristics and thus need to be considered separately. The coolant density feedback in the fuel-region is input in the RELAP5 default density-reactivity table, while the coolant density feedback in center tube region is determined by a "control variable". This "control variable" defines the reactivity feedback as a polynomial function of the averaged density in the center tube of each channel. The weighting factors for coolant density and fuel temperature W_i are based on power-squared weighting as suggested in [32].

$$W_i = \frac{\mathrm{f_i}^2}{\sum_1^n \mathrm{f_i}^2} \tag{3-14}$$

where f_i is the power fraction in the i-th node.

In addition to the fission power, the power generation from radioactive decay of fission products and actinides is also included. RELAP5 has two built-in decay power models based on the ANS standard proposed either in 1973 or in 1979 for Decay Heat Power in Light Water Reactors [30]. The default ANS-73 model uses one isotope (U-235) as the fission source and 11 groups of fission products, whereas in the ANS-97 model, 23 groups of fission products for each of the three isotopes (U-235, U-238, Pu-239) are used for decay power calculation.

The Canadian SCWR utilizes a Thorium-Plutonium mixture fuel and the fission sources include U-233, Pu-239 and Pu-241. Thus the RELAP5 default decay heat curves are unsuitable. A specific decay heat curve for this Th-Pu fuel provided by Canadian National Laboratory (CNL) [33] is incorporated using a "power table" to describe the decay power in this work. This term and the fission power computed by the point kinetics model combine to determine the total thermal power.

3.3 Heat transfer

Thermal power generated in the fuel elements is transferred from the fuel pellet to the cladding through solid conduction and then to the coolant by forced convection. Under accident transients where the sheath temperature is elevated, radiation to the other channel components may provide a significant contribution to fuel cooling.

3.3.1 Conduction heat transfer

The heat equation in cylindrical coordinates is given as:

$$\rho c_p(r,T)\frac{\partial}{\partial t}T(r,t) = \nabla \cdot [k(r,t)\nabla T(r,t)] + q'''(r,t) \tag{3-15}$$

where $c_p(r,T)$ is the specific heat capacity, $k(r,T)$ is the thermal conductivity of the solid, $T(r,t)$ and $q'''(r,t)$ are the spatial and temporal temperature distribution and volumetric power density. RELAP5 solves the heat conduction equation for each heat structure (e.g. fuel element, pressure tube, center flow tube) at each time step based on the surrounding coolant conditions.

3.3.2 Convection heat transfer

The heat transfer from fuel cladding surface to the coolant is mainly convection and governed by Newton's Law as following:

$$q'' = -hA(T_{fuel} - T_{coolant}) \tag{3-16}$$

where q'' is the surface heat flux and has a relationship with the volumetric wall heat transfer rate in equation 3-9 as $q'' = \frac{r}{2}Q_{wf}$ (r is the fuel element radius). h is the heat transfer coefficient and A is the surface area.

Water at supercritical pressure is artificially regarded as single-phase liquid in RELAP5 and the widely applied Dittus-Boelter correlation for forced flow heat transfer is chosen to compute the heat transfer coefficient:

$$N_u = \frac{hL}{k} = 0.023Re^{0.8}Pr^{0.4} \tag{3-17}$$

where Reynolds number $R_e = \frac{vD}{\nu}$ and the Prandtl number $P_r = \frac{c_p\rho\nu}{k}$

At a given supercritical pressure, the water properties undergo large variation as a function of temperature (Figure 3-3 shows properties at typical SCWR operating pressure of 25 MPa). The density and dynamic viscosity decrease drastically near the pseudo-critical point. The thermal conductivity has a similar trend yet with a local maximum near pseudo-critical temperature. A sharp peak in the Prandtl number is also observed due to the large increase in specific heat near the pseudo-critical point.

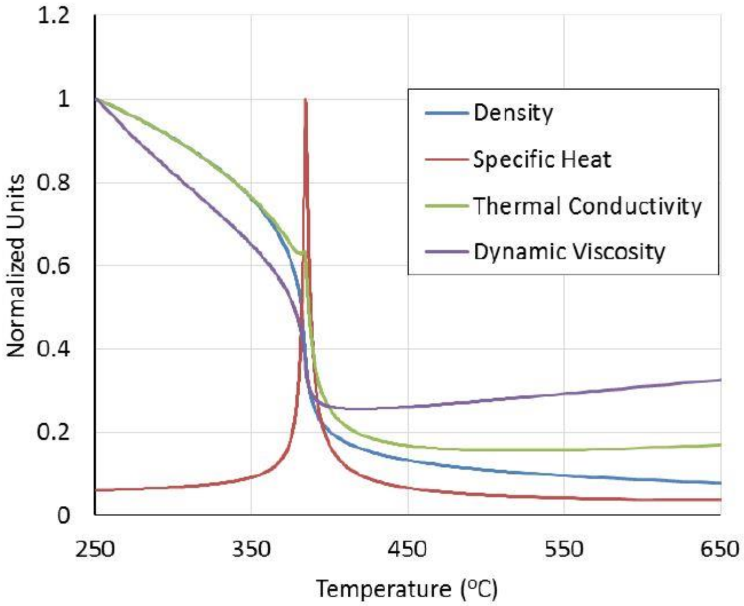

Figure 3-3 Normalized water properties at 25MPa [41]

The strong variation of water properties in the vicinity of the pseudo-critical line complicates the evaluation of the convective heat transfer coefficient. The heat transfer characteristics in supercritical water have been studied by various experiments and CFD simulations and many new empirical heat transfer correlations have been proposed for application in SCWRs and summarized in [5]. While it is generally agreed that the Dittus-Boelter correlation provides poor prediction of the convective heat transfer coefficient near pseudo-critical temperature, it does provide reasonably accurate predictions at temperatures either above or below this threshold (i.e. for nodes less/more than 5 K from the pseudo-critical temperatures the correlation appears to behave reasonable well). Given the temperature range of coolant in the channel spans 350 to 625 ℃, the inaccuracies near the pseudo-critical temperature likely occur in only a few nodes and hence system response is likely not affected. Furthermore, in all transients the peak MCST occurs at coolant temperature well above the pseudo-critical temperatures and hence the MCST is likely not highly sensitive to the Dittus-Boelter inaccuracies. Therefore, in the interim until the SCWR community develops a suitable bundle heat transfer correlation, the D-B correlation is adopted here.

3.3.3 Radiation heat transfer

Under normal and some transient conditions, heat generation by thermal power is removed predominately by conduction and convection. However in the unusual events when the reactor core flow and power are no longer matched, fuel temperatures tend to elevate and radiation heat transfer then provides an additional mechanism for decay heat removal. Stephen-Boltzmann's law describes the radiation emission rate over all wavelengths and in all directions from a surface per unit area, which is

$$E = \varepsilon\sigma {T_s}^4 \tag{3-18}$$

where ε is the user-defined emissivity, σ is the Stephen-Boltzmann constant which equals to 5.67E-8 $W/(m^2 \cdot K^4)$. The emissivity is in general not well characterized for stainless steel sheath under SCWR accident conditions, and is treated parametrically in this thesis.

RELAP5 incorporates a lumped-system method to calculate the rate of radiation exchange between grey diffuse surfaces contained in an enclosure. This method assumes that [30]:

- No radiant thermal energy is emitted or absorbed in the fluid within the enclosure;
- Temperature, reflectance, and radiosity are constant over each surface;
- The surface reflectance is independent of incident, reflected direction or radiation frequency

The radiosity from a surface is the total radiation leaving from a surface (i.e. the emitted energy and the reflected energy) and has the mathematical expression for the i-th surface as:

$$R_i = \varepsilon_i \sigma T_i^4 + \rho_i \sum_{j=1}^{n} R_j F_{ij} \tag{3-19}$$

The net radiation heat flux at surface "i" is the difference between radiosity at surface "i" and radiation reflected from the other surfaces, which is

$$Q_i = R_i - \sum_{j=1}^{n} R_j F_{ij} \tag{3-20}$$

The view factor F_{ij} is defined as the fraction of the radiation leaving surface "i" that is intercepted by surface "j". There are two constitutive relations defined for the view factors in an enclosure:

$$\sum_{i=1}^{n} \mathrm{F_{ij}} = 1 \tag{3-21}$$

$$\mathrm{A_i F_{ij}} = \mathrm{A_j F_{ji}} \tag{3-22}$$

In this study, the view factors are generated by an external program GEOFAC, which is developed by CNL at Chalk River. The view factor matrix is discussed specifically in the next chapter.

4. Modelling of Canadian SCWR using RELAP5

This chapter first describes the conceptual design of Canadian SCWR reactor coolant system including the inlet and outlet plenum, main feedwater line, vertical fuel channels and the steam line. Following the high-level descriptions the detailed RELAP5 models of main heat transport system are provided. The hydraulic components, heat structures, point kinetics model, radiation heat transfer model and system control models are described separately in the following subsections.

4.1 Canadian SCWR systems description

The Canadian SCWR proposed by CNL consists of 336 vertical fuel channels each housed by a pressure tube. It is cooled with supercritical light water passing through the channels and moderated with a separate low pressure and low temperature heavy water. The distributed pressure tube design is similar to current CANDU technologies with an innovative insulation layer in lieu of a separate annual gas and calandria tube [36]. Such arrangement ensures the pressure tube to be maintained at lower temperature (comparable to the moderator temperature) which allows for existing materials to be used in the higher pressure SCWR design. A unique thermal insulator is used between the pressure tube and coolant so as to prevent heat loss at normal operational condition but also provide a heat removal path under accidental circumstances. The use of pressure tubes avoids a single large pressure vessel in the reactor core thereby avoiding fabrication issues which may arise for larger vessels under such extreme conditions. Furthermore, and similar to CANDU, the use of a separate low pressure moderator allows for reactivity control devices to be operated under less extreme conditions, thereby avoiding the potential for fast control rod ejections which are possible in other SCWR designs.

An advanced fuel cycle of Plutonium and Thorium mixture is utilized in the Canadian SCWR to achieve the sustainability goals of the GIF. Enrichment of the fuel is targeted to optimize fuel cycle length and burnup. The following paragraphs present a detailed description of the heat transport system.

Reactor core

The schematic figure of the Canadian SCWR reactor core was shown in Figure 1-2 in Chapter 1. Four identical loops supply cold coolant to the inlet plenum while four hot-leg pipes deliver higher temperature fluid from the core through the Main Steam Isolation Valves (MSIVs) to the turbines. Coolant discharged from four feedwater pumps enters the inlet plenum via the feedwater lines at 25.8MPa and 350℃. Flow passes from the inlet plenum to each individual fuel channel via the channel inlet orifice and flows downward through the central flow tube. Once the coolant reaches the bottom of each channel, it is redirected upwards in the outer portion of the channel and through the fuel containing region taking away the thermal energy, where the coolant goes through pseudo-critical transition (384℃ at 25MPa). The hot coolant from the 336 channels gets uniformly mixed in the outlet plenum with a temperature of 625℃ at 25.0MPa and subsequently flows into the steam turbine through the main steam lines.

The mass flow rates in each channel are matched to the channel power via the inlet orifice similar to BWRs [34]. In this thesis the channel power distribution at the middle of cycle (MOC) from Hummel's quarter-core physics calculation has been used as the axial power profile thus the orifice sizes in this study are only for MOC [7].

Fuel channel

The SCWR fuel assembly design has evolved from the CANDU-type short bundle to a long fuel assembly and from the horizontal core to a vertical core layout in order to achieve the goals of high exit burnup, low negative coolant void reactivity, low linear power rate and low fuel cladding temperature through iterative reactor physics and thermalhydraulic calculations [35]. The most recent fuel assembly concept is the HERC.

Figure 4-1 shows a cross-sectional view of the HERC. It consists of a central down-flow orientated coolant path and an outer upward-flow orientated flow path through the fuel region. The stainless-steel central flow tube physically separates the coolant into two regions. Surrounding the outer flow path is the Zirconia insulator (Yitria-stablized Zirconia ceramic) with inner and outer liners which serves to isolate the pressure tube from the high temperature coolant. The liners are zirconium-modified stainless steel and are adopted to prevent mechanical failure of the insulator. The pressure tube is in direct contact with the low pressure and low temperature heavy water moderator and acts as the pressure boundary of the primary heat transport system.

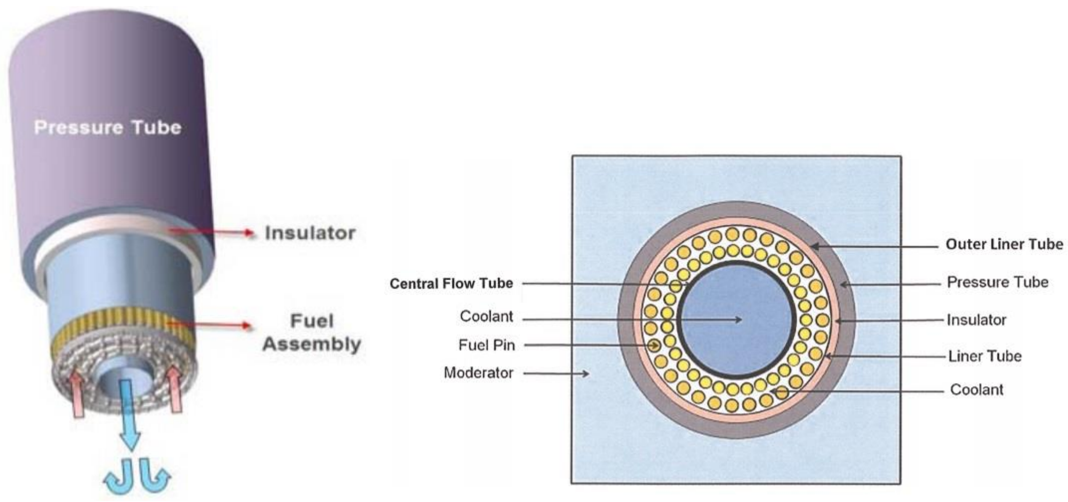

Figure 4-1 HERC fuel channel for the Canadian SCWR

The 64-element fuel assembly consists of two concentric rings, referred to as inner ring and outer ring, each containing 32 identical fuel pins. The fuel pins in the outer ring have a slightly bigger radius of 0.005m with a power fraction of 51.9% while the inner ring fuel pins have a radius of 0.00475m with a power fraction of 48.1% [7]. 13% weight of reactor grade Plutonium is mixed with Thoria and fabricated as ceramic fuel. While cladding materials have not been finalized, Stainless Steel 316S is used as an interim cladding material for the current fuel assembly design.

4.2 Modeling of the Canadian SCWR

In this study, the 336 fuel channels were assembled into two groups, that is, the highest power channel as the high power (HP) group and the remaining 335 channels as the average power (AP) group. HP group reveals the limiting parameters such as maximum cladding surface temperature (MCST) during the transient to obtain the safety margin. The AP group provides the general behavior of the fuel channels and primary heat transport system response.

The RELAP5 system model consists of 158 hydraulic volumes, 8 heat structures, a point kinetics model and several trips and valves which are intended to simulate the break and corresponding system responses. These components will be described separately in the subsequent paragraphs.

4.2.1 Hydraulic components

Boundary conditions

RELAP5 provides two ways to define the boundary conditions: i) using time dependent volumes (TDVs) ; ii) using time dependent junctions (TDJs). TDVs provide users options to set the boundary state condition of the fluid, such as pressure, temperature, phasic internal energy and static quality. TDJs are used to set the boundary flow conditions such as mass flow rate or phasic flow velocity. TDJs can control the flow rate/velocity as a function of time after certain signal is tripped by other state variables (e.g., trip signals generated when a parameter reaches a safety system setpoint).   .

To generate the initial steady-state for the HTS system, two TDVs at the inlet and outlet boundaries were used to specify the fluid states. Since the detailed pump selection for the SCWR design is unavailable at this time, a default Westinghouse pump model is included to draw coolant from the feedwater tank and provide the demanded coolant flow and pressure at the core inlet. To simulate the feedwater tank depletion and pump rundown during transients, the coolant mass flow rate is modeled with a TDJ and linearly decreased to 0 within 6s after a reactor scram.

The moderator system has a constant inlet flow rate and boundary conditions of 1800kg/s, 55℃ and 0.65MPa and with the outlet boundary temperature of 80℃ for the steady-state conditions. Under accident conditions the mass flow rate in the moderator system is reduced to 5% to simulate a loss of active moderator cooling.

Table 4-1 Boundary conditions for coolant and moderator systems

Parameter	**Coolant system**		**Moderator system**	
	Inlet	Outlet	Inlet	Outlet
Pressure[MPa]	24.8[2]	25.0	0.65	0.45
Temperature [K]	623	898	328	353
Mass flow rate [kg/s]	-(1281)	-	1800	-

[2] This pressure boundary is defined such that the pressure from the pump discharge side is 25.8MPa

Non-boundary hydraulic components

The coolant path was modeled volume by volume, starting from the feedwater storage tank and main feedwater pumps through the reactor core to the main streamline pipes, as shown in Figure 4-2. There are four identical cold-leg pipes with a 310mm inner diameter linking the feedwater tank and the inlet plenum, only one of which is assumed to break. Figure 4-2 shows the broken path (volume 304 to pipe 102) and the other three intact pipes were lumped together as an averaged flow path (volume 404 to pipe 202).

After the coolant from the broken and intact flow paths merge in the inlet plenum (volume 105), it flows down through the 5-metre long center flow tube inside the fuel channels (pipe 111 for the AP group and pipe 211 for the HP group) and reverses direction at the bottom. The 180-degree bend at the channel bottom was modeled by two identical volumes with opposite directions connecting the center flow tube and the outer fuel channel flow path with a forward flow resistance factor of 1.16 and reverse flow resistance factor of 1.36 consistent with Reference [7]. The coolant then passes through the outer channel region, referred as the fuel region or outer coolant volume (pipe 117 and 217), and absorbs the heat from the fuel elements before merging with flow from the other channels in the outlet plenum. The 5-meter active core region, including the center flow tube and the fuel region is divided into 20 nodes in this study. After the outlet plenum, the high temperature vapor-like coolant flows to the high pressure turbine through the main steam lines (pipe 129) before it is condensed and pumped back to the reactor core. The four main steam lines are simulated using a single pipe with equivalent hydraulic diameters, total area, total flow and length. The turbine and condenser are omitted in this study for simplification and the node immediately upstream of the turbine is used to specify the system model outlet boundary condition.

Prior to generating the steady-states, the orifice sizes were determined to match the flow to power in each channel. A servo valve with a controllable open fraction was used to model the orifice at the inlet of the center flow tube for each channel-group. The valve position is adjusted using a PI controller until the desired outlet temperatures are achieved in each channel group. Once the valve position is selected, it is then fixed for all subsequent transient simulations. The coolant temperature from each group (volume 125 and 225) were controlled by a *steamctl* control variable to be 625℃.

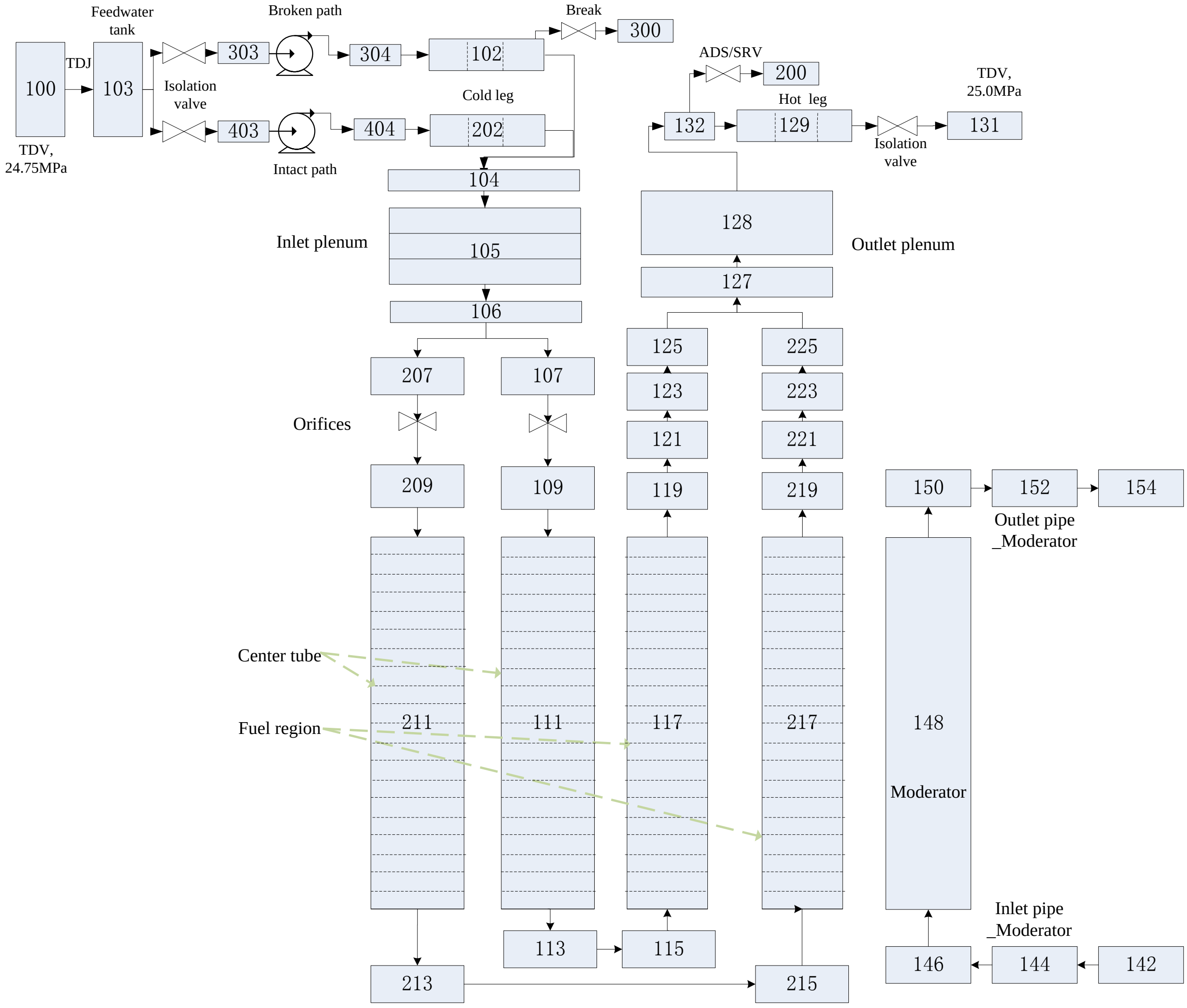

Figure 4-2 RELAP5 model of the Canadian SCWR

A servo valve (320) connecting the cold-leg pipe and a standard atmospheric volume (200) was to model the break. The user defined cross-section area is adjustable to model different break sizes along with the opening rates (break opening time was less than 0.1s for all breaks in this study). Two isolation valves (302 and 402, one for each channel group) on the cold-leg side and one isolation valve (130 for the lumped 4 steam lines) on the hot-leg side would isolate the reactor core once a certain trip was activated. A trip valve (201) connecting the hot-leg pipe and a standard atmospheric volume (300) was used to model the ADS/SRV safety systems in this design. The following table summarizes the parameters for each valve component.

Table 4-2 Parameters for valve component in the RELAP5 model

Valve number	**Valve type**	**From/to component**	**Flow area [m^2]**	**Open fraction**	**open/close trip**	**change rate[s^{-1}]**	**Initial position**	**Note**
302	mtrvlv	103/303	0.07548	1.0	501/502	0.2	1.0	Isolation
402	mtrvlv	103/403	0.22643	1.0	501/502	0.2	1.0	Isolation
320	mtrvlv	102/300	0.07548	1.0	505/501	6.17	0.0	Break
108	srvvlv	107/109	6.6476E-3	3.9371E-2	-	-	-	Orifice
208	srvvlv	207/109	2.22694	3.0202E-2	-	-	-	Orifice
201	trpvlv	132/200	0.03774	1.0	604	-	-	ADS/SRV
130	mtrvlv	129/131	0.58088	1.0	501/506	2.0	1.0	Isolation

The combined active and passive components of the moderator cooling systems were simplified to be an upward flow path from volume 142 to volume 154 as shown in Figure 4-2. Pipe 148 represents the moderator tank surrounding the pressure tubes and was divided into 20 nodes consistent with the active core region nodelization. This system acts as the hydraulic boundary for the heat structure modeling the pressure tube wall and is capable of removing approximately 3% to 5 %FP as per the BERC fuel channel specifications (3.6%FP was used in this study unless otherwise noted). The heat structures involved in this study are described in the following section. Post reactor SCRAM, the active components of the MCS are assumed to fail and only passive components remain operable. To simulate the reduction in moderator flow the time-dependent mass flow boundary conditions is ramped linearly from its 100% value to 5% within 5s. Sensitivity studies show that the MCST is relatively independent of the moderator flow rate.

4.2.2 Heat structures

Eight solid heat structures are used to represent:

a) the inner ring of fuel elements in AP group
b) the outer ring of fuel elements in AP group
c) the center flow tube separating coolant in central tube and the outer fuel region for the AP group
d) the pressure tube, insulator and liner tube solid conduction from the outer region coolant to the moderator for the AP group
e) Same as (a) (b) (c) (d) except for the HP group.

The heat structure dimensions and materials are listed in Table 4.3 and the specifications for each are described below.

Table 4-3 Dimensions and materials of heat structures

Structure	Inner radius[m]	Outer radius[m]	No. per channel	Material	Note
Center tube	0.046	0.047	1	SS	-

Inner fuel pins	0.000	0.00475	32	12%wt Pu	SS cladding thickness
Outer fuel pins	0.000	0.005	32	15%wt Pu	0.006m, fuel properties obtained from [7]
Inner liner	0.072	0.0725	1	SS	-
Insulator	0.0725	0.0780	1	YSZ	properties obtained from Ref [7]
Outer liner	0.0780	0.0785	1	SS	-
Pressure tube	0.0785	0.0905	1	Zirconia	properties used the internal Zircaloy

The 64 fuel pins in each channel are configured in two concentric rings equidistant between the inner liner tube and the central flow tube. The fuel rings were modeled separately with 48.1% of the channel power generated in the inner ring and 51.9% in the outer ring, respectively. In the axial direction, the 5-meter long fuel model is divided into 20 axial nodes consistent with the hydraulic discretization of the fuel channel. The axial channel power distribution varies from beginning of cycle (BOC), middle of cycle (MOC) and end of cycle (EOC). Consistent with Hummel [7], the power profile at MOC is selected in this study as representative of the equilibrium core and is shown in the Figure 4-3. The fuel pins in each ring were modeled as 32 identical cylinders coupled to the fuel region hydraulic volumes. The heat source was determined by the reactor point kinetics model which advances the total thermal power based on various reactivity feedback terms and is described in detail in Section 4.2.4.

The Canadian SCWR fuel concept utilizes a "collapsible" fuel sheath which eliminates the design of gas gap between the fuel and the cladding in the CANDU reactors and allows for direct contact with the fuel pellets. Therefore no gap was included in the fuel model and instead a 6mm-thick stainless steel cladding was assumed to be in direct contact with the fuel material. The effect of fission gas and potential sheath lift off during a LOCA are not considered in this work. The mixed Thorium and Plutonium fuel thermo-physical properties provided by CNL are listed in Table 4-4.

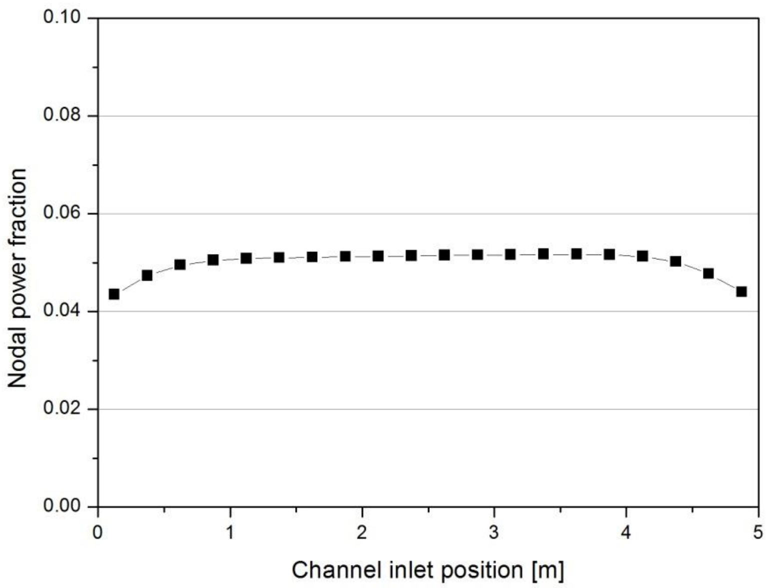

Figure 4-3 Axial power profile in the fuel elements at MOC [7]

Table 4-4 Canadian SCWR fuel thermal properties for inner and outer ring

<table>
<tr><th rowspan="2">Temperature [K]</th><th colspan="2">Inner ring</th><th colspan="2">Outer ring</th></tr>
<tr><th>Thermal conductivity</th><th>Volumetric heat capacity</th><th>Thermal conductivity</th><th>Volumetric heat capacity</th></tr>
</table>

	[W/m/K]	[J/m^3/K]	[W/m/K]	[J/m^3/K]
300.	3.8	2.18E+06	4.77	2.17E+06
400.	3.42	2.39E+06	4.20	2.38E+06
500.	3.11	2.51E+06	3.75	2.50E+06
600.	2.86	2.60E+06	3.39	2.59E+06
700.	2.64	2.66E+06	3.10	2.64E+06
800.	2.45	2.70E+06	2.85	2.69E+06
900.	2.29	2.72E+06	2.63	2.71E+06
1000.	2.15	2.74E+06	2.45	2.73E+06
1100.	2.02	2.75E+06	2.29	2.74E+06
1200.	1.91	2.75E+06	2.15	2.74E+06
1300.	1.81	2.75E+06	2.03	2.74E+06
1400.	1.72	2.75E+06	1.92	2.74E+06
1500.	1.64	2.75E+06	1.82	2.74E+06
1600.	1.57	2.76E+06	1.73	2.75E+06
1700.	1.5	2.76E+06	1.65	2.75E+06
1800.	1.44	2.78E+06	1.58	2.77E+06
1900.	1.38	2.79E+06	1.51	2.79E+06
2000.	1.33	2.82E+06	1.45	2.82E+06
2100.	1.28	2.86E+06	1.39	2.86E+06
2200.	1.23	2.91E+06	1.34	2.91E+06
2300.	1.19	2.98E+06	1.29	2.98E+06
2400.	1.15	3.06E+06	1.24	3.06E+06
2500.	1.11	3.15E+06	1.20	3.16E+06
2600.	1.08	3.26E+06	1.16	3.27E+06
2700.	1.05	3.40E+06	1.12	3.41E+06
2800.	1.01	3.55E+06	1.09	3.57E+06
2900.	0.99	3.73E+06	1.06	3.75E+06
3000.	0.96	3.93E+06	1.03	3.96E+06

The center flow tube wall was modeled by a 20-node hollow cylinder with no heat source, separating the hydraulic volumes of center flow tube and fuel region. The RELAP5 model is consistent with the most recent conceptual design and removes the insulation layer within the central flow tube. In this model the RELAP5 internal properties for stainless steel were used for center flow tube wall.

The pressure tube heat structure consists of four material regions including the inner liner tube, the insulation layer, the outer liner and the pressure tube. The Yttria-Stabilized Zirconia (YSZ) insulator is to prevent heat loss at normal condition but provide a heat transfer path under accidental condition for decay heat removal to the moderator system. This structure is quite different from the traditional CANDU fuel channel design, where the pressure tube is insulated by a gas gap from the calandria tube. The YSZ thermal properties used in this study are listed shown in Table 4-5 [7].

Table 4-5 Canadian SCWR fuel thermal properties for YSZ insulator

Temperature [K]	Thermal conductivity [W/m/K]	Volumetric heat capacity [J/m^3/K]
323.	2.51	2.7497E+06
373.	2.52	2.8991E+06
423.	2.47	3.0545E+06
473.	2.39	3.1783E+06
523.	2.31	3.2834E+06
573.	2.22	3.3458E+06
623.	2.15	3.4292E+06

673.	2.09	3.5075E+06
723.	2.03	3.5493E+06
773.	1.99	3.5649E+06
823.	1.96	3.5828E+06
873.	1.93	3.6379E+06
923.	1.91	3.6738E+06
973.	1.90	3.7045E+06
1023.	1.90	3.7208E+06
1073.	1.92	3.7659E+06
1123.	1.94	3.7630E+06
1173.	1.97	3.8086E+06
1223.	2.00	3.8377E+06
1273.	2.06	3.8632E+06

4.2.3 Trip, control variable and general table

"Trip", "control variable" and "general table" are three types of control models used in RELAP5 as control systems within the model. Such control can be continuous (i.e. control of liquid level in a PWR pressurizer) with or without feedback terms, or it can be in the form of a discrete action (for example opening the SRV when the simulated set pressure exceeds a pre-specified value). "Trip" inputs in RELAP are self-explanatory and often used to actuate hydraulic components such as valves and pumps. "Control variable" allows generic control of certain user-defined variables as a function of other variables via operators such as SUM, MULT, DIV, DIFFRENI, and etc. "General table" defines a one-dimensional look up table which defines certain functional relationships between a simulated variable and a desired quantity which is a function of that variable. For instance, the thermal properties for heat structures are input as general tables as functions of the heat structure temperatures.

Trips

RELAP5 provides two types of "trips" for the transient simulations, i.e. "variable trips" and "logical trips". A "variable trip" becomes true if the relationship between a variable and a predefined limit is met. The relationship may be EQ, NE, GT, LT or LE, where the symbols have the standard FORTRAN meaning. A "logical trip" defines a logical relationship between two variable trips using operator AND, OR or XOR. All trips used in this model are listed in Table 4-6 and explained in the following paragraph.

Table 4-6 Trips in the RELAP5 model

Trip number	Condition of true	Application component	Action
501	Time < 305s	valve 302/402/130	open
		valve 320	close
502	Time>timeof (605)+0.55s	valve 302/402	close
505	Time>=305s	valve 320	open(break)
506	Time >timeof (605)+0.6s	valve 130	close
507	Time >timeof (605)+0.55s	scram curve	insertion
		pump 301/401	power detach
510	Pressure of 105<2.4E7 Pa	-	-
511	Mass flow rate of 126<1152.7kg/s	-	-
605	510 or 511	either scram signal detected	
503	Pressure of 132>2.6E7 Pa	This group of trips are designed for the	

504	Pressure of 132>2.525E7 Pa	relief valves:
602	-604 and 503	
603	604 and 504	valve 201 open when pressure>2.6E7 Pa
604	602 or 603	and close when pressure<2.525E7 Pa

For instance, the cold-leg break modeled by valve 320 remains closed for the first 305s and opens at 305s to simulate the sudden break (305s is used to ensure that an adequate steady-state has been established prior to initiating the transient). Trip 510 and 511 are the two reactor trip signals representing steam flow rates smaller than 90% of nominal value (a low-flow trip) or the inlet plenum pressure lower than 24 MPa (a low-pressure trip). Trip 605 is initiated when either trip 510 or 511 is true. Trip 502 (core isolation) and 507 (reactor scram and pump trip) become true with a delay of 0.55s after detection of 612 to account for instrumentation response time to the signal, while trip 506 (turbine trip) has a delay of 0.6s to account for actuation time of the turbine trip.

The trips 503, 504, 602, 603 and 604 are used as a logical group to open the relief valve 201 when the hot-leg pipe pressure is greater than 26.0 MPa and to close it when the pressure drops to 25.25 MPa. The setpoints are consistent with reference [19]. The SRV control logic is explained in detail in Appendix A.

Control variables

A *steamctl* control variable was used to adjust the orifice size so as to regulate individual channel flow in pre-simulations to ensure a uniform coolant temperature of 625℃at the channel exit. This component works similar to a Proportional-Integrated (PI) controller [37]. The difference between channel exiting node temperature and the target value is sent back to recalculate the orifice size (i.e. valve opening fraction). A new flow rate distribution and temperature profile are then determined by the current orifice sizes. This procedure is repeated until the target temperature is reached. It is worth noting that this control component operates only to determine the initial steady-state flow orifice sizes. Once the orifice sizes are obtained, these control components become constant for the rest of transient simulation.

In this study, another important application of the control variable model is to compute the reactivity feedback from center tube coolant density as reactivity contribution to the point kinetics model. The power-squared weighted average density in the center tube region is calculated using a SUM operation and considering that the average channel group represents the vast majority of the channels (i.e. the power-squared weighted average is also weighted according to the number of channels represented by each channel group in the core). The average density is then used as an independent variable to calculate the corresponding reactivity feedback through a fifth-order polynomial function (Section 4.2.4).

General tables

RELAP5 allows for limited look up tables defining functional relationships such as thermal conductivity/heat capacity/density/heat transfer coefficient versus temperature, power/heat flux/heat transfer coefficient/temperature versus time and normalized area versus normalized valve-stem position. For instance, the general table is used to define the reactivity insertion rate as a function of time corresponding to shut off rod insertion speed once a SCRAM signal is detected (a equivalent -11$ reactivity is introduced within 3s) [22].

4.2.4 Point kinetics model

The point kinetics model updates the reactor thermal power based on the various reactivity feedbacks and provides a total thermal power of 2540MW for steady-state. The typical six delayed neutron group is used here and the kinetics data from Reference [7] is used in this study and summarized in Table 4-7. The mean neutron generation time for MOC is determined to be 2.22E-4 seconds consistent with [7].

Table 4-7 Delayed neutron data for the point kinetics model

Group #	Yield fraction (β_i)	Decay constant(λ_i) [s^{-1}]
1	$7.180* 10^{-5}$	0.0117727
2	$7.410* 10^{-4}$	0.0277209
3	$5.467* 10^{-4}$	0.1151299
4	$1.002* 10^{-3}$	0.2993739
5	$3.615* 10^{-4}$	1.0469525
6	$9.070* 10^{-5}$	2.5418856

For this thermal spectrum reactor, reactivity feedbacks from coolant density and fuel temperature are of great importance and considered as the main reactivity contributions in this point kinetics model. The separated coolant flow pathways are significantly different from the unidirectional flow configuration in a CANDU fuel channel. Figure 4-4 shows that the reactivity induced from a decrease in coolant density is negative under equilibrium conditions (i.e. when both the coolant in the inner flow tube and outer flow tube void uniformly). However, there may be transients wherein a significant, albeit short duration, difference of void appears between these regions. This differential voiding effect was examined extensively by Hummel and Novog [37] and their study showed that the reactivity feedback effects of coolant density in the inner and outer channel regions need to be considered separately. This is in contrast to the work of Shen [42] which applied a uniform reactivity feedback assuming a constant coolant density across the assembly.

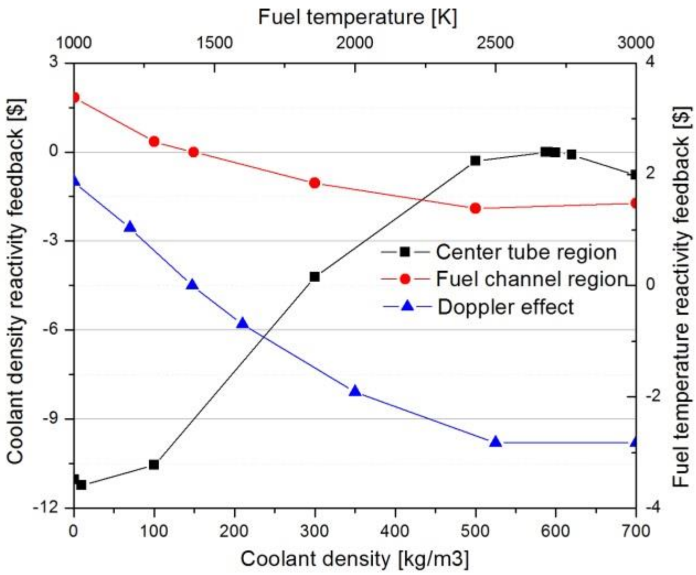

Figure 4-4 Coolant density and fuel temperature reactivity feedback for SCWR

A separated reactivity feedback mechanism was adopted for the point kinetics model to update the thermal power during the transient. The flux-squared weighted reactivity feedback in outer fuel channel region was modeled as the default "coolant density feedback table" in the RELAP5 kinetics model. The fuel temperature feedback was also modeled using the standard RELAP5 "Doppler feedback table". An additional reactivity feedback determined by a control variable is used to simulate the center tube region coolant density effect and is explained in the following paragraph. Table 4-8 to Table 4-10 list the three reactivity feedback terms generated with SCALE for MOC consistent with the models in Reference [7].

Based on the density-reactivity data in Table 4-9, a fifth order polynomial function was fitted to describe the relationship between center tube coolant density and the reactivity feedback:

$$\rho = -11.04076 - 0.0189973 * \bar{d} + 3.073 * 10^{-4} * \bar{d}^2 - 7.67453 * 10^{-7} * \bar{d}^3 + 7.84992 * 10^{-10} * \bar{d}^4 - 3.10933 * 10^{-13} * \bar{d}^5 \quad (4.1)$$

where $\bar{d}$ is the flux-squared weighted density and ρ is the corresponding reactivity feedback.

The RELAP5 kinetics model updates the total power in each time step as a result of the individual reactivity contribution from the center tube and fuel region coolant densities as well as the fuel temperature.

Table 4-8 Coolant density feedback in center tube region

Density [kg/m3]	Reactivity [mk]	Reactivity feedback [mk]
700	109.6920	-2.3125
620	111.7151	-0.2895
600	111.9318	-0.0727
590	111.9939	-0.0106
587.56	112.0045	0.0000
500	111.1158	-0.8887
300	99.5270	-12.4775
100	80.6818	-31.3227
10	78.6785	-33.3260
1	79.2501	-32.7544

Table 4-9 Coolant density feedback in fuel region

Density [kg/m3]	Reactivity [mk]	Reactivity feedback [mk]
700	106.8862	-5.1183
500	106.3699	-5.6346
300	108.9093	-3.0953
149.33	112.0045	0.0000
100	113.0408	1.0363
1	117.4565	5.4520

Table 4-10 Fuel temperature reactivity feedback

Temperature [K]	Reactivity [mk]	Reactivity feedback [mk]
1000	120.0180	5.5256
1200	117.5584	3.0660
1420.62	114.4924	0.0000
1600	112.4318	-2.0606
2000	108.8148	-5.6776

2500	106.0999	-8.3925
3000	106.0990	-8.3934

As stated in Section 3.2, the built-in decay heat curves in RELAP5 are not suitable for the Canadian SCWR. Thus a decay heat curve provided by CNL [33] for Th-Pu fuel was incorporated using a "power table" to describe the decay power. The decay power combines with fission power computed by the point kinetics model to determine the total thermal power.

4.2.5 Radiation heat transfer model

Radiation heat transfer becomes significant when the fuel sheath temperature exceeds approximately 800 to 900℃ during postulated accident transients. Therefore it is essential to include radiation heat exchange in the enclosure consisting of the center flow tube wall, inner fuel ring, outer fuel ring and insulated pressure tube. In RELAP5 the radiation heat exchange in the axial direction is omitted and only that amongst the solid surfaces at the same axial level is calculated. Each heat structure consists of 20 axial nodes thus 20 enclosure sets are defined for each channel group.

As discussed in Section 3.3, the following parameters are important in radiation heat transfer calculations: the solid surface temperatures, the emissivity and the view factor matrix. The surface temperatures are calculated internally by solving a series of spatial conduction and convection equations within the code. The emissivity is a function of solid material and surface treatment. It is input by the user and assumed to be 0.8 for all the surfaces. A sensitivity analysis of the fuel emissivity is performed in Section 5.3. The view factors matrix for each surface has been calculated by an external computer program GEOFAC version 1.0.2. This GEOFAC code is specially designed for CATHENA radiation heat transfer model by CNL for calculation of the view factor matrix. The view factor matrix generated by GEOFAC is then used in RELAP5 for the radiation heat transfer calculation (Figure 4-6).

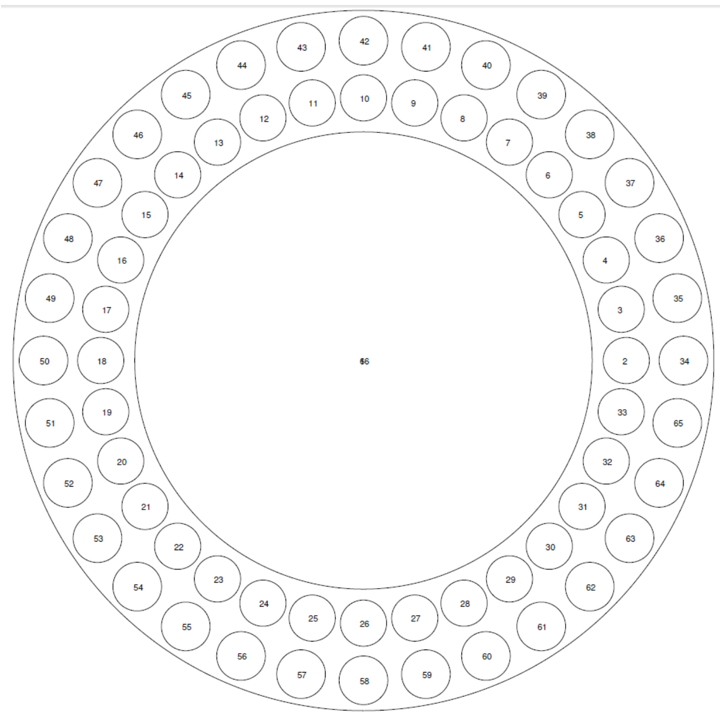

Figure 4-5 View factor matrix of the radiation heat transfer enclosure

4.3 Code-to-code benchmark

RELAP5 has been widely used to simulate transients and accidents in LWRs with subcritical coolant and has been validated by a large number of experimental data. Its mature capacity of modeling nuclear power plants is accepted throughout the nuclear industries and academic institutes. The RELAP5/MOD4 has incorporated water properties extended to supercritical region and special techniques were created by code developers from Innovative Software System (ISS), LLC for application in SCWRs. As part of this research, a benchmark test was performed to demonstrate the acceptability of RELAP5/MOD4 via a code-to-code comparison with CATHENA.

CATHENA is a two-fluid one-dimensional thermalhydraulic code developed by CNL in Chalk River. It has been frequently utilized for preliminary thermalhydraulic simulation and safety analysis of SCWR in the conceptual design stage. Although the current version of CATHENA is unable of model the system behavior during the trans-critical process as stated in [19], it has been employed for thermalhydraulic simulations above the critical pressure.

To confirm the simulation capability of RELAP5/MOD4, the CATHENA model from reference [7] was replicated, i.e. the RELAP5 model discussed above is modified by removing the pumps and storage tank components, and defining the inlet boundary conditions as 25.8MPa and 350℃ consistent with [7], as illustrated in Figure 4-6. While neither code has specific validation in the region, the significant differences in theoretical framework in the codes and independence in their development means that code-to-code comparisons are useful as a consistency check (but not their accuracy since validation is still not available under SCWR conditions). Furthermore, the CATHENA simulations were performed using a 3-dimensional coupled neutronic solver (DONJON with cross sections computed by

DRAGON) while RELAP5 uses point kinetics with reactivities determined from the SCALE physics code package. Hence in all aspects the CATHENA and RELAP5 results are independent.

In this benchmark, the inlet pressure decreased exponentially from 25.8 MPa to 23.0 MPa within 5 seconds while the outlet boundary pressure remained at 25.0MPa through the transient, shown as the black lines in the top plot of Figure 4-7.

The model ran for 300s before the transient initiation and the steady-state parameters obtained from the two codes are listed in Table 4-11. The referenced values in the last column are the neutronic/thermalhydraulic coupling results from [7] at MOC. It is noted that the steady-state results from RELAP5 are fairly close to the reference values, which indicates a good performance of the RELAP5 model for SCWR steady-state conditions.

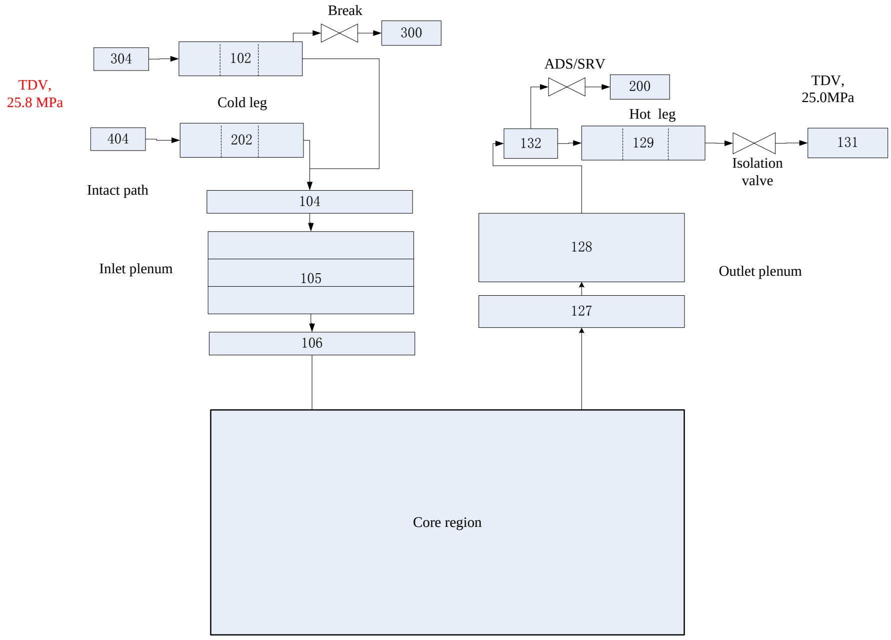

Figure 4-5 RELAP5 model for the LOCA-like transient replicating the CATHENA model in [7]

Table 4-11 Steady-state calculation results compared between RELAP and CATHENA

Parameter	RELAP5/MOD4	CATHENA	Reference value
Power [MW]	2542.0	2539	2540
Core flow [kg/s]	1280.0	1265.0	1272.0
MCST [K]	1058.3	1037.6	1052.0
MCT [K]	2635.2	2596.4	-

Figure 4-7 and Figure 4-8 show the predictions during the LOCA-like transient by CATHENA and RELAP5. The reactor core flow reduced as the the inlet pressure decreased and became reversed shortly after the transient initiation. The reverse channel flow drived high-temperature low-density coolant in the outlet plenum through the outer fuel channel, center tube and eventually reached the inlet plenum. Also during this period the coolant density in fuel region and center tube reigon decreased unevenly. This non-equilibrium density decrease in the two regions introduced a temporary positive reactivity in the first 2 seconds which in turn initiated the power excursion up to 163%FP. This power peak value agrees well with the 160%FP predicted by coupled DONJON/CATHENA simulation in [7].

After the short postive-reactivity period, further coolant density decrease in the two regions combined to cause a large negative reactivity insertion thus the power dropped rapidly to decay heat levels. This confirms the overall negative CVR effect in the Canadian SCWR and demonstrates the reactor's ability of self-shuttdown with no shutdown systems involvement. The MCST increased as a result of early-stage high power pulse and degraded heat transfer condition caused by high-temperature coolant due to reverse channel flow. When the heat convected to the hot coolant exceeded the decay heat generation (occurred at around 4s) the cladding temperature started to decrease. The maximum centerline temperature presents the same trends in both codes.

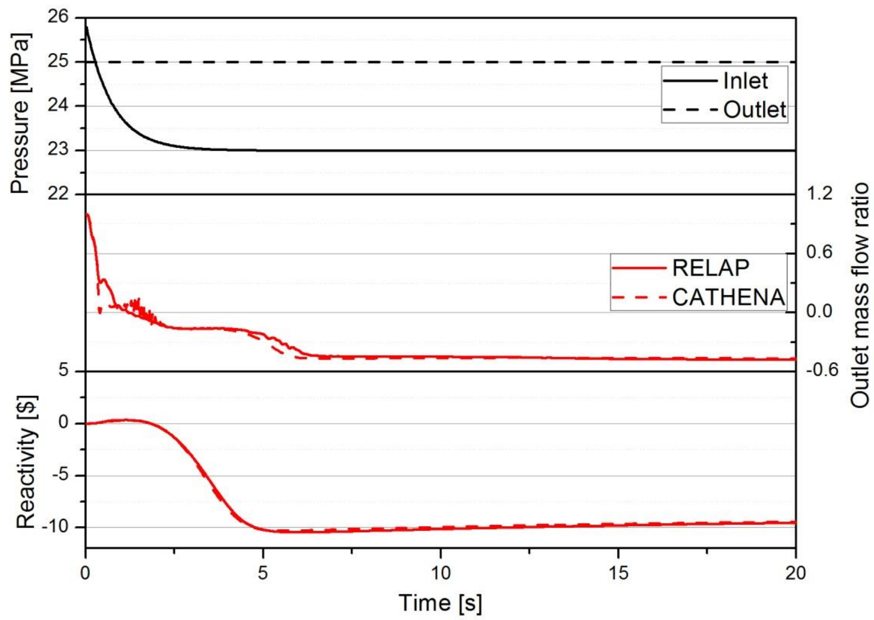

Figure 4-6 Pressure boundary conditions, core-flow ration and reactivity feedback for LOCA-like transient modeled by RELAP and CATHENA

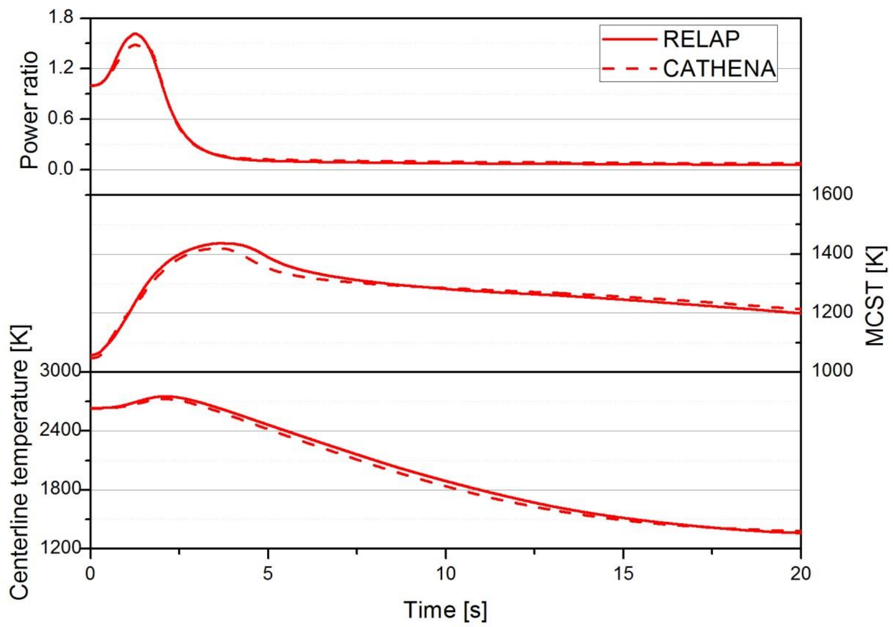

Figure 4-7 Thermal power, MCST and maximum centerline temperature during the LOCA-like transient by RELAP and CATHENA

To summarize, the simulation results for both steady-state and the LOCA-like transient from RELAP5/MOD4 model agree quite well with the fully coupled CATHENA/DONJON simulations for this benchmark.

4.4 Summary

This chapter provides the detailed Canadian SCWR system description, including the primary cooling system from feedwater tank to the main steamline, the specification of the reactor core and HERCs. The chapter continued with a detailed procedure of establishing the RELAP5 model for the Canadian SCWR, which consists of hydraulic components, heat structures, radiation heat transfer models and a point kinetcs model. A code-to-code benchmark was then performed with CATHENA. The test results of RELAP5 agreed well with CATHENA for both steady-state and the LOCA-like transient, which enhances the confidence in using RELAP5 for this study.

5. Results and discussions

The simulation results based upon the 2-group PT-SCWR model are discussed in this chapter, including the steady-state conditions and the cold-leg pipe break LOCA transients. The typical large break (100%) LOCA transient simulation was split into four phases for discussion purpose so that the phenomena and sensitivities in each phase can be addressed. The effectiveness of core-cooling is examined by simulations with a hypothetical failure of ADS and LPCI. The PMCS was assumed to operate effectively for all the simulations performed in this study. Under the worst possible condition when the large LOCA is combined with a loss of ADS and coolant injection, the predicted MCST still has a considerable safety margin relative to the safety criteria discussed in Chapter 2.

A 5% cold-leg break transient representing a SBLOCA is also investigated given that other SCWR conceptual design analyses have shown SBLOCA to be more limiting than larger breaks. At this break size, the reactor stays above the ADS setpoint for a long period of time, thus the ADS and the coolant injection are excluded from the transient. Consistent with other designs in literature, the simulation results suggest that the SBLOCA is more hazardous in terms of MCST, especially in the early stage of transient, though it is still well below the safety criteria.

Given the above analyses, a parametric study was performed to examine the MCST as a function of break sizes and sensitivity assumptions on emissivity, ADS actuation time and SDS timing. In general, the maximum sized small break (i.e. 15%) LOCA is most limiting and while for the reference analysis assumption the MCST was acceptable, some of the cases with degraded emissivity or SDS actions showed unacceptable results.

5.1 Steady-state simulation results

As stated in Section 4.2 the 336 fuel channels were divided into HP channel group and AP channel group. Due to batch refueling and fuel depletion, the channel power and axial power distributions change from day to day. Typically the power profiles and other thermo-physical parameters at BOC, MOC and EOC are studied as representative states for the core level simulations. This study focuses on the MOC power distribution, consistent with Hummel [7].

The maximum channel power at MOC is determined to be 9.62MW by the coupled neutronic/ thermalhydraulic simulations in Reference [7]. The key steady-state parameters are listed in Table 5-1. The HP channel group has a higher mass flow (i.e. it is flow-power matched) than the AP channel group. The orifice sizes for the channel groups are computed according to the group power such that the outlet coolant temperatures are 625℃.

In Table 5-1 one can see that the steady-state MCST in the outer ring fuel elements is slightly higher than that of the inner ring, while the maximum centerline temperature occurs in the inner ring. This can be explained by the differences in geometry and power distribution in the two rings. The power fraction in the inner ring is assumed to be 48.1% and the rest (51.9%) in the outer ring [7]. The fuel element radii are 0.00475 m and 0.005 m, for the inner and outer rings, respectively. At steady-state, the heat flux per unit area on the inner ring cladding surface is smaller than that of the outer ring, which results in a smaller cladding temperature with the same heat transfer coefficient and coolant temperature. The higher centerline-cladding temperature difference is on the other hand caused by a higher volumetric power density. As discussed in Section 4.3, the steady-state simulation results agree well with that of CATHENA, providing an ideal initial condition for the transient simulation.

Table 5-1 Steady-state parameters for the 2-group modeling

Group	Power [MW]	Power fraction	Mass flow rate [kg/s]	Orifice size [%]	MCST [K] (inner/outer)	MCT [K] (inner/outer)
HP	9.62	0.0037874	4.8532	3.937051	1058.0/1060.4	2634.3/2594.7
AP	7.55*335	0.9962126	3.8093*335	3.020228	1051.6/1053.8	2186.6/2151.2
Total	2542.8	1.0	1281	-	-	-

Figure 5-1 and Figure 5-2 show the axial distribution of coolant temperature and density in both the center tube region and the outer fuel region. There is a small temperature rise and a slight density decrease in the center tube region coolant, which is caused by thermal leakage from the hot coolant in the fuel region being conducted through the center tube wall. The coolant temperature in the fuel region increases gradually from 643K at the entrance node to 673K at the 9-th node, while the density decreases vastly from 540 kg/m^3 to 167 kg/m^3. The pseudo-critical transition occurs at approximately 657 K (25MPa) in node 5 in both channel groups. The large coolant specific heat in the pseudo-critical region and non-uniform axial heat flux cause the temperature increase to change non-linearly with elevation.

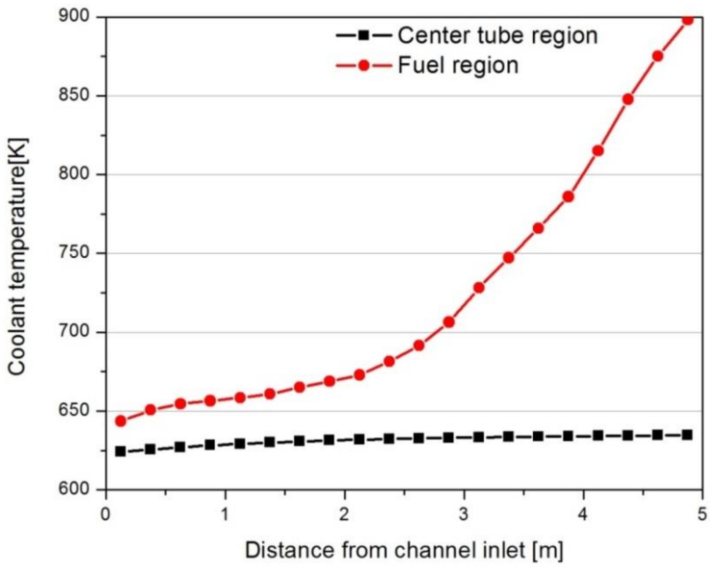

Figure 5-1 Steady-state coolant temperatures in two regions of HP group

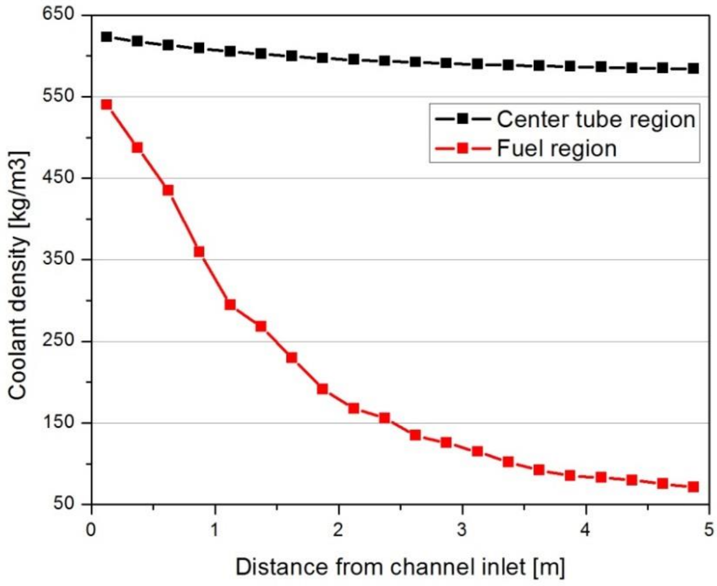

Figure 5-2 Steady-state coolant densities in two regions of HP group

Figure 5-3 and 5-4 show the steady-state cladding surface and centerline temperature distributions along the fuel channel in the two fuel rings of HP group. The temperature variation in the AP group has the same trend yet with constantly lower values. The cladding temperature decreases slightly near the pseudo-critical point indicating the enhanced heat transfer caused by the strong variation of thermodynamic properties. As discussed earlier, this heat transfer coefficient enhancement is likely caused by the sharp peak of Prandtl number in the Dittus-Boelter correlation. The inclusion of a properly validated heat transfer correlation for supercritical water is recommended for future improvement of the RELAP5 code to predict more accurate cladding temperatures in this region. After the short period of reduction, the cladding temperature increases monotonically and approaches the maximum value at the channel exit. The centerline temperature stays constantly higher in the inner ring than the outer ring due to the higher power density and the maximum value appeared at the 18-th node in both fuel rings.

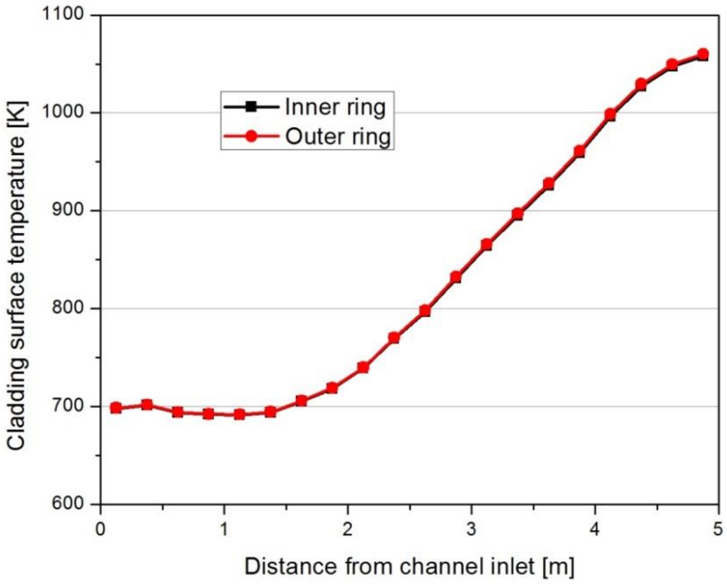

Figure 5-3 Steady-state cladding temperatures in two fuel rings of HP group

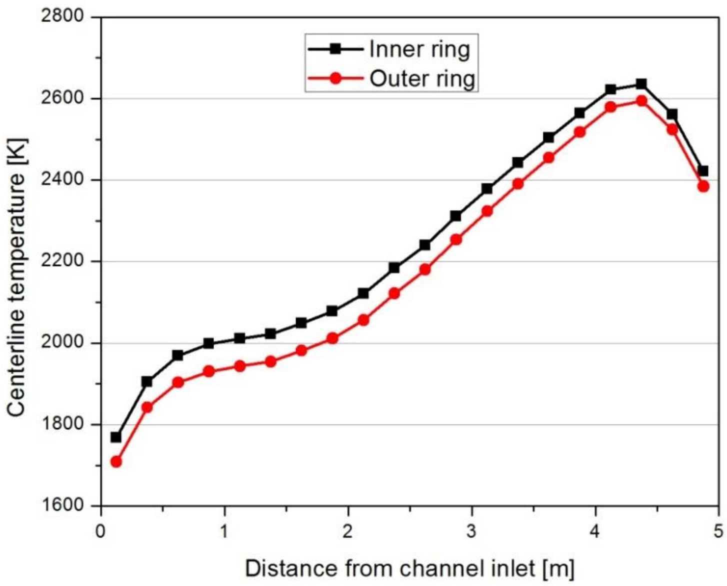

Figure 5-4 Steady-state centerline temperatures in two fuel rings of HP group

5.2 100% break LOCA transient with/without passive safety systems

The LOCA transients initiated by a break in the cold-leg piping are studied below. The basic requirement to ensure that the reactor safety criterion are met (i.e. MCST), is to maintain the core flow and reduce reactor power. This is achieved by:

- maintaining the coolant supply from cold-leg pipe to the greatest extent practicable. While the SCWR design includes feedwater pumps with high inertia (via large flywheels) and check valves to prevent reverse coolant flow from the cold-leg out of reactor core, for example, in breaks in downstream of the check valve reverse flow is possible. Hence alternative systems such as ADS may be used to ensure continuous flow from the inlet to outlet plena during the initial break phases.
- maintaining the steam outflow from the hot-leg pipe. In response to a LOCA, the system is designed to close the MSIVs and open the ADS system, thereby maintain a flow path on the hot-leg to the suppression pool, and avoid steam transport outside the containment.
- triggering fast acting SDS to terminate high-power operation in a timely manner. Due to non-uniform voiding effects, some LOCAs may result in power excursions caused by the positive feedback resulting from the voiding of the outer flow path in the fuel channel. Therefore the SCWR design includes safety systems of comparable speed (both in detection, actuation and reactivity depth) as current CANDU designs.

Prior to each LOCA, a "null-change" transient is simulated for a sufficient period of time such that an adequate steady-state is maintained. Once the break is initiated, the event sequence is as follows:

1. Main heat transport system is depressurized and most of the core coolant is discharged rapidly from the break, resulting in reverse flow in the fuel channels;
2. The low steam flow (90% of the steady-state value) signal and/or a low pressure (24.0MPa) signal are detected early in the transient initiating the shutdown system which

rapidly insert negative reactivity of approximately 11 dollars with a delay of 0.55 s [22];

3. The feedwater pumps are tripped coincident with the SDS trip signals and the reactor core inlet isolation valves close within 5s of the trip signal;
4. Following the signal for inlet isolation, the main steam isolation valve (or turbine isolation valve) close with an additional delay of 0.05s;
5. The feedwater tank was assumed to linearly drain out within 6s after the pump trip;
6. The ADS is assumed to operate at the detection of low pressure signal (24MPa) with a delay of 2.0s;
7. Low-pressure coolant injection (LPCI) system starts to deliver cold coolant into the core as the pressure drops to 3MPa with a total reservoir mass of 10,000kg. The coolant injection will stop once inventory is depleted. Subsequently injection will be maintained by either the active pumped system from the containment sumps of the GFCIS as described previously (note, the simulation of PCCS and GFCIS are not within the scope of this work);
8. Lacking core-injection, the coolant in the fuel channel is boiled off during the later phase of the transient and decay heat is primarily removed by radiation heat transfer to the liner tube and eventually deposited into the moderator cooling system.

5.2.1 LOCA transient with ADS and coolant injection

A 100% cold-leg break (i.e. a break with a cross-sectional area of a main feedwater pipe, 0.07548m^2) LOCA transient simulation is discussed below. As shown in Table 5-2, the break occurred at 5.0s and the low coolant flow signal was registered 0.09 s later, initiating the reactor trip and the main coolant pump trip at 5.645 s (with a 0.55s delay). The low pressure signal occurred slightly later at 6.45s. Then the main steam isolation valve closed at 5.695 s while the coolant flow from the feedwater storage tank decreased linearly and flow stopped at 11.645 s. The ADS initiated 2s after the detection of a low pressure (24MPa) signal at 8.45 s. The LPCI was initiated at 18.53 s when the system pressure drops below 3MPa and continued until 106.94 s when the total make-up inventory of 10,000kg was depleted. The simulation continued for 500s after the break. This transient scenario represents the reference case, or Case 1 for against the ones in the subsequent section. "Case 1" column in Table 5-2 denotes the transient sequence for this reference case.

Table 5-2 Transient sequences for the 100% break LOCA cases

Event sequence	Case 1	Case 2	Case 3
Break occurrence	5.00	5.00	5.00
Reactor trip signal/low flow	5.09	5.09	5.09
Reactor trip	5.645	5.645	5.645
Main coolant pump trip	5.645	5.645	5.645
Main steam isolation	5.695	5.695	5.695
ADS activation	8.45	8.45	-
LPCI initiation	18.53	-	-
LPCI drain out	106.94	-	-
Feedwater tank drain out	11.645	11.645	11.645

Figure 5-5 shows the normalized power ratio and the integrated mass outflow for the reference case. The green line is the accumulated mass lost from the break. It increases immediately after the break and then its rate of increase slows as the pressure difference between the circuit and containment decreases. Beyond about 120s the core inventory is depleted such that the break discharge is no longer significant. The red line shows the normalized power ratio during this transient. It is noticeable that the short-period power excursion at early stage due to temporary positive reactivity is caused by the uneven coolant density decreases in the center tube region and the outer fuel region.

During the LOCA transient, the mass flow rate in the fuel containing region of the fuel channels is important as it provides convective cooling of the fuel. In particular in the early phases of the transient, convective cooling is essential since the power levels are high, while later phases of the transient convective cooling requirements are reduced since the heat loads become smaller. Therefore the transient is divided into the following phases based on the important phenomena: 1) initial MCST excursion phase; 2) blowdown cooling phase; 3) interim heat-up phase; 4) sustained cooling phase. During Phase 1 the LOCA initiates a short-termed power excursion due to non-equilibrium voiding in the channel which is terminated by the action of the shutdown system and negative reactivity feedback due to further density decrease. Flow during this period quickly reverse due to large inlet break. ADS actuation acts to re-establish forward flow during this phase but the combination of energy deposition and degraded fuel cooling conditions causes the temperature to increase. Phase 2 begins after the first MCST peak. In Phase 2 the blowdown cooling provided by combined flow from the ADS and the LPCI actuation is sufficient to cool the fuel at smaller power level. Phase 3 begins after the coolant inventory is depleted and degraded heat transfer under near stagnation flows causes the MCST to increase. Heat rejection during this phase is primarily via radiation heat transfer from the fuel to the PT assembly and ultimately to the PMCS. Phase 4 begins when the heat removal exceeds the decay heat and the MCST begins to decrease. Phase 4 cooling can be achieved either by core-injection, gravity-fed systems, or by radiation heat transfer to the PMCS. The mode of heat transfer in Phase 4 is dependent on the availability of safety systems and will influence the timing and magnitude of the secondary peak in MCST.

Figure 5-7 indicates that the early MCST peak occurs at the 18^{th} heat structure nod (i.e. close to the fuel channel exit). Thus the mass flow rate in the corresponding hydraulic volume is regarded as a representative channel flow rate for the following discussions. Figure 5-6 illustrates the mass flow rate per channel in both HP and AP groups. A strong reverse flow was induced immediately after the break. The flow rate in HP channel group was greater than that of AP channel group due to the larger orifice size since the channels are flow-power matched at steady-state, resulting in a relatively smaller flow resistance to the reverse flow. The blue line in Figure 5-6 illustrates the discharge flow through the ADS valve once it was activated. Additional HTS inventory is lost via the ADS discharge, which accelerates the system depressurization process and allows for earlier core-injection or gravity-fed systems. The coolant injection is modeled by a TDV defined as a constant pressure of 3MPa and is capable to provide a total mass of 10,000kg (the actual setpoints and total injection volume could be optimized to reduce the MCST during the later phases, but this optimization is beyond the scope of this work). The pink line indicates that the coolant injection lasted for approximately 100 seconds and provides additional coolant flow in the fuel channel to prolong the convection-dominated heat transfer regime for a certain period of time as shown in Figure 5-7 by the MCST variation.

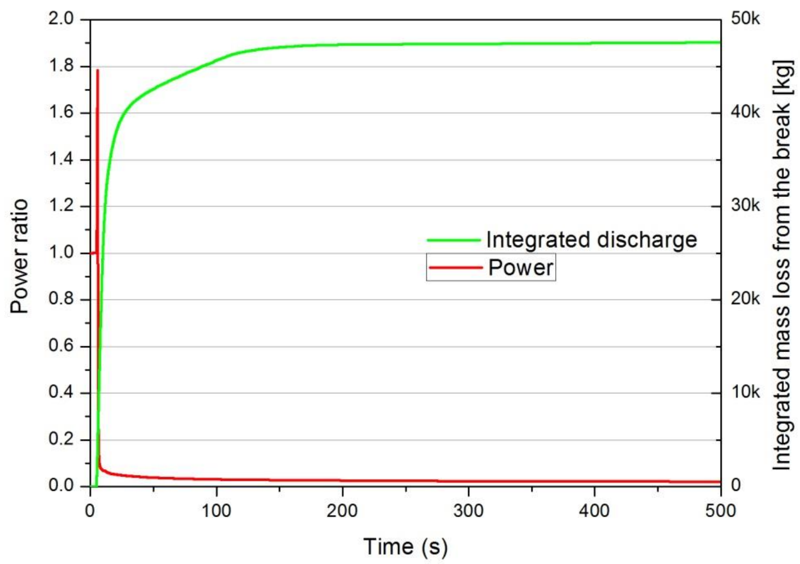

Figure 5-5 Normalized thermal power and the integrated mass loss during 100% break LOCA in the reference case

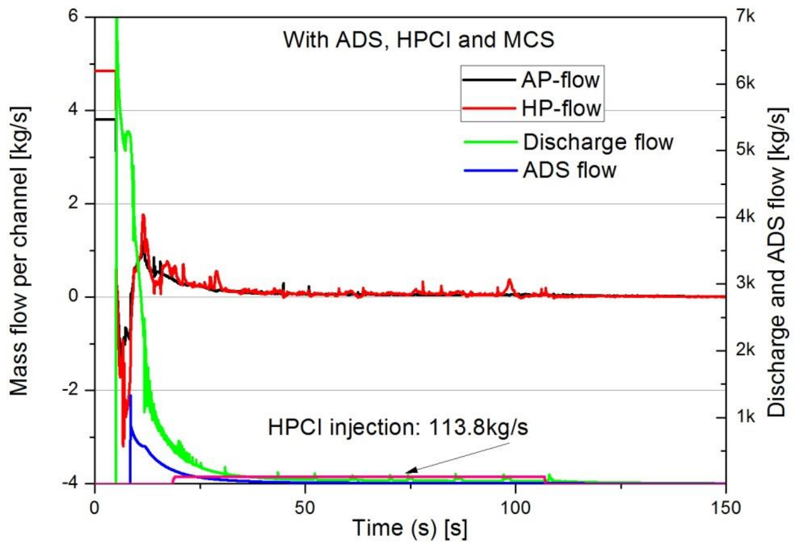

Figure 5-6 Discharge from break and ADS, LPCI injection and channel flow at 4.125m during the 100%break LOCA in the reference case

The MCST value and location varies (Figure 5-7). Initially it is located at the position consistent with that under normal operating conditions. This is typical for designs where the power profile along the channel is not very peaked. As the accident progressed and location moves upstream to the location of maximum power in the channel, indicating radiation heat transfer (which dependent only on surface temperature and is independent of coolant conditions along the channel) is making larger contribution to heat transfer.

Figure 5-7 also indicates that the outer ring MCST is slightly higher than that of the inner ring in the first 50s as the fuel elements were still surrounded by certain amount of coolant and convection dominated the heat transfer, similar to the steady-state temperature profile. While in the later phases of the transient the inner ring cladding temperatures are more limiting since radiation heat exchange with the cooler liner tube was limited as compared to the outer fuel ring. The highest MCST, 1315 K, appeared at 15.9 s at the 4.5-meter node in the outer ring, which is 218K lower than the safety criteria for stainless-steel cladding. As a result of the ADS and coolant-injection system actuation, the secondary peak MCST at the end of Phase 3 is not as severe as that of the first peak. To focus on the transient phenomena, each of the four phases is analyzed in detail below.

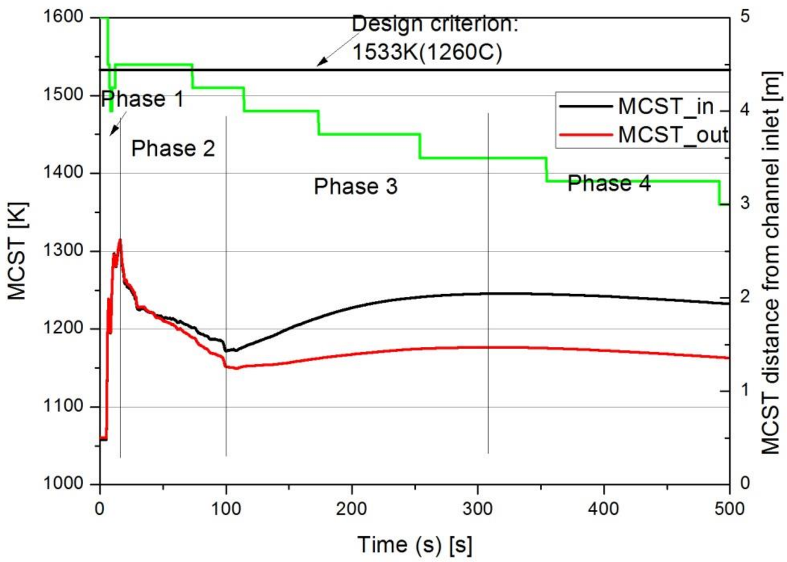

Figure 5-7 Maximum cladding surface temperature and position in HP group during 100% break LOCA in the reference case

<u>Phase 1(5-16s)</u>

As discussed previously, the reactivity feedback from multiple region coolant densities can be temporarily positive during a cold-leg LOCA due to the non-uniform density changes at a given cross section. This was reported in Hummel's [7] LOCA-like transient results (Section 4.3). A similar power pulse was observed in the first few seconds of the 100% break LOCA transient shown in Figure 5-8. To be specific, the early flow reversal moved low density coolant from the outlet plena towards the bottom of the fuel channel, thereby decreasing the coolant density in the outer channel region while the center tube region coolant was less affected. The net effect is a positive reactivity feedback until such time as reversing flow carries low density coolant to the center flow tube. Once the center flow tube density decreases, a large negative reactivity sufficient to shut down the reactor is generated. The increase in fuel temperatures during this phase also provides negative reactivity feedback. As a result, the thermal power increases to 178% FP over the first second of the transient before the further coolant density decrease introducing a negative reactivity and driving the core power to decay heat levels. Compared to Section 4.3, the power excursion observed in this transient has a higher peak and lasts for a shorter period of time, which is caused by the faster depressurization in this LOCA case. Note also, fast acting shutdown systems are included to further limit the initial power excursion.

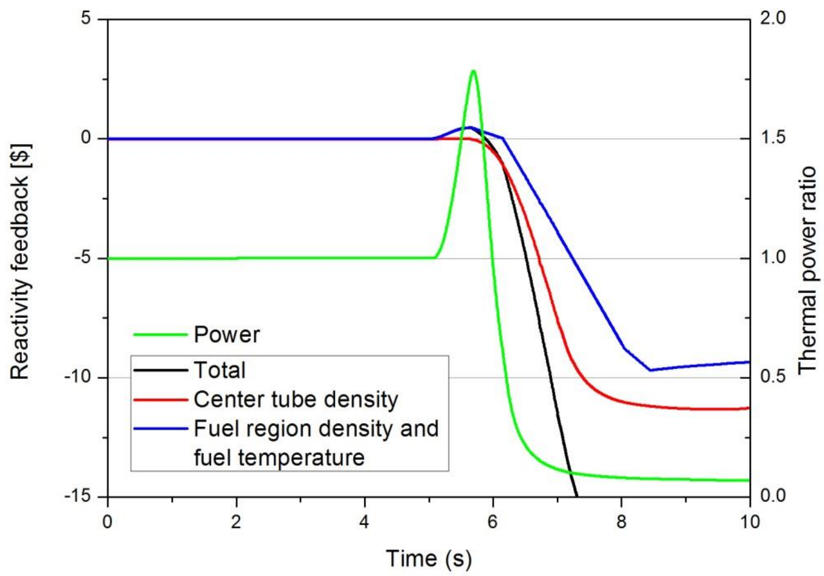

Figure 5-8 Reactivity feedback and thermal power variation in the initial stage of 100% break LOCA in the reference case

Figure 5-9 shows the system inlet and outlet pressure and the average channel flow in each group in Phase 1. The cold-leg break caused a sudden systematic drop in the inlet plenum pressure which propagates to the outlet plenum over a short period of time. During this period of time, the resultant pressure differences quickly initiated reverse flow in all channels, resulting in hot coolant flow from the outlet plenum being transported into the fuel region. As stated, this causes not only a brief positive reactivity insertion, but also the higher temperature coolant acting to increase the MCST. The outlet plenum depressurization was accelerated once the ADS valve opened, as shown by the blue line in Figure 5-9. Meanwhile, ADS overcame the reverse pressure gradient and restored flow to the forward direction. The brief near stagnation at the flow direction transition point may exacerbate the surface temperatures temporarily.

Despite the fact that the reactor was tripped early in Phase 1, the relatively high decay power in combination with the energy deposition during the power pulse exceeded the heat removal capability of the channel flow. The integration of impaired cooling condition and high energy deposition led to fuel temperature increase in Phase 1 as shown in Figure 5-10.

Two local MCST dips (at around 7s and 12s) were observed in Phase 1 when the maximum reverse/forward channel flow occurred. These heat transfer enhancements are confirmed by the relatively high convective heat flux in Figure 5-11. In the early phase of the 100% break LOCA transient, convection dominated the heat transfer over radiation. The fraction of heat removed by radiation is less than 30% of the total heat flux.

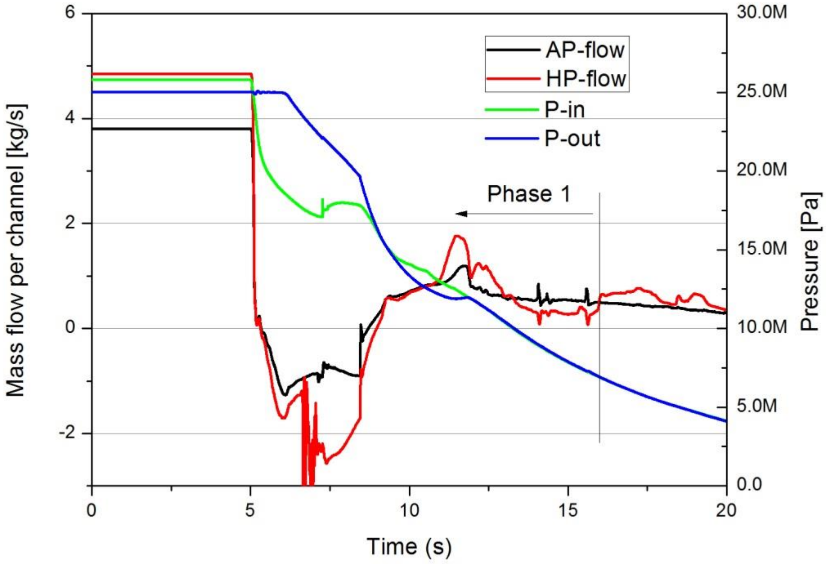

Figure 5-9 System pressure and channel flows in phase 1 of the 100% break LOCA in the reference case

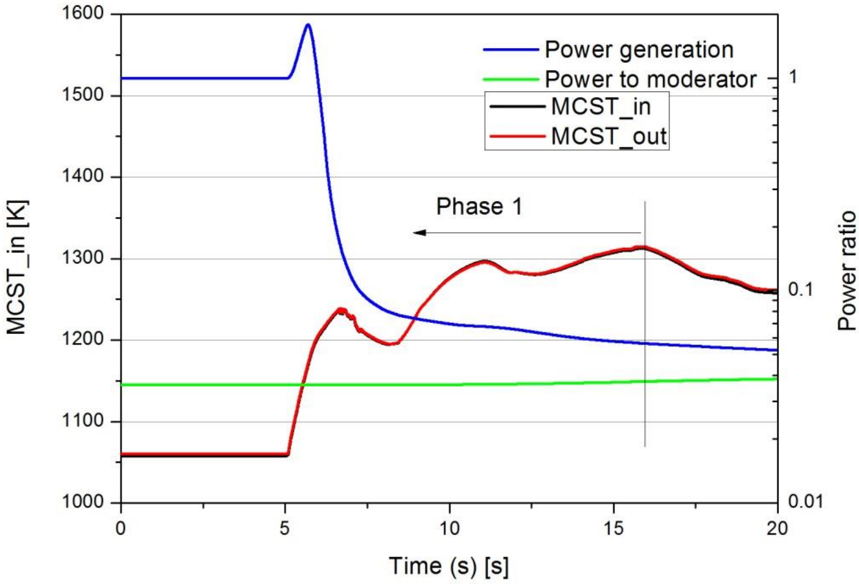

Figure 5-10 Power generation, removal and MCSTs in Phase 1 of the 100% break LOCA in the reference case

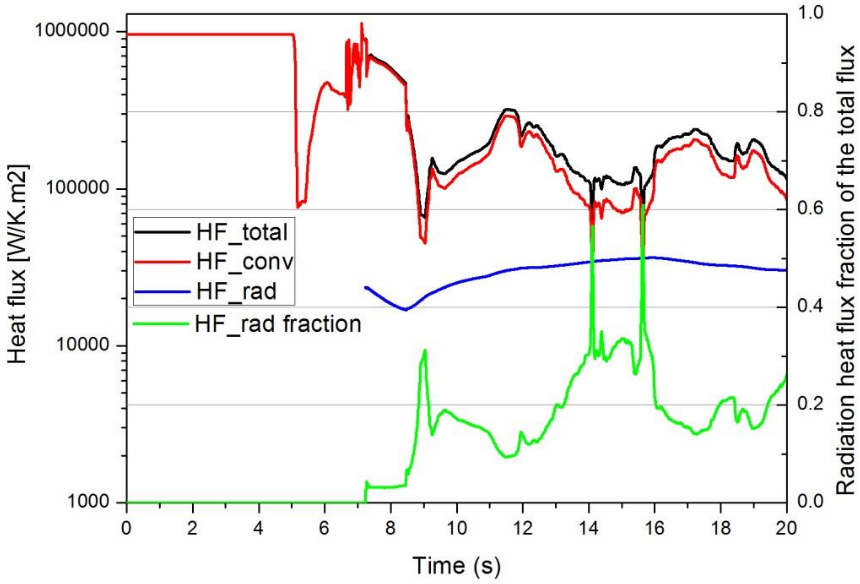

Figure 5-11 Convection and radiation heat flux rate in Phase 1 of the 100% break LOCA in the reference case

<u>Phase 2 (16-100s)</u>

Phase 2 is defined as the interval of time with decreasing MCST after the first peak. During this phase the system pressure decreased smoothly and blowdown combined with coolant injection maintained a small amount of mass flow in the channels (Figure 5-12). The combined effects of radiation and convection heat transfer exceeded the energy production in the fuel and the temperatures began to decrease. At the end of Phase 2, the local minimum MCST was achieved (Figure 5-13).

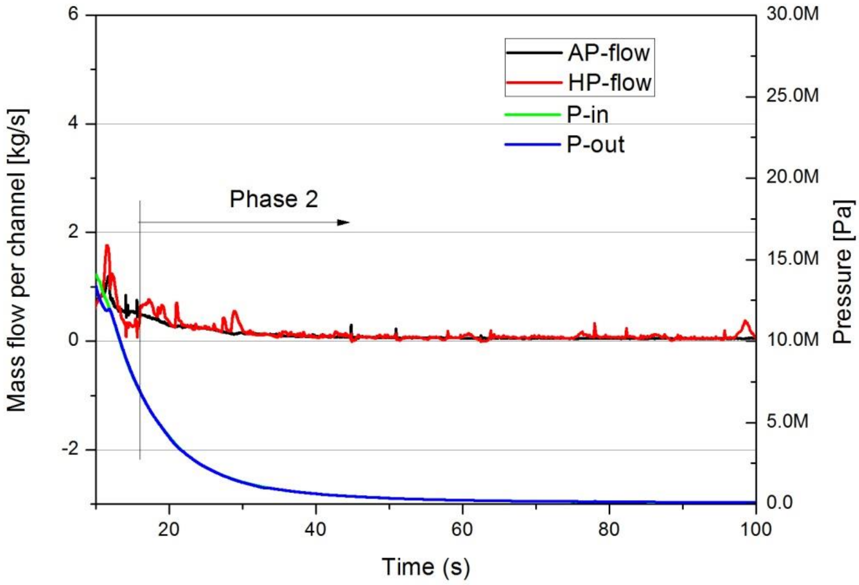

Figure 5-12 System pressure and channel flow in Phase 2 of the 100% break LOCA in the reference case

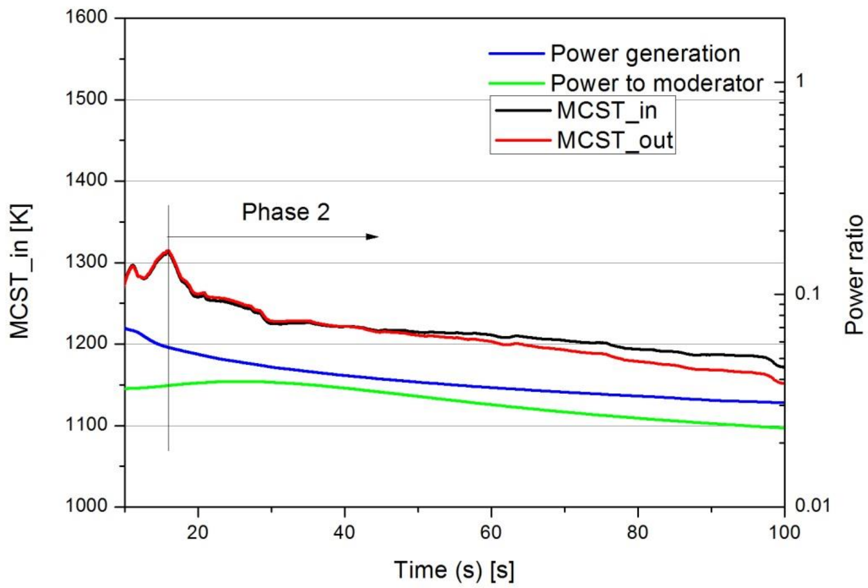

Figure 5-13 Power generation, removal and MCST in Phase 2 of the 100% break LOCA in the reference case

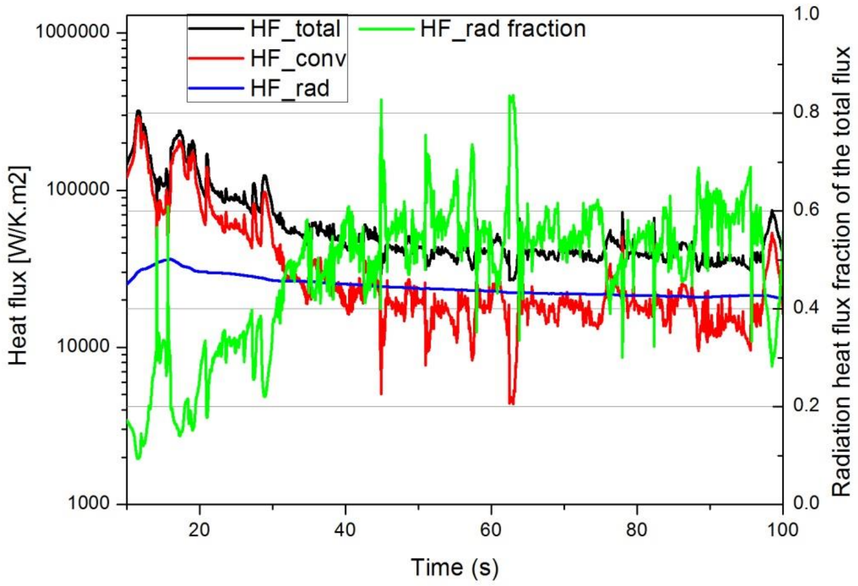

Figure 5-14 Convection and radiation heat flux in Phase 2 of the 100% break LOCA in the reference case

Phase 3 (100-320s) and Phase 4 (320-500s)

The reactor core inventory was nearly depleted at the beginning of Phase 3 due to the limited capacity of the coolant injection. If LPCI was transferred to containment sumps, or pressure fell below the GDCI capability, additional long term injection would continue to drive down fuel sheath temperatures. In the event that these systems are inoperable, heat removal then proceeds to the PMCS mode. In Phase 3 radiation dominated the heat transfer as a fraction of nearly 80% of the total heat flux (Figure 5-16). During Phase 3 the MCST increases until such time as the radiation heat transfer balances the decay heat, beyond which time Phase 4 starts.

In Phase 3 and Phase 4, the temperature at each fuel heat structure node is a balance between heat removal and heat generation (Figure 5-15). As stated in Phase 3 the radiation is insufficient to remove decay heat and thus the temperature increases. In Phase 4, MCST has risen such that all the decay heat is being removed and temperatures drop with the decay in power level. The second peak MCST (1245.7 K) was observed in the inner fuel ring by the end of Phase 3. The MCST in the outer ring approached its local maximum point at the same time, yet with a smaller value due to the fact that it radiates more effectively to the cooler pressure tube assembly.

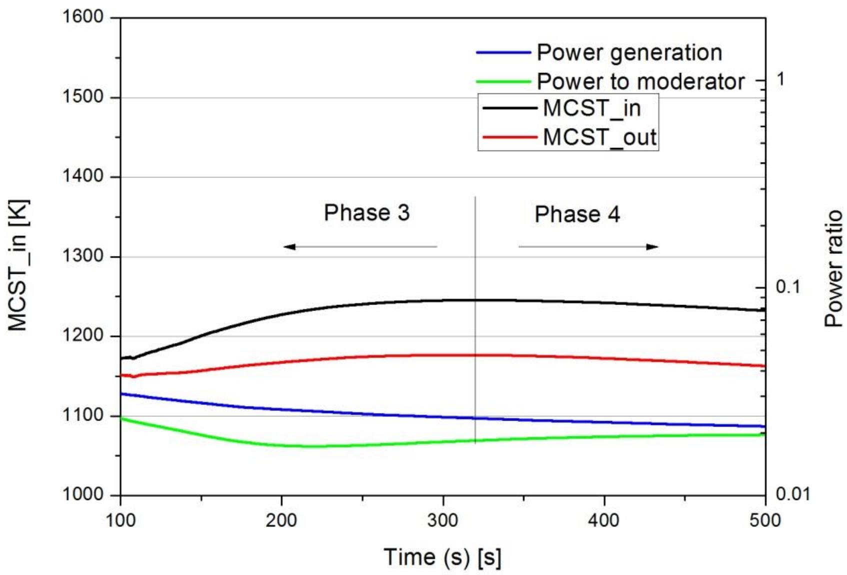

Figure 5-15 Power generation, removal and MCSTs in Phase 3 and Phase 4 of the 100% break LOCA in the reference case

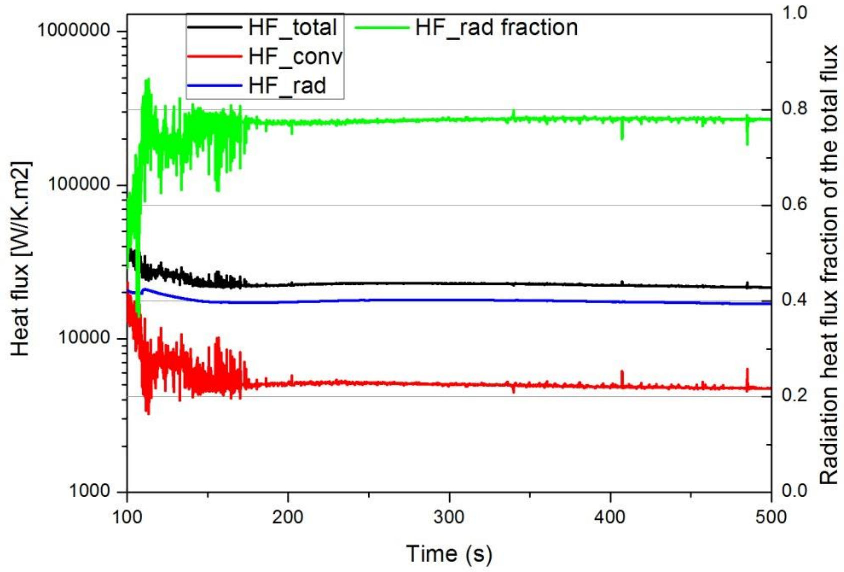

Figure 5-16 Convection and radiation in Phase 3 and Phase 4 of the 100% break LOCA in the reference case

5.2.2 LOCA transient with partial or total loss of ECCS

In contrast with the above discussed 100% LOCA with actuation of ADS and LPCI (Case 1, reference case), a single failure of LPCI for a 100% break (Case 2) and a simultaneous failure of ADS and LPCI for a 100% break (Case 3) were also studied. The transient sequences are listed in Table 5-2. The system behaviors in the initial stages are identical for the three cases. Note the single failure of ADS is not simulated because the coolant supply from LPCI will be mostly discharged along with the reverse channel flow through the break in case of no ADS actuation. Thus LPCI without ADS is not expected to mitigate the transient consequence and it is not studied.

For Case 2, since no coolant is injected after the ADS valve opening, core cooling is expected to be degraded for later phases of the transient, hence the second MCST peak will be larger.

As shown in Figure 5-17, the system responses in Case 2 started deviating from the reference case beyond 18.53s (coolant injection initiation time in Table 5-2). In absence of coolant injection the channel was stagnated early and flow was not reestablished. The discharge flow from the break decreased slightly compared to the reference case which implies that part of the injected coolant in Case 1 left the reactor core via the break.

For Case 3 the reverse channel flow from the outlet plenum initiated by the break remained reversed for the duration of the transient and the coolant was depleted at around 50s, after which the convection heat transfer became minor and radiation heat exchange dominated the decay heat removal. In absence of the ADS, the system was depressurized at a slightly lower rate and the discharge flow rate was greater in the early phase (due to a higher system pressure). As a consequence of the prolonged reversed flows, the feedback effects are reduced relative to Case 1, and hence the initial power pulse and initial MCST peak are reduced.

Figure 5-18 shows the MCST variations in Case 2 and Case 3 compared to the reference case. The faster coolant depletion in Case 2 shortened the effective cooling period and the MCST began to increase earlier compared to that of Case 1. Hence, the subsequent heat-up in Phase 3 takes place at higher decay heat levels which leads to higher secondary MCST peaks.

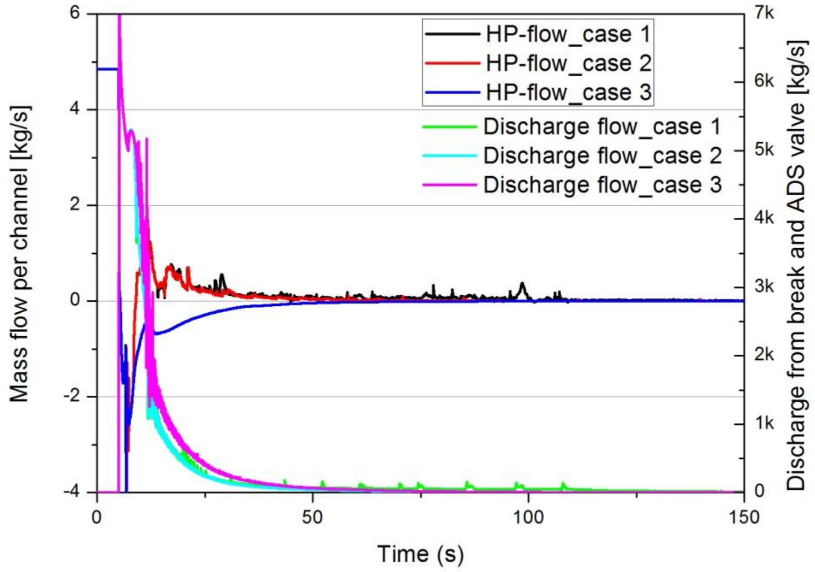

Figure 5-17 Channel mass flow and discharge flow in Case 2 and Case 3 of 100% break LOCA compared to the reference case

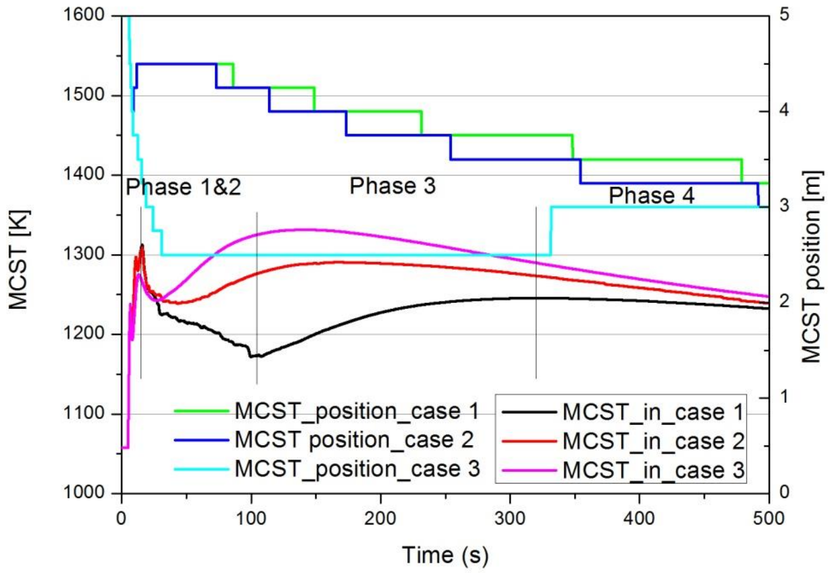

Figure 5-18 MCST in the Case 2 and Case 3 of 100% break LOCA compared to the reference case

In Case 2 the limiting MCST remains the first peak similar to Case 1.

The higher reverse channel flows in Case 3 lead to a reduction in power pulse as compared to

Case 1 and Case 2. Furthermore, since the flow remains reversed, the temporary degradation in heat transfer that occurs as the channel transitions back to forward flow in Case 1 are avoided. However, since LPCI is unavailable in Case 3, the subsequent phases take place earlier at higher decay heat levels. As such the limiting MCST occurred at the secondary peak.

The transients are summarized in Table 5-3.

Table 5-3 Time frame and MCST peak value in the three cases of 100% break LOCA

Parameters	Phase	1	2	3	4	Highest MCST [K]
Time frame[s]	Case 1	5-16	16-100	100-320	320-500	-
	Case 2	5-15	15-49	49-168	168-500	-
	Case 3	5-13	13-27	27-141	141-500	-
Phase-ending temperature[K]	Case 1	1315.1	1172.1	1245.7	1232.4	1315.1
	Case 2	1311.2	1239.8	1290.8	1239.1	1311.2
	Case 3	1275.5	1242.8	1331.5	1247.4	1331.5

The following observations are made for Phase 1 and Phase 2:

Case 2 - the MCST values and locations are identical to the reference case in Phase 1 and early portion of Phase 2. In later stage of Phase 2, further reduction in MCST is restricted due to the lack of coolant injection. A local minimum value is achieved at the balance of power generation and removal at the end of Phase 2.

Case 3- in Phase 1 the fuel temperatures rise mainly for two reasons, one being the power accumulation from the short-period power pulse and relatively high decay heat generation, the other being the impaired heat transfer induced by reverse flow. Figure 5-19 shows the comparison of heat flux between Case 3 and the reference case for Phase 1 and Phase 2. In the first 30s, the total heat flux in Case 3 is somewhat more advantageous. The fuel channels in the two cases are both filled with hot coolant as a result of the reverse flows and the energy depositions from thermal fission and decay power are also the same. The convection heat transfer coefficient is believed to be more favorable for larger magnitude flows, regardless of the flow direction. At around 13s the convection heat transfer exceeds the power generation in Case 3 and the first peak MCST is reached, while the reference case undergoes the flow direction transition and the temporary small magnitude flow rate provides insufficient heat transfer and the fuel temperature keeps increasing until forward flow is reestablished. This explains the slightly lower and earlier first-peak MCST by the end of Phase 1 in Case 3.

Phase 2 in Case 3 is rather short compared to the reference case. Since no external coolant is injected, the effectiveness of forced convection rapidly declines. Once the energy generation rate exceeds the decay heat removal rate, Phase 2 ends and the fuel temperature starts increasing in the subsequent phase.

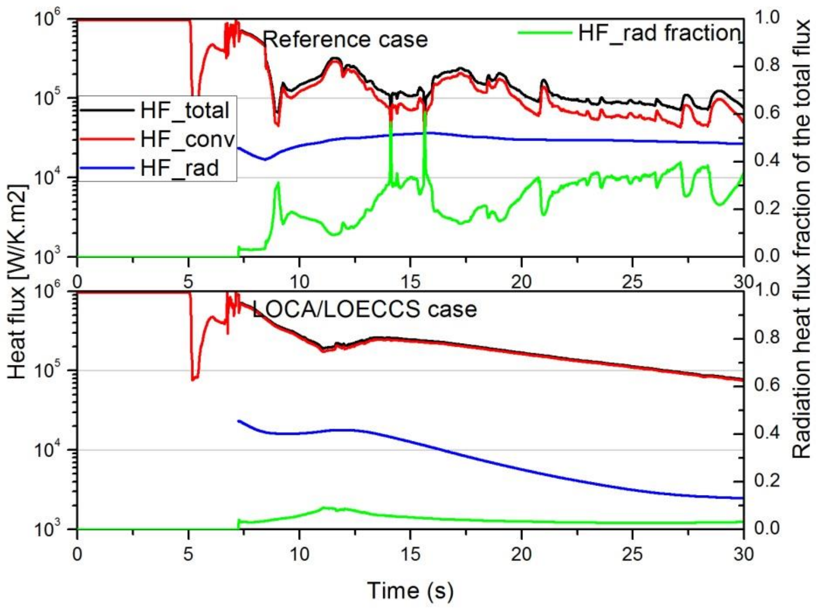

Figure 5-19 Convection and radiation in Phase 1 & 2 in the LOCA/LOECC case compared to the reference case

The following observations are made for Phase 3 and 4 for the multiple failure scenarios:

Case 2 - Similar to Phase 3 in the reference case, the MCST increased until radiation was able to reject sufficient heat to balance the decay heat. However, Phase 3 in this case lasted for a shorter time period with a higher MCST (1290.8K), although the overall limiting temperature still remains the first peak.

Case 3 - Figure 5-21 presents the fuel cladding temperature change during Phase 3 and 4. During Phase 3 the contribution of convection drops to insignificant levels as the core inventory is depleted (Figure 5-20). The energy production in the fuel exceeds the available radiative cooling and the fuel temperature begins to increase. The maximum value of MCST, i.e. 1331.5 K, occurred at the end of Phase 3. Figure 5-20 shows the fraction of heat removed by radiation increases to 80% in this phase and remains at this level for the remainder of the simulation time.

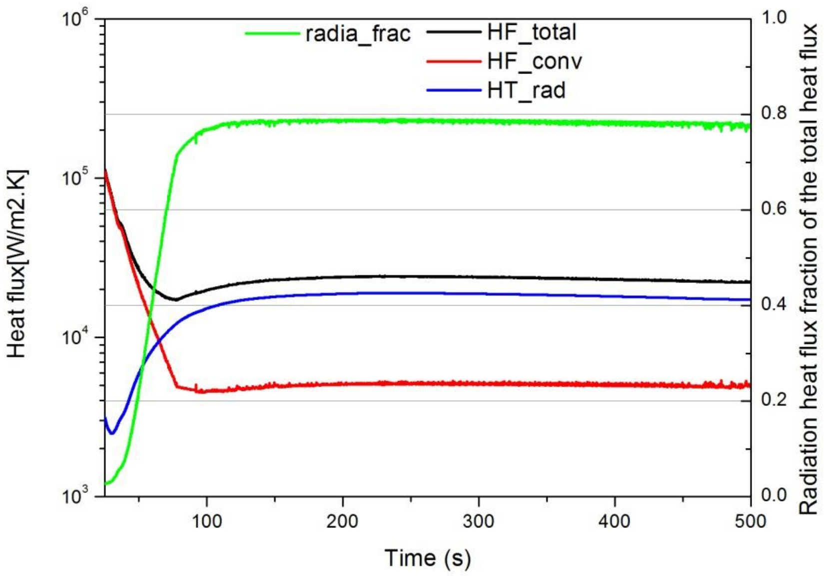

Figure 5-19 Convection and radiation heat of Case 3 compared to the reference 100% break LOCA

At the beginning of Phase 4, the cladding surface temperature has risen sufficiently such that the heat radiated from the fuel balances the further reduced decay heat, resulting in a decrease in fuel temperature. Figure 5-21 shows that the heat removal stayed higher than the decay heat generation for the rest of the transient which ensures the long term cooling of the fuel and core components.

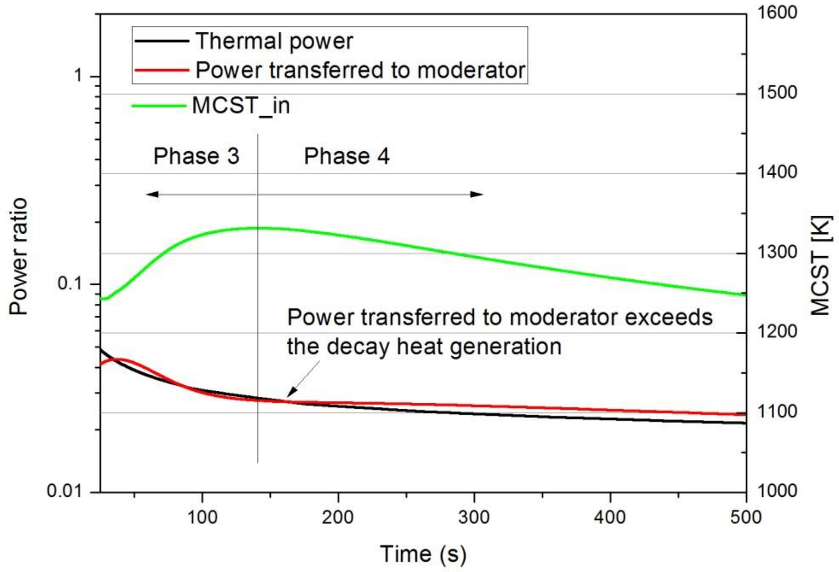

Figure 5-20 Power generation, removal and MCST in Phase 3 and Phase 4 of Case 3 compared to the reference case 100% break LOCA

5.2.3 Summary

This section discussed the behavior of the Canadian SCWR heat transport system during the 100% cold-leg break LOCA transient. Three different safety systems combinations, i.e. ADS, LPCI and PMCS; ADS and PMCS; PMCS only, are credited separately in three transient cases. The transients can be split into four different phases based on heat transfer and fuel temperature characteristics, which have been investigated in detail. Generally speaking, there are two peak values of MCST: the first one appears in the first phase due to the combined effects of short-term power pulse and heat transfer deterioration due to reverse flow of hot coolant from the outlet plenum; the secondary peak occurs later in the transients after the core coolant is depleted and a heat balance between decay power and radiation exchange is achieved.

Table 5-3 summarizes the time frames and limiting MCST for the three cases. For the 100%

break LOCA, the worst case is observed with the highest MCST being 1331.5 K (secondary peak) at dual failure of ADS and LPCI. The ADS maintains a forward flow in the fuel channels and propels the secondary peak MCST to a lower value. The inclusion of LPCI together with ADS promotes the long term cooling even further by providing inventory for prolonged convective cooling. However, the involvement of ADS also has a side effect on the first peak MCST. The temporary heat transfer degradation as the channel coolant changes direction from reverse flow to forward flow caused the temperature to continuously increase relative to the case with no ADS.

5.3 Parametric study for critical break size

As stated in the literature review, the sensitivity study regarding to the break sizes performed for the Japanese Super LWR indicated that the SBLOCA gives a higher MCST compared to the LBLOCA [28] since the induced hot assembly flows are lower and the reactor trip timings are extended. The SBLOCA in the Canadian SCWR is characterized by a slow depressurization process whereby the core remains at high pressure for a longer time than the large break cases. In the current SCWR model, breaks with a size bigger than 15% of the cold-leg flow area are denoted as the LBLOCA, while the others are regarded as SBLOCA. The reason for 15% break case being the boundary size is that for breaks below 15% the heat transport system undergoes pressurization due to the resultant flow-power imbalance and thus it is the largest size where the relief valve actuates. This chapter starts with a 5% break LOCA with simultaneously loss of ADS and LPCI transient to investigate the distinctive system behavior of a typical SBLOCA. Following the detailed analysis of the 5% break, a parametric study is performed to determine the most limiting LOCA break size.

5.3.1 5% break LOCA transient with loss of ADS and LPCI

As discussed in the previous section, the unlikely concurrence of a loss of coolant accident and the loss of ADS and LPCI systems presents the worst consequence for the 100% cold-leg break LOCA. The first peak, related to the net energy deposition during the high power portion of the transient is slightly reduced in the dual failure case since the prolonged reverse flow acts to reduce the non-equilibrium void feedback effects (and no temporary stagnation is observed during the switch-over to forward flow in the ADS case). In these transients the secondary MCST peak occurring under decay heat conditions becomes limiting. Since the SBLOCA power excursions due to non-uniform voiding are expected to be less severe than the LBLOCA case, and thus the secondary MCST peak will likely again be limiting. The same dual failure transient scenario is performed for the 5% break as a representative SBLOCA transient. The 5% break LOCA event sequences are listed in Table 5-4.

Table 5-4 Transient sequences for 5% break LOCA

Even sequence	Time[s]
Break occur	5.00
Reactor trip signal/low flow	5.41
Reactor trip	5.97
Main coolant pump trip	5.97
Main steam isolation	6.02
Feedwater tank drain out	11.97

As shown in Figure 5-22, the outflow rate from the 5% break was approximately one eighth of that in the 100% break case. The accumulated mass loss from the break at 500s was about 87% of that in the 100% break, indicating the coolant was not yet completely depleted. The combination of the smaller break size, reduced coolant flow, delayed coolant pump trip and closure of the isolation valves leads to a temporary pressurization of the heat transport system up to the SRV setpoint. In this case core isolation causes the reactor to be isolated from a heat sink leading to fuel heat-up and system pressurization. Such phenomena are also predicted in Loss of Flow Accident similar to those reported by Wu [19]. The frequent SRV actions cause a periodic pressure oscillation, resulting in a fluctuating channel flows in early stage of the transient. ICS action is not credited in this analysis, but such systems may provide some short term cooling/inventory dependent on break size and location. Similar to the 100% break case, the transient is split into several phases depending on the MCST behavior, with a typical early pressurization phase where flow oscillations driven by SRV action dominate (Figure 5-23, Figure 5-24).

During Phase 1 the system is characterized by flow pulses stemming from SRV actions downstream of the reactor core, and a small power excursion to 108.5% FP, followed by a small reverse flow driven by the cold-leg break. Due to the combined effect of the net energy deposition and insufficient core cooling, the MCST increases rapidly to about 1390 K. Phase 2 in the 5% break LOCA lasted for a longer period of time since coolant depletion is significantly delayed relative to the LBLOCA case (Figure 5-24). Phase 3 and Phase 4 are less discernable since the modest reverse flows provide cooling for a long duration. A small secondary peak is observed at the end of Phase 3 when the heat transfer regime transitions from convection to radiation dominated. However due to the extended Phase 2 cooling mode, the decay heat levels are very low by this time and the secondary peak MCST is small.

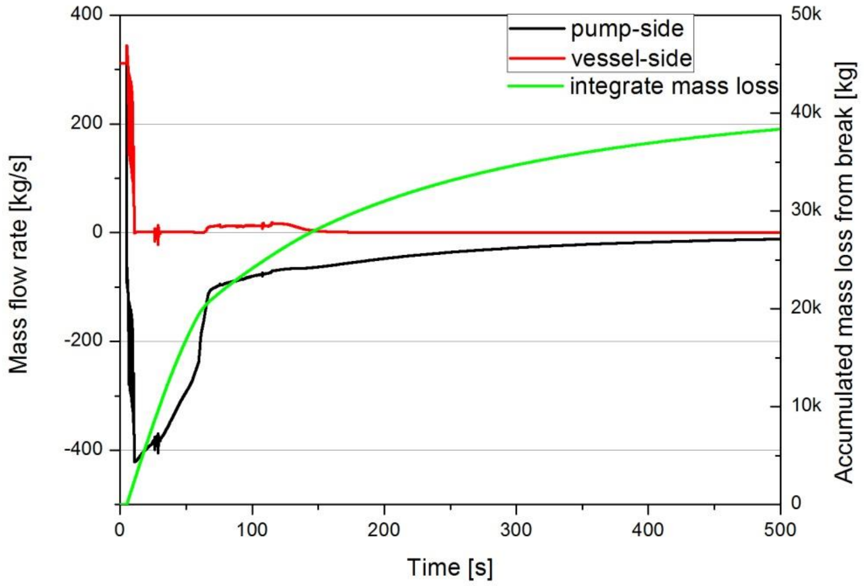

Figure 5-21 Discharge flow rate and mass loss for the 5% break LOCA/LOECC

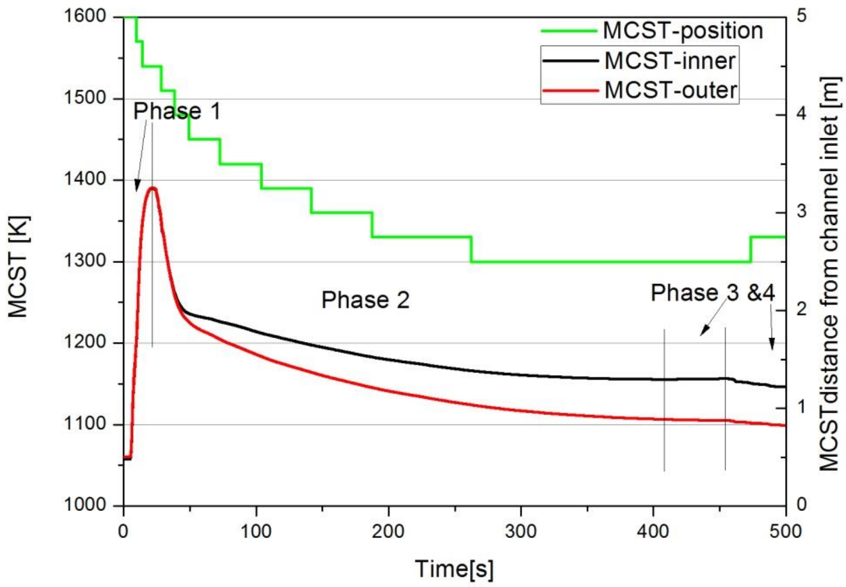

Figure 5-22 MCST value and position variation for the 5% break LOCA/LOECC

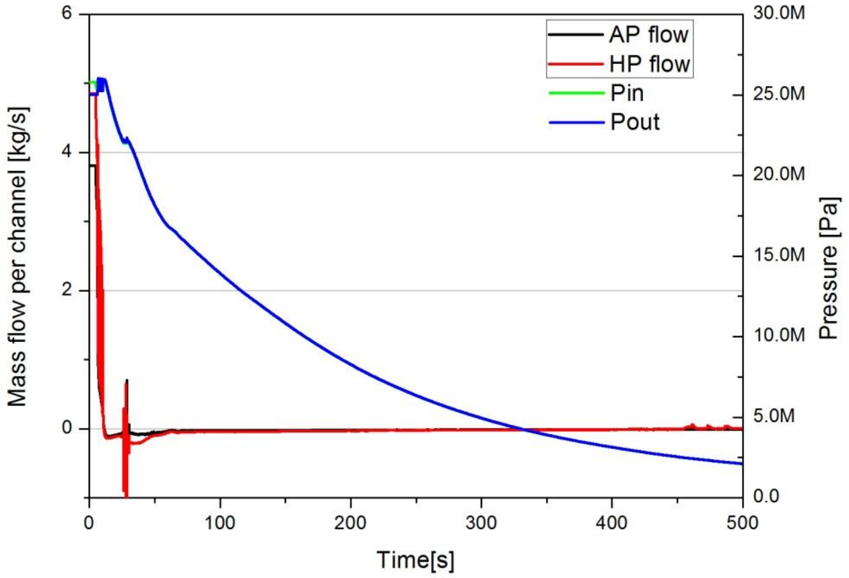

Figure 5-23 Pressure and channel flow rate for the 5% break LOCA/LOECC

After the break, the reactor system responses are listed in Table 5-5. The combination of loop isolation, coolant pump trip and the small break outflow causes early flow stagnation in the core and the imbalance between heat generation and heat removal, resulting in the system pressurization. A smaller power pulse (108.5% FP) occurs at 6.09s since the difference in the center flow tube and outer fuel region coolant density is lower compared to the 100% break LOCA. As system pressure increases to the setpoint of the SRV, it is activated to release the pressure and closes as the pressure decreased. Subsequent pressurization occurs after the valve closure and the SRV opens again to relieve pressure (Figure 5-25). During this initial oscillatory phase the SRV actions oppose the reverse flow while some improved cooling is observed it is much smaller than the SRV cooling effects in a LOFA as noted by Wu [19]. At approximately 11s the coolant inventory is depleted to the extent that the bulk pressure drops and SRV action is terminated. Beyond this time, continuous small reverse flow occurs in all channels.

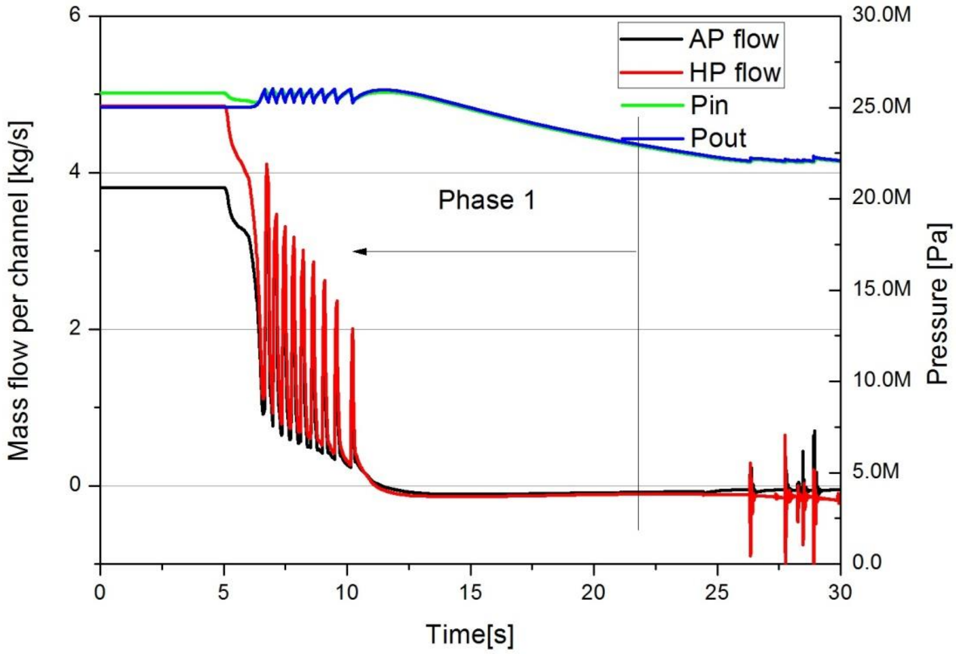

Figure 5-24 Pressure and channel flow behavior in phase 1&2 for 5% break LOCA

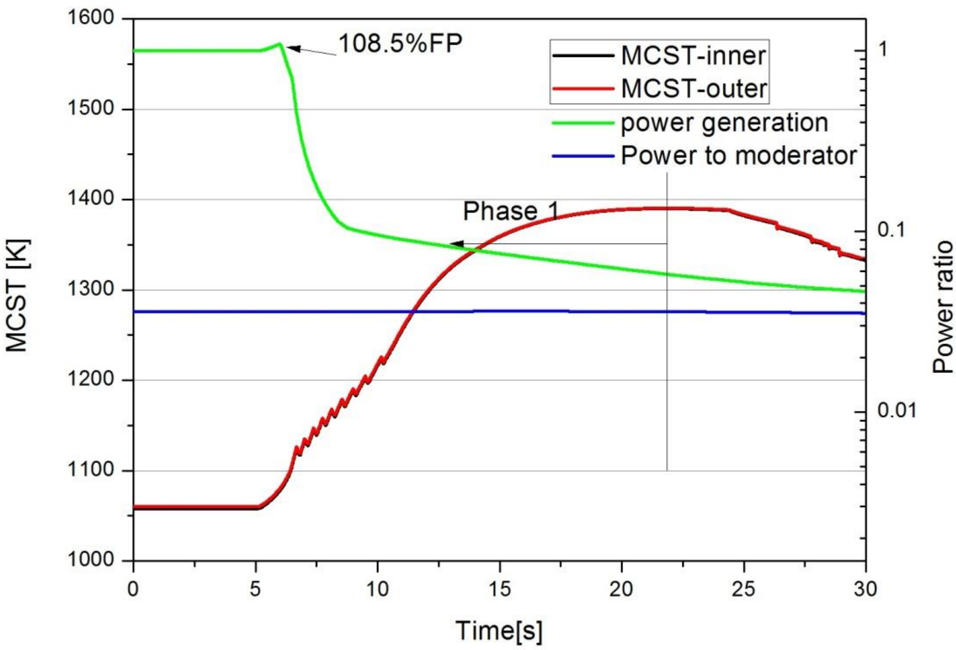

Figure 5-25 Reactor power and MCST variation in phase 1&2 for 5% break LOCA

Figure 5-26 shows that the first peak MCST value is 1389.9 K at the 22s and (17s after the break) is more limiting than the 100% LOCA case by a smaller safety margin. Figure 5-27 shows the net energy deposition (NED) at the MCST node (node-18) in early phase of the 5% break compared to the 100% break. Even though the energy deposition due to the initial power pulse is much larger in the 100% break case, the subsequent large reverse flows limit the temperature excursion. In the SBLOCA case, the initial blowdown cooling is insufficient to remove the NED and thus the peak MCST is higher than that in LBLOCA. Beyond the peak at the end of Phase 1, the reverse flows provide adequate convection for these decay heat levels. Radiation plays only a small role since the fuel temperatures remains low in Phases 2, 3 and 4.

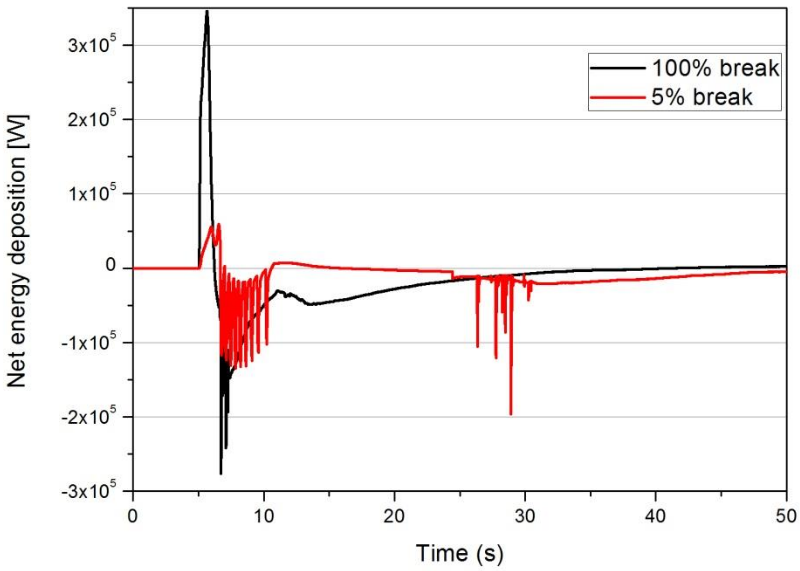

Figure 5-26 Net energy deposition in early phases for the 5% break LOCA compared to the 100% case

A series of channel flow oscillations are observed in Figure 5-25 at about 28s as the system undergoes transition from supercritical to subcritical pressure. This is likely caused by the code limitation in dealing with the drastic coolant property variations near critical point. Such variations take place rapidly in the 100% break case and hence are less noticeable in the predictions. For smaller breaks, the duration of time in the trans-critical region is much longer and hence some addition code issues are observed. Such oscillations, while likely artificial, require further more study and/or validation beyond the scope of this work. These artificial flow spikes caused some unrealistic heat transfer enhancement for a few seconds as shown in Figure 5-28 and thus partially contribute to the early temperature decreasing in Phase 2. Apart from these temporary flow pulses, the reverse flow effectively removes decay heat and reduces the fuel temperature.

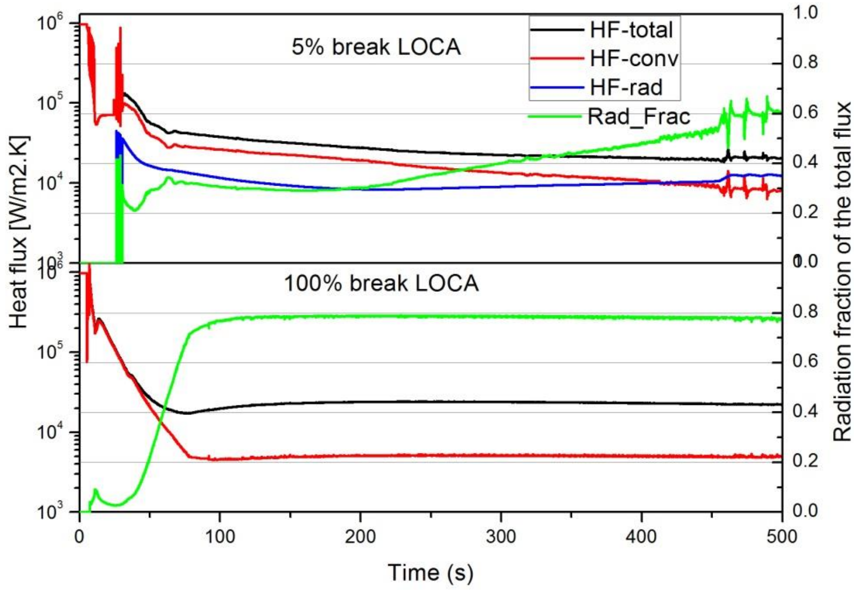

Figure 5-27 Convection and radiation heat flux for 5% break LOCA compared to the 100% break case

5.3.2 Parametric study for various break sizes

The objective of this section is to investigate the impact of break sizes on the LOCA transient consequences and find the critical break with the most limiting MCST. Various break size LOCAs, from 5% to 100% of the cold-leg cross-sectional area were simulated to investigate the system behavior. The largest SBLOCA size for this design corresponds to approximately 15% as larger breaks do not cause early pressurization to the SRV setpoint, while smaller breaks have an initial pressurization period. ADS and LPCI are not credited to represent the worst possible consequences.

Figure 5-29 shows the depressurization process as a function of break size from 100% to 5%. The slower depressurization rate in SBLOCAs provide longer periods of flow reversal (Figure 5-30), and hence the secondary peak MCST is expected to be reduced in magnitude with decreasing of the cold-leg break size.

In terms of the maximum cladding temperature in Figure 5-31, generally two peak MCSTs appeared in all cases. Consistent with the previous discussion, the first peak is related to NED during the power pulse phase and reduced cooling, while the secondary peak is related to the transition from convective to radiation heat transfer. For LBLOCA, the second peak MCST is more limiting since the first peak is mitigated by the relatively large reverse channel flow in the early phase. However, the first peak MCST becomes more restrictive for SBLOCAs due to a reduction in the reverse channel flows and SRV action in an opposing direction to the reverse flow. The SBLOCA second peak is reduced due to longer sustained reverse channel flows and a much later transition to radiation heat transfer. Compared to the 5% break, the first peak MCST in the 15% break is much higher because of the larger energy deposition caused by a higher power pulse. Table 5-5 summarizes the power pulse and MCSTs for all the LOCA transients conducted with coincidental loss of coolant injection and ADS. The highest MCST (1450.4 K) in the 15% break LOCA occurs at 12.86s.

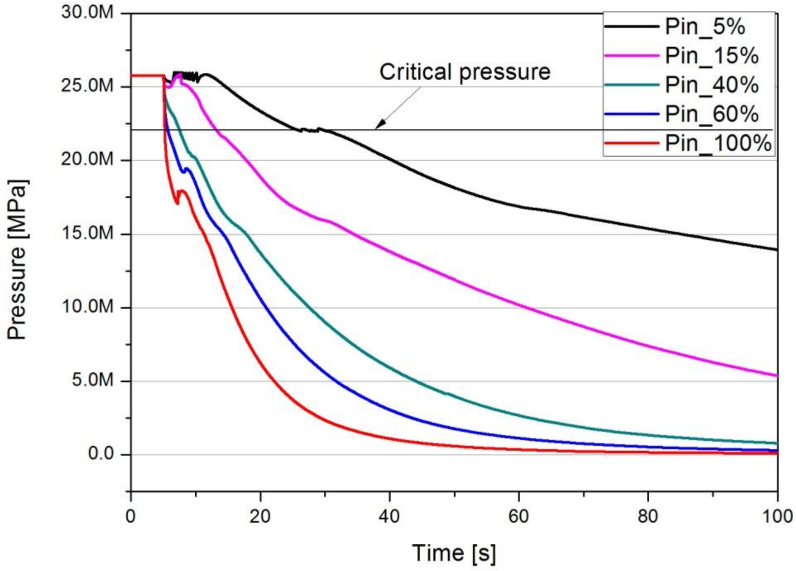

Figure 5-28 Depressurization progress for LOCAs with various break sizes

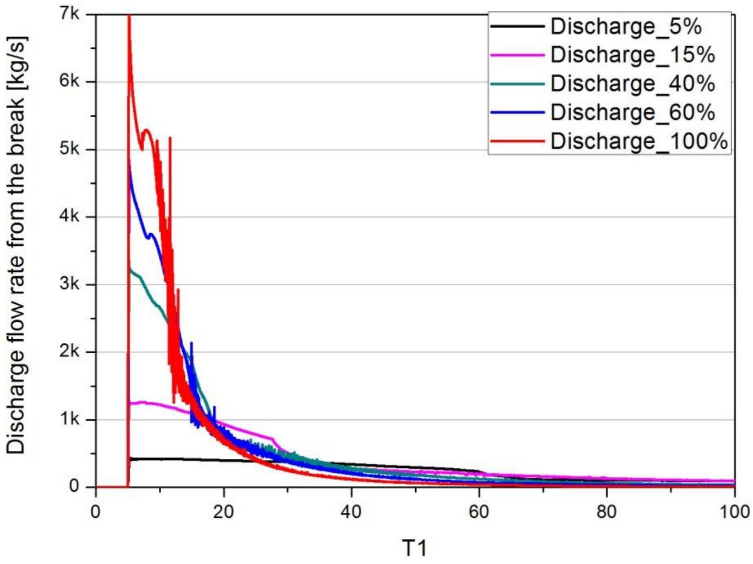

Figure 5-29 Discharge flow from the break in LOCAs with various break sizes

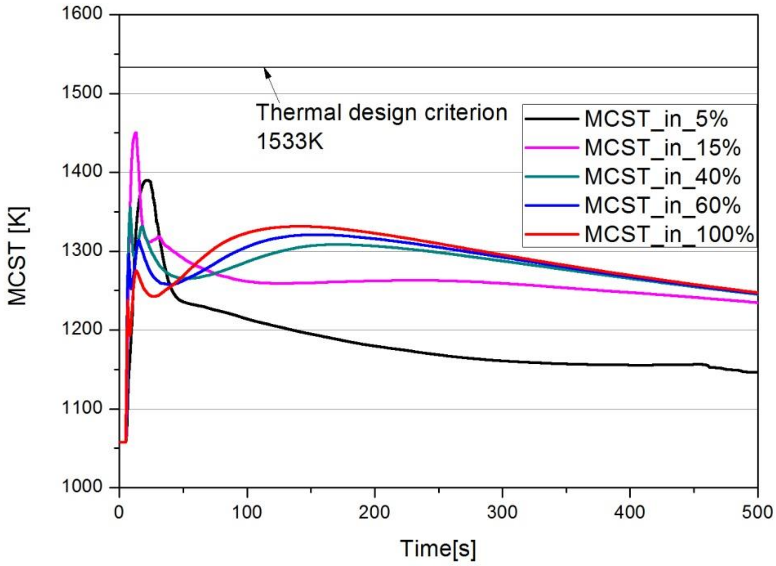

Figure 5-30 MCST variations for LOCAs with various break sizes

Table 5-5 Two peak MCSTs and occurrence time for LOCAs with different break sizes

Break size	Power pulse [%FP]	First Peak MCST [K]	First peak MCST time [s]	Second peak MCST [K]	Second peak MCST [s]
5%	108.5	1389.9	21.8	1156.5	454.0
15%	118.6	1450.4	12.86	1263.2	228.0
40%	143.4	1331.7	17.73	1308.6	171.0
60%	156.8	1313.7	14.96	1320.9	155.0
100%	178.3	1275.5	13.1	1331.5	141.0

5.3.3 Summary

This section described the differences between SBLOCA and LBLOCA behavior in the Canadian SCWR. SBLOCA is characterized by an early pressurization phase, small reverse flows, and frequent SRV actions. The first peak MCST is higher than that of 100% break LOCA due to the much smaller reversed channel flow. The longer period of sustained reverse flow ensures that the secondary peak occurs much later and at a lower decay heat level than the LBLOCA cases. A parametric study of MCST as a function of break size reveals that the

15% break case (largest SBLOCA) has the highest MCST with a safety margin of 83 K. Faster SDS action or early intervention of the ADS system may temper the fuel heat-up and provide considerable safety margin. This is confirmed by several sensitivity analyses in the following section.

5.4 Other Sensitivity analysis

5.4.1 ADS sizes

The ADS design for the Canadian SCWR has not been finalized yet and the accident behavior may be sensitive to the ADS size, setpoints and valve-stroke timing. A larger ADS valve causes larger magnitude forward flows for LBLOCA events however it leads to earlier inventory depletion and hence in the absence of coolant injection leads to an earlier and therefore higher secondary MCST peak. On the other hand, a small ADS valve size may not ensure forward flow in a LBLOCA event. The ideal ADS flow area is such that it is the minimum that can still ensure forward flow in the largest LOCA. A key aspect of the reverse flow in Phase 1 of a LBLOCA is that it quickly brings hot coolant from the outlet plenum to the central flow tube in each channel, thereby terminating any reactivity excursion. Therefore, if ADS initiates very early in the transient it prevents reverse flow and the power pulse maybe larger. ADS must also not come in too late, since it ensures that flow stagnation does not occur until later in the transient (when decay heat is lower).

The sensitivity study regarding to the ADS valve sizes have been conducted by varying the ADS valve area in the 100% LOCA case while assuming LPCI failure. Simulations with the ADS sizes of 30%, 50% and 70% of the cold-leg pipe flow area have been conducted and the results are shown in Figure 5-32. As the ADS size increases, the peak cladding temperature decreases. The power pulse induced peak MCST reaches 1402.6 K for the case with 30% cold-leg area and the channel flow nearly stagnates after the ADS opening. Inclusion of an ADS valve with such size only exacerbates the transient consequences since it cannot fully restore forward flow. The 70% ADS size provides sufficiently large forward flow to cool the fuel elements and a peak value of 1277.9 K is achieved at earliest time among the three cases. The MCST drops below 1200 K after 20s. The results for ADS flow area of 50% also show adequate cooling, and since smaller ADS size can prolong the blowdown cooling phases, it is selected as the optimal.

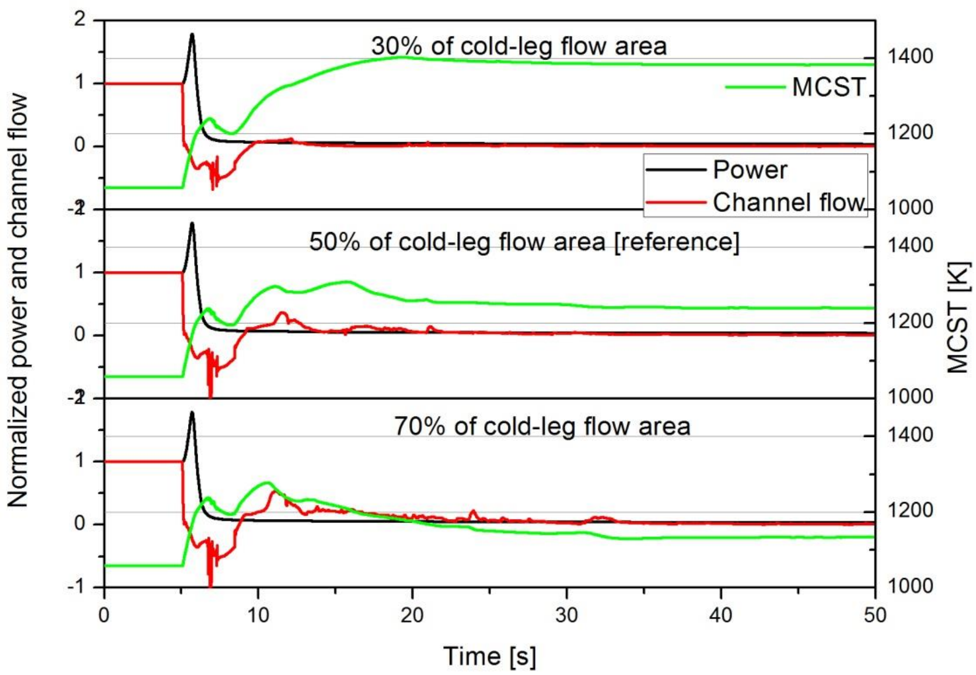

Figure 5-31 Normalized power, channel flow and MCST for different ADS sizes

5.4.2 Elements affecting long term cooling

Radiation heat transfer plays an essential role in removing the decay heat in later phases of the LOCA transients after the coolant is depleted, especially for LBLOCAs where LPCI is unavailable. The highest MCST occurs during the transition from convective to radiation dominated regimes. In this section the sensitivity of MCST to emissivity and thermal resistance to the moderator system is performed. The 100% break LOCA/LOECC transient in Section 5.2.3 is used as the reference case.

Emissivity

One of the key parameters that affect radiation heat transfer is the surface emissivity, as explained in section 3.3. It varies from 0 (complete reflectance) to 1 (black body) depending on the solid material and its surface conditions. The sheath material for the Canadian SCWR design has not yet been finalized and stainless steel is used in this study assuming a constant emissivity of 0.8. However, due to the uncertainty in cladding conditions the emissivity may vary considerably.

Table 5-6 summarizes the simulation results for the 100% break LOCA cases as emissivity varies from 0.2 to 1. Simulations using fuel sheath emissivity lower than 0.2 demonstrate surface temperatures which exceed the safety limit for SS cladding. For the other cases, the sheath decreases with increasing emissivity as expected and remains below the acceptance criteria; the lower emissivity gives a higher prediction of the MCST (Figure 5-33).

Table 5-6 Peak MCST and occurrence time of different emissivities for 100% break LOCA

Case No.	Emissivity	Peak MCST [K]	Time [s]
1	0.2	1533	244.0
2	0.4	1428.8	241.0
3	0.6	1368.3	171.5
4(Ref)	0.8	1331.5	141.0
5	1.0	1306.8	121.0

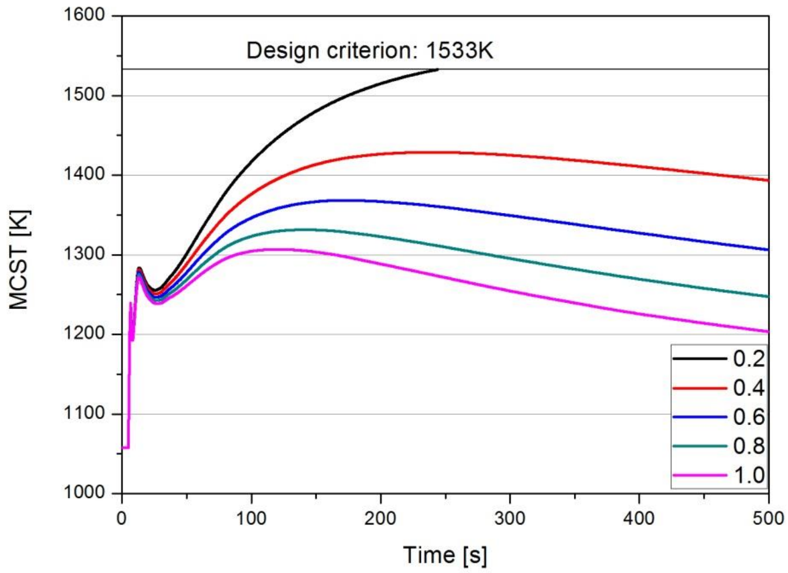

Figure 5-32 MCST variations at different solid emissivity conditions

<u>Insulation layer properties</u>

Another factor that may affect the heat transfer to the moderator system during the LOCA transient is the insulation heat resistance (i.e. the thermal conductivity). This also influences the power lost to the moderator at steady-state. A good insulator is supposed to prevent excessive energy loss during the steady-state and be able to remove decay heat to the PMCS under accident condition as required.

The thermal properties used in this study are determined based upon those used by Hummel [7]. To examine the sensitivity, a multiplier is applied on the original thermal conductivity so as to change the power fraction conducted to the moderator systems. The simulation results are listed in Table 5-7 with the 100% break LOCA/LOECC as the reference case. It implies that the MCST remains below the safety criteria if the power transferred to the moderator system is higher than 2%FP at steady-state operation.

Table 5-7 Insulator thermal conductivity impacts on the 100% break LOCA transient

Thermal conductivity multiplier	MCST [K]	Occurrence time [s]	steady-state power to moderator[%FP]
1.0(Ref)	1331.5	141	3.62
0.8	1349.2	143	3.05
0.5	1395.3	174	2.10

5.4.3 Elements affecting the early phase fuel heat-up

While LBLOCA with loss of injection is dominated by the secondary thermal peak, SBLOCA is dominated by the early phases of transient as discussed in Section 5.3. In particular, the most severe accident consequence was found with the 15% break case. The early peak MCST is caused by the power pulse and insufficient convective heat transfer. It is expected to be reduced by: 1) reduced power generation; 2) enhanced heat transfer. Improvements to SDS timing can lower the power more quickly and hence reduce the initial MCST peak. The sensitivity to instrumental delay in reactor scram is shown below. In addition the ADS initiates strong forward channel flows and can reduce fuel heat-up if its actuation is moved earlier in time. Hence the sensitivity to ADS actuation is also investigated. The following analysis uses the 15% break LOCA/LOECC from Section 5.3 as the reference case.

<u>Reactor scram delay</u>

Table 5-8 shows the highest MCST of 15% break LOCA with loss of ECC with different reactor shutdown system delays. As expected by decreasing the delay in SDS action, the peak power is reduced and so is the subsequent MCST. In the case of zero instrument delay, the resultant peak MCST will be 1393.7 K with a safety margin of 140 K. Alternative detection systems (such as neutronic based as in CANDU) may provide much earlier indication and hence much faster shutdown, so some optimization of the SDS is still required.

Table 5-8 MCST sensitivity upon the reactor shutdown delay

Shutdown delay[s]	MCST[K]	MCST Time [s]
1.0	1503.3	13.10
0.55(Ref)	1450.4	12.86
0.4	1432.5	12.70
0.2	1410.5	12.50
0.0	1393.7	12.50

ADS trip setpoint

In the current model, the ADS is assumed to be actuated by a low pressure (24MPa) signal. For the limiting SBLOCA the system pressure remains higher than that until 11.065 s, however by this time the peak MCST has already reached a high value of 1441 K. In addition to the low pressure signal, a low steam flow (6% nominal flow) signal was proposed by the Japanese Super LWR as an alternative ADS trip signal. This low flow signal is registered about 3s earlier than low pressure and hence would provide significant benefit in the SBLOCA case. The maximum cladding temperature declines to 1356.8 K compared to the case where ADS is registered on low pressure. Once the ADS is activated, strong forward flow is established in the fuel channel and fuel temperature decreases to rather low level (Figure 5-34).

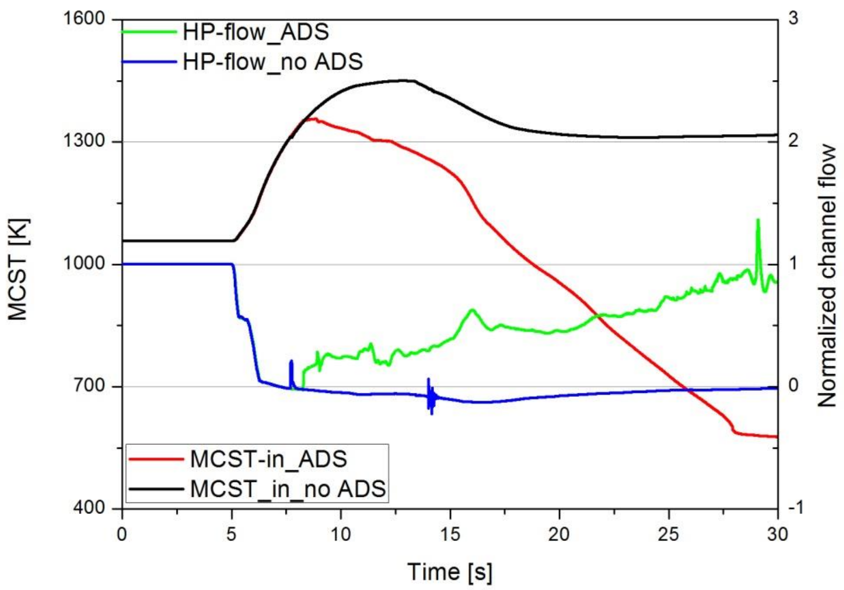

Figure 5-33 MCST sensitivity to an early ADS intervention for 15% break LOCA

5.4.4 Different choking models

Critical flow is a phenomenon when the discharge flow from a break reaches a maximum velocity and will not increase with a further decrease in the downstream pressure while the upstream pressure is fixed. The critical flow initiated by a break in a supercritical system has unique characteristics due to its thermo-physical properties. Some experiments and CFD simulations have been performed to understand the mechanisms of critical flow from supercritical pressure [40]. Since no SCWR specific model exists in RELAP5, a simple comparison between the two accessible choking models in RELAP5 is conducted to inspect their impacts on the discharge flows.

There are two choking models available in the current version of RELAP5, i.e. the default Ransom-Trapp choking model and the modified Henry-Fauske model [30]. The latter has been evaluated to provide better prediction for subcooled choking flow and low-pressure choking through thin orifice plates [30]. The breaks in this study occur at the cold-leg which is initially filled with water in a pseudo-liquid state and therefore the modified Henry-Fauske choking model is selected for all the simulation discussed in previous sections.

However, the aforementioned statement is not confirmed by experiments in supercritical region yet. Therefore significant uncertainties exist in the critical fluid model. Hence, one additional simulation with the Ransom-Trapp choking model for the 100% break LOCA was performed. Figure 5-35 shows that the modified Henry-Fauske model predicts a slightly quicker depressurization process with a larger discharge flow rate above the critical point. After the trans-critical point, the discharge rate predicted by the Ransom-Trapp model shows some oscillations and is slightly higher than that of the Henry-Fauske model. The reason causing the oscillations is not clear, but the discharge rate and system pressure have mutual effect on each other.

In the large break LOCA transient, faster depressurization and larger break flows cause faster inventory depletion and hence an earlier secondary peak. These results imply that the modified Henry-Fauske model predicts more conservative results compared to the Ransom-Trapp model.

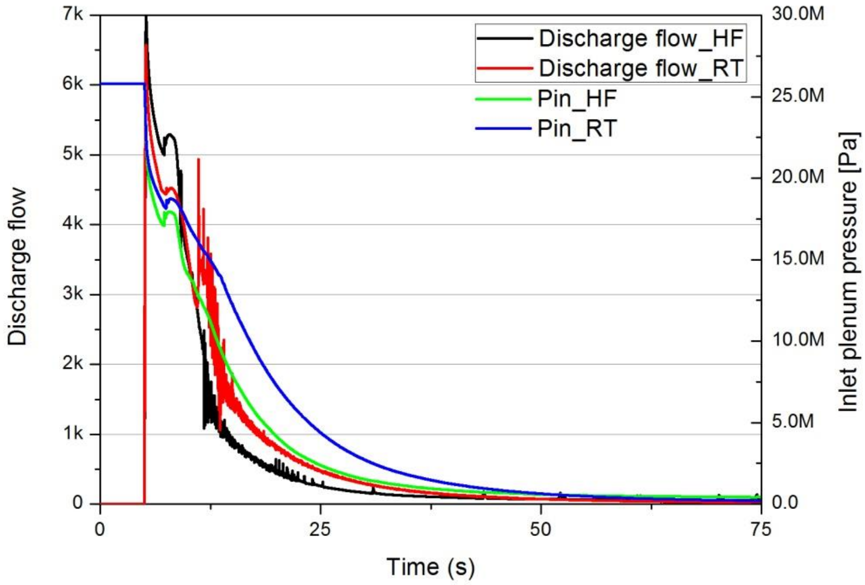

Figure 5-34 100% break LOCA/LOECC simulations with two different choking models

6 Conclusions and future work

6.1 Conclusions

The primary objective of this study is to investigate the PT-SCWR transient behavior under postulated loss of coolant accidents and to demonstrate the effectiveness of the proposed safety systems. A RELAP5 idealization including coolant and moderator systems has been constructed based on the current design of the Canadian PT-SCWR. The 336 vertical fuel channels are divided into two groups, one with the highest channel power and the other with the remaining 335 channels. The channel power and axial power fractions at MOC are used consistent with Hummel [7]. The orifice sizes are adjusted to achieve power/flow match in steady-state and remain constant throughout the transients. A point kinetics model with two coolant density feedbacks from two regions (center tube and fuel region) and the fuel temperature feedback is used to compute the fission power. The decay power is incorporated by an input table based on the values provided by CNL. A benchmark test is then performed by comparison with an identical CATHENA model, showing good agreement for both steady-state and transient conditions.

6.1.1 LBLOCA transients

The 100% cold-leg break LOCA transients with/without ECCS are performed. A short-termed power pulse was observed as a result of the non-equilibrium voiding in the fuel channel. The power pulse in combination with the reverse flow induced by a sudden cold-leg break contributes to the fuel heat-up within first 15s. The ADS actuation induces forward channel flow with temporary heat transfer degradation at the flow direction transition, resulting in a slightly higher MCST (1315 K) than the no-ADS case (1257K), although the most limiting condition occurs at the secondary peak for LBLOCA/LOECC case. This secondary peak MCST was observed during the transition from convective to radiation heat transfer regime. The ADS and LPCI in combination reduce the second peak from 1331 K to 1245 K by maintaining the forward channel flow for a longer period of time. It should be noted that if the GCIS system was credited, then the secondary peak would not occur and the system would stay in the convection dominated regime. The sensitivity analysis indicated that fuel surface emissivity higher than 0.2 result in acceptable fuel sheath temperatures. The thermal resistance of the channel walls was also investigated and showed that even for the case of only 2% FP heat flow to the moderator system, acceptable results occur.

6.1.2 SBLOCA and Critical break size

Break size smaller or equal to 15% is defined as SBLOCA in this design (the boundary may vary depending on the cold-leg pipe size) and is characterized by pressure/flow oscillations induced by frequent SRV actions. The smaller break introduced a less-significant, longer-lasting reverse channel flow, which mitigated the second peak MCST. However the reduced reverse flows cause higher initial MSCT peaks, even the NED is less than the LBLOCA case.

The most severe result is observed at the 15% break case with a highest MCST (1450 K) in the early stage of the transient. This is caused by a moderate power pulse (119% FP) and rather small reverse flows. Improvement in the SDS characteristics, early ADS intervention, alternative SRV characteristics were shown to provide significant benefit to SBLOCAs and hence further optimization of these systems is required.

6.2 Recommendations for future work

Some limitations have been found during this study and future work is required to improve the code for more accurate and reliable predictions. As discussed earlier, the Dittus-Boelter heat transfer correlation can either overestimate or underestimate the heat transfer rate near the pseudo-critical temperature. Some correlations specially recommended for heat transfer under supercritical pressure such as Jackson's and Bishop's should be incorporated. The same is true for pressure drop characteristics.

Although RELAP5 is robust enough to simulate the critical-transition in the depressurization process, it predicts some unlikely flow pulse near the critical pressure in the 5% break LOCA. Furthermore, some code failures still occur at some break size and nodalization combinations, typical by a thermal property error. These failures are also observed when a large number of channel groups is simulated. This suggests that the water property interpolation procedure near critical pressure can be further improved. Another possible improvement is to generate denser property tables with smaller grid length near the critical point so as to provide more accurate properties in the vicinity.

References

[1] OECD Nuclear Energy Agency for the Generation IV International Forum. Technology Roadmap Update for Generation IV Nuclear Energy Systems. January 2014.

[2]M. Yetisir, Generation IV Supercritical Water-cooled Reactor. 2012 Deep River Science Academy Summer Lecture, July 12-2012.

[3] T. Schulenberg, L. K. H. Leung, Y. Oka, Review of R&D for supercritical water cooled reactors. Progress in Nuclear Energy 77 (2014) 282-299.

[4] I. Pioro, S. Mokry, Thermophysical Properties at Critical and Supercritical Conditions, University of Ontario Institute of Technology, Canada. www.intechopen.com.

[5] X. Cheng, T. Schulenberg, Heat transfer at Supercritical Pressures- Literature Review and Application to an HPLWR. Institut für Kern- und Energietechnik, Programm Nukleare Sicherheitsforschung, Forschungszentrum Karlsruhe GmbH, Karlsruhe, 2001.

[6] J. D. Jackson and W. B. Hall. Influence of buoyancy on heat transfer to fluids flowing in vertical tubes under turbulent conditions. Advanced study Institute book: Turbulent Forced Convection in channels and bundles, 1979, p.613-640

[7] D. W. Hummel, D. R. Novog, Coupled 3D Neutron kinetics and thermalhydraulic characteristics of the Canadian Supercritical Water Reactor. Nuclear Engineering and Design, Volume 298, March 2016, p.78-89.

[8] T. Schulenberg, L. K. H., D. Brady, Y. Oka, et al., Supercritical Water-Cooled Reactor (SCWR) Development through GIF Collaboration. IAEA-CN-164-5S06

[9] M. Gaudet, M. Yetisir and Z. Haque, Physical aspects of the Canadian Generation VI Supercritical Water-Cooled Pressure-Tube Reactor plant design. 2014 Canada-China Conference on Advanced Reactor Development. Niagara, Ontario, Canada, 27-30April, 2014

[11] Thorium fuel cycle-Potential benefits and challenges. IAEA-TECDOC-1450, May 2005.

[12] M. Perez, C. M. Allison, R. J. Wagner, et al. The Development of RELAP5/SCDAPSIM/ MOD4.0 for Advanced Fluid Systems Design and Analysis. Proceeding of ICONE-23, Chiba-Japan , 17-21May 2015.

[13]C. M. Allison and J. K. Hohorst. Role of RELAP5/SCDAPSIM in Nuclear Safety. Science and Technology of Nuclear Installations. Volume 2010, Article ID 425658.

[14] http://www.nist.gov/srd/nist10.cfm

[15] M. Hanninen and J. Kurki, Simulation of flows at supercritical pressures with a two-fluid code. The 7th International Topical Meeting on Nuclear Reactor Thermal Hydraulics, Operation and Safety. Seoul, Korea, October 5-9, 2008.

[16] P. Wu, J. Gou, J. Shan, et al., Safety analysis code SCTRAN development for SCWR and its application to CGNPC SCWR. Annals of Nuclear Energy 56 (2013) 122-135.

[17] S. W. Fu, X. J. Liu, C. Zhou, et al., Modification and application of the system analysis code ATHELET to trans-critical simulations. Annals of Nuclear Energy 44 (2012) 40-49.

[18] R. Riemke, C. Davis and R. Schultz, RELAP5-3D Code For Supercritical-Pressure, Light-Water-Cooled Reactors, 11th International Conference On Nuclear Engineering. April 20, 2003. Tokyo, JAPAN.

[19] Y. Wu, D. R. Novog, Prediction of the Response of the Canadian Super-Critical water Reactor to potential Loss of Forced Flow Scenarios. The 7th International Symposium on Supercritical Water-Cooled Reactors, 15-18 March 2015, Helsinki, Finland.

[20] Kito et al. Fefinement of transient criteria and safety analysis for a high-temperature reactor cooled by supercritical water. Nuclear Technology, 135[3], 252(2001)

[21] Y. Ishiwatari, Y. Oka, et al., Safety of Super LWR, (II)-Safety analysis at Supercritical Pressure. Journal of Nuclear Science and Technology, Vol. 42. No. 11, p. 935-948 (November 2005).

[22] P. MacDonald, J. Buongiorno, et al. Feasibility Study of Supercritical Light Water Cooled Reactors for Electric Power Production. Idaho National Engineering and Environmental Laboratory Bechtel BWXT Idaho, LLC. January 2005.

[23] I. Ituen, D. R. Novog. Analysing Supercritical water reactors (SCWR's) special safety systems using probabilistic tools. The 5th International Symposium on Supercritical Water-cooled reactors, Vancouver, Canada, Mar 16-2011.

[24]D. Novog, G. McGee, D. Rhodes and M. Yetisir. Safety concepts and systems of the Canadian SCWR. The 3rd China-Canada Joint Workshop on Supercritical-Water-Cooled Reactors(CCSC-2012), Apr 18-20,2012. Xi'an,China

[25] X. Huang, M. Gaudet, M. Yetisir, et al., Analysis of passive residual heat transfer systems for the Canadian Supercritical Water-cooled reactor. 2014 Canada-China Conference on Advanced Reactor Development, Niagara Falls, Ontario Canada, 27-30 April, 2014.

[26] P. Wu, J. Gou, L. K. H. Leung. Heat transfer effectiveness of cooling of Canadian SCWR fuel assembly under the LOCA/LOECC scenario. Ann. Nucl. Energy (2015), http://dx. doi.org/10.1016/j.anucene.2015.03.006

[27]Y. Oka, S. Koshizuka, Y. Ishiwatari, et al, Super light water reactors and super fast reactors, Springer, New York/Dordrecht/Heidelberg/London, 2010.

[28] Y. Ishiwatari, Y. OKA, S. Koshizuka, et al., LOCA analysis of Super LWR. Journal of Nuclear Science and Technology. Vol.43, No.3, page 231-241(2006).

[29] X. J. Liu, S. W. Fu, Z. H. Xu, et al., LOCA analysis of SCWR-M with passive safety system. Nuclear Engineering and Design, Volume 259, June 2013, p 187-197.

[30] RELAP5/MOD3.3 code manual/volume4: models and correlations. Information Systems Laboratories, Inc., Idaho Falls- US, December 2001

[31] The International Association for Properties of Water and Steam, Release on the IAPWS Formulation 2011 for the Thermal Conductivity of Ordinary Water Substance, September 2011.

[32] J. Sharpe, A. Moghrabi, D. R. Novog, et al., A benchmark Comparison of the Canadian Supercritical Water-cooled reactor (SCWR) 64 element fuel lattice cell parameters using carious computer codes. 35th Annual Canadian Nuclear Society (CNS) Conference, Saint John, NB Canada, May31-June 3, 2015.

[33] J. Pencer, M. McDonald and V. Anghel, Parameters for transient response modeling for the Canadian SCWR. The 19th Pacific Basin Nuclear Conference (PBNC2014), Vancouver, BC, Canada, August 24-28, 2014.

[34] Y. Oka, Review of high temperature water and steam cooled reactor concepts. Proceedings of the SCR-2000, 6-8 November 2000, Tokyo, Japan.

[35]A. Nava-Dominguez, E. N. Onder, Y. F. Rao and L. K. H. Leung. Evolution of the Canadian SCWR Fuel-assembly concept and assessment of the 64 Element Assembly for Thermalhydraulic Performance. Proceedings of Global 2015, September 20-24, 2015-Paris(France).

[36] D. F. Torgerson, B. A. Shalaby, S. Pang, CANDU technology for Generation III+ and IV reactors. Nuclear Engineering and Design 236 (2006) 1565-1572.

[37] D. W. Hummel, D. R. Novog, Optimized channel inlet orifice sizing for the pressure tube type supercritical water-cooled reactor. 19th Pacific Basin Nuclear Conference, Vancouver-Canada, 24-28 August, 2014

[38] Status report 71-Japanese Supercritical Water-Cooled Reactor (JSCWR) [online]. Available: https://aris.iaea.org/sites/..%5CPDF%5CJSCWR.pdf.

[39]RELAP5/MOD3.3 code manual volume I: Code structure, system models, and solution methods. Information System Laboratories, Inc.,Rockville, Maryland, December 2001.

[40] M. Chatharaju, Computational Study of Critical Flow Discharge in Supercritical Water Cooled Reactors. Master thesis, McMaster University, August 2011.

[41] F. Zhou, CFD study on convective heat transfer on Carbon Dioxide and water at Supercritical pressure in vertical circular pipes. Master thesis, McMaster Unversity, 2014.

[42] J. Shan, W. Chen, et al. Coupled neutronics/ thermal-hydraulics analysis of CANDU-SCWR fuel channel. Annals of the Nuclear Energy 37(2010) 58-65.

Appendix

A. Trip logic of the SRV

In this SCWR model, the SRV is designed to open as the system pressure increases above 26.0MPa and stay opened until the pressure drops back to 25.25 MPa. Techniques from Boolean algebra are used here to assist in building the logic statements. A Boolean variable has one of the two values, false (0) or true (1). The Boolean variables are defined as following:

1) V_1 is to be true when the valve should be opening;

2) V_2 is the current value of the valve motion (1 for opening and 0 for closing);

3) P_1 is true when the pressure is greater than 25.25 MPa;

4) P_2 is true when the pressure is greater than 26.0 MPa;

Table A1.1 lists all possible combinations of the three input variables. The following expression can be written based on the truth table A1.1:

$$V_1 = (\overline{V_2} \otimes P_2 \otimes P_1) \oplus (V_2 \otimes \overline{P_2} \otimes P_1) \oplus (V_2 \otimes P_2 \otimes P_1) \quad \text{(Eq1.1)}$$

where $\otimes$ donates AND , $\oplus$ donates OR and the bar donates the complements. The relationships between P_2 and P_1 are: $P_2 \otimes P_1 = P_2$ $P_2 \oplus P_1 = P_1$. Thus the logical expression in equation A1.1 can be simplified as

$$V_1 = (\overline{V_2} \otimes P_2) \oplus \left((V_2 \otimes P_1) \otimes (P_2 \oplus \overline{P_2})\right) = (\overline{V_2} \otimes P_2) \oplus (V_2 \otimes P_1) \qquad \text{(A1.2)}$$

Table A1.1 Truth table of the Boolean variables in the trip statements defining a trip valve

Output	Input		
V_1	V_2	P_2	P_1
0	0	0	0
0	0	0	1
impossible	0	1	0
1	0	1	1
0	1	0	0
1	1	0	1
impossible	1	1	0
1	1	1	1

The following trip input implements the above logic. Trip 602 and 603 specify the first and second term on right hand side of equation A1.2. Trip 604 implements the open trip in a trip valve.

```
503   p   132010000   gt   null   0   2.6E7     n
504   p   132010000   gt   null   0   2.525E7   n
602   -604   and   503   n
603   604    and   504   n
604   602    or    603   n
```